MARTIN EVERARDUS REYNERS

A MICROEARTHQUAKE STUDY OF THE PLATE BOUNDARY,

NORTH ISLAND, NEW ZEALAND

Submitted for the degree of

Doctor of Philosophy

Institute of Geophysics

Victoria University of Wellington

New Zealand

November, 1978

ABSTRACT

The seismicity, structure and tectonics of the North Island plate boundary have been studied by means of a microearthquake traverse oriented in the direction of dip of the subducted Pacific plate and stretching from southern Hawke's Bay to northern Taranaki.

The geometry of the top of the Pacific plate is inferred from a band of concentrated microearthquake activity which can be identified with the crust of the plate. The Pacific plate appears to have two knee-like bends, one between the east coast and the Ruahine Range, where the top of the plate is about 25 km deep, the other below the volcanic front, where it is about 70 km deep. The shallower bend and subsequent restraightening of the plate can be related to phase changes in the plate, while the deeper bend can be related to volcanism.

Composite focal mechanisms indicate that seaward of its shallower bend the Pacific plate is being loaded by the Indian plate, whereas landward of this bend the Pacific plate is sinking under its own weight. Both composite focal mechanisms and the distribution of microseismicity in the Pacific plate suggest the existence of a major discontinuity striking down the dip of the plate and passing beneath the Tongariro volcanic centre.

A conspicuous lack of microseismicity in the Indian plate in the eastern North Island revealed in this study can be related to the plates being unlocked in this region. A feature of the seismicity of the Indian plate in the region of the Wanganui Basin is the concentration of activity in the 25-42 km depth range, shallower activity being largely confined to the northeast edge of the basin, near Mt Ruapehu and Waiouru. Composite focal mechanisms suggest the 25-42 km deep activity reflects stresses set up by locking and unlocking of the plates, while the shallower activity reflects local stresses related to volcanic phenomena.

ACKNOWLEDGEMENTS

CONTENTS

LIST OF FIGURES

LIST OF TABLES

CHAPTER 1

INTRODUCTION

The North Island of New Zealand exhibits all the principal features typically found at a plate boundary with subduction. These features include an oceanic trench, large negative gravity anomalies, andesitic volcanism, and crustal and mantle seismicity. Yet the plate boundary in the North Island is unusual, in that the subducted Pacific plate does not begin to dip steeply until well beneath the North Island (e.g. Hamilton & Gale, 1968). As a result, a larger proportion of the plate boundary can be subjected to land-based geophysical observation than is possible with most other subduction zones, where the shallow part of the subducted plate is offshore.

The Seismological Observatory of the Geophysics Division of the New Zealand Department of Scientific and Industrial Research (DSIR) operates a nationwide permanent network of seismographs with a typical station spacing of some 140 km. This network enables detailed study of the intermediate depth and deep earthquakes associated with subduction of the Pacific plate beneath the North Island (e.g. Ansell & Smith, 1975; Adams & Ware, 1977; Smith, 1977). However, the large station spacing of the permanent network leads to generally poor depth control for shallow earthquakes, and up to 1976 all shocks recognized as crustal by the Seismological Observatory have been routinely restricted to depths of 12 km or 33 km for purposes of computation.

The advent of microearthquake surveying has now made the detailed investigation of shallow seismicity feasible. Microearthquake surveying involves the location of small earthquakes, usually of magnitude less than 3.0, using closely-spaced, high-gain seismographs at selected sites. Given good recording conditions, earthquakes of magnitude less than 0.0 can be located with a microearthquake array. Consequently, a sample of the microearthquake activity in a given region can be obtained in a relatively short time, since the frequency of occurrence of earthquakes increases by a factor of about eight for each unit drop in magnitude (e.g. Richter, 1971). In New Zealand,

microearthquake surveys have been used to study regional seismicity (e.g. Scholz et al., 1973a; Robinson & Arabasz, 1975; Arabasz & Robinson, 1976), the seismicity of a geothermal area (Evison et al., 1976), and the long-term behaviour of an aftershock sequence (Robinson et al., 1975).

This thesis describes a microearthquake traverse carried out across the North Island, from Porangahau in the southeast to Whangamomona in the northwest. The traverse strikes at 311°, approximately parallel to the direction of dip of the underlying Benioff zone determined by Adams & Ware (1977). The principal aims of the study were:

(1) To obtain a detailed picture of the seismicity of the North Island plate boundary through the accurate location of well-recorded microearthquakes close to the traverse.

(2) To determine the stress regime in the subducted and overlying plates through the study of microearthquake composite focal mechanisms.

(3) To combine the results of (1) and (2) with other geophysical data pertaining to the North Island and thus arrive at a better understanding of active deformation at the North Island plate boundary.

CHAPTER 2

THE TECTONIC SETTING, SEISMICITY AND STRUCTURE
OF THE STUDY AREA

2.1   TECTONIC SETTING

In terms of plate tectonics (Le Pichon, 1968), New Zealand
straddles the boundary between the Pacific and Indian plates (fig. 2.1).
This boundary is marked by the Tonga-Kermadec subduction zone (Oliver &
Isacks, 1967) to the northeast of New Zealand, and by the Macquarie
Ridge complex (Hayes et al., 1972) to the southwest. The boundary
within New Zealand has been described as a 200 km-wide zone of
pervasive deformation manifest in seismic activity, distortion of
triangulation nets and differential vertical movements of the land
(Walcott, 1978a).

Sea-floor spreading magnetic evidence suggests that an active
plate boundary has passed through the New Zealand region since the
Paleocene, but since the pole of rotation of the Pacific/Indian plate
pair has always been close to the boundary during this time, evidence
of plate interactions in New Zealand continental geology is generally
variable and sometimes subtle (Weissel et al., 1977). Indeed, there
is very little direct information on the relative motion of the Pacific
and Indian plates, and Chase (1978) does not use any data from the
Pacific/Indian plate boundary in calculating a pole of rotation for
this plate pair for post-Miocene times based on global sea-floor
spreading rates, transform fault trends and earthquake slip vectors.
The velocity of the Pacific plate relative to the Indian plate predicted
by this pole is shown in fig. 2.1.

The mode in which the relative motion between the Pacific and
Indian plates is presently accommodated in New Zealand varies along the
length of the plate boundary. In the Fiordland region (in the southwest
of the South Island) the offshore seismicity, thrusting earthquake
mechanisms and intermediate depth activity all suggest subduction of
the Indian plate, whereas in the Alpine fault zone in the central South
Island the plate boundary has been described as a zone of oblique
continental convergence (Scholz et al., 1973a). In the North Island
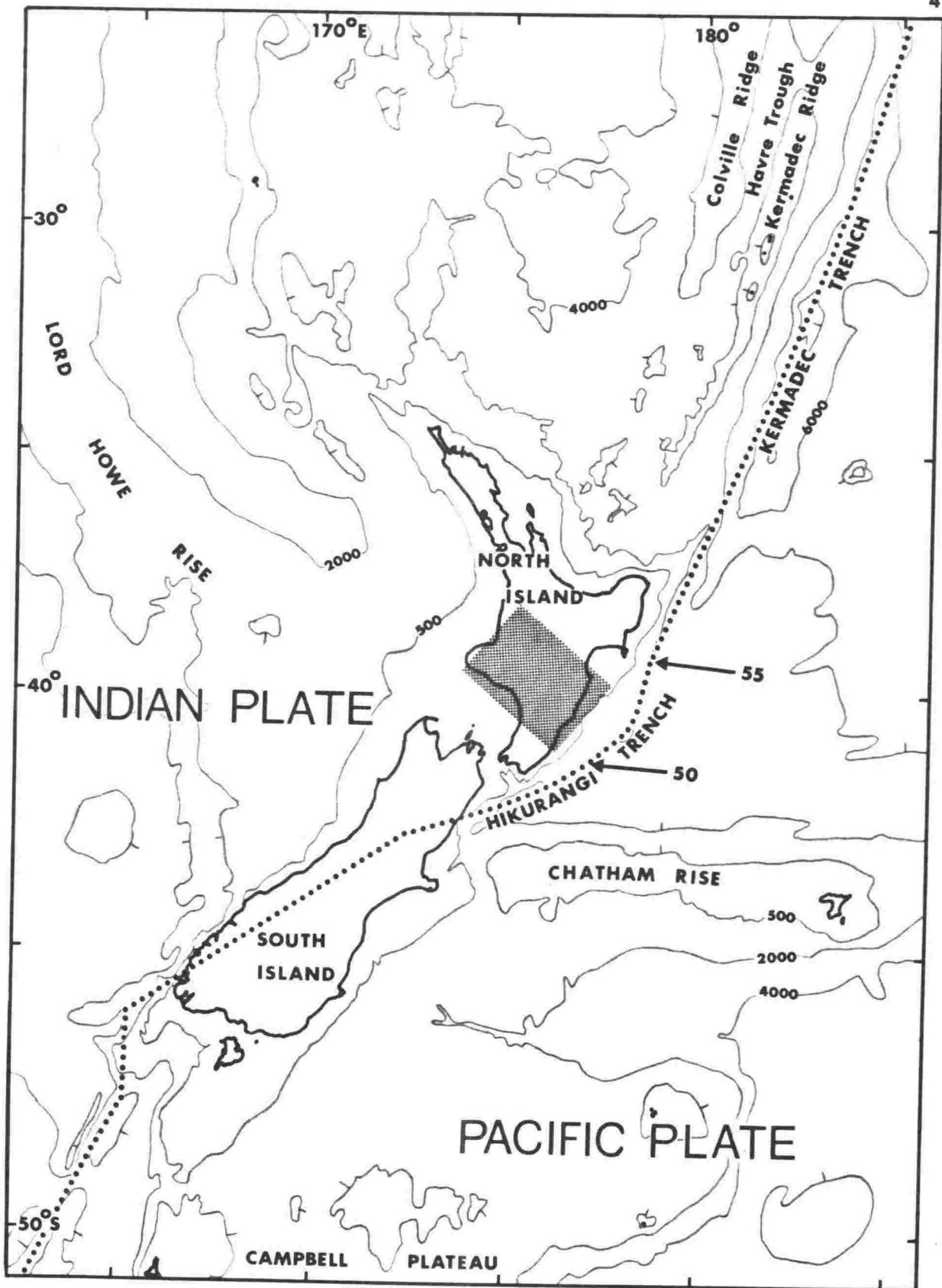
Figure 2.1   Tectonic setting of the New Zealand region.   The area of this study is shaded.   Bathymetry is in metres, and is taken from Lawrence (1967). The dotted line marks the approximate position of the boundary between the Pacific and Indian plates of Walcott (1978a), while the arrows indicate the velocity, in mm/yr, of the Pacific plate relative to Indian plate predicted by the Pacific/Indian pole of Chase (1978).

and northern South Island, intermediate-depth earthquakes, active volcanism and a shallow trench indicate that subduction of the Pacific plate is currently occurring. Hereafter this portion of the plate boundary will be referred to as the Hikurangi Margin, following Hatherton (1971).

2.2 SEISMICITY

The Hikurangi Margin incorporates the Main Seismic Region of Eiby (1971), and its seismicity has been extensively discussed (e.g. Eiby, 1958, 1964, 1971; Hamilton & Gale, 1968, 1969). The most definitive study to date of the morphology of the Benioff zone associated with the subducted Pacific plate at the margin has been that of Adams & Ware (1977). These authors have located subcrustal earthquakes using a laterally inhomogeneous velocity model in which velocities along ray paths presumed to lie entirely in the Benioff zone have been increased by 11% compared with the standard Jeffreys-Bullen model. They have determined the Benioff zone to be essentially planar, with a strike of 045° and a dip of 50° to the northwest (see fig. 2.2); the lower limit of Benioff zone activity shoals towards the southwest, making an angle of some 15° with the horizontal (fig. 2.3).

The southwesterly shoaling of the lower limit of Benioff zone activity is more rapid than that predicted by a linear decrease in subduction rate as the Pacific/Indian pole of rotation is approached. Scholz et al. (1973a) argue that this shoaling provides strong evidence for a southerly migration of the Hikurangi Trench. However, as pointed out by Arabasz & Robinson (1976), the shoaling may simply result from the "fold axis" of the subducted plate being oblique to the direction of plate convergence (compare figs. 2.1 and 2.2). If the vertical cross sections of the Benioff zone of Adams & Ware (1977) are rotated to the surface, it becomes apparent that the subducted plate is almost uniformly wide between 36°S and 40.5°S, the leading edge of the plate being nearly parallel to the Hikurangi and Kermadec Trenches.

Subcrustal earthquakes in the northwest of the South Island mark a clear southwestern edge to the Benioff zone of the Hikurangi Margin (fig. 2.3). The northeastern boundary of the Benioff zone shown in figs. 2.2 and 2.3 is arbitrary, being the limit of the area studied by
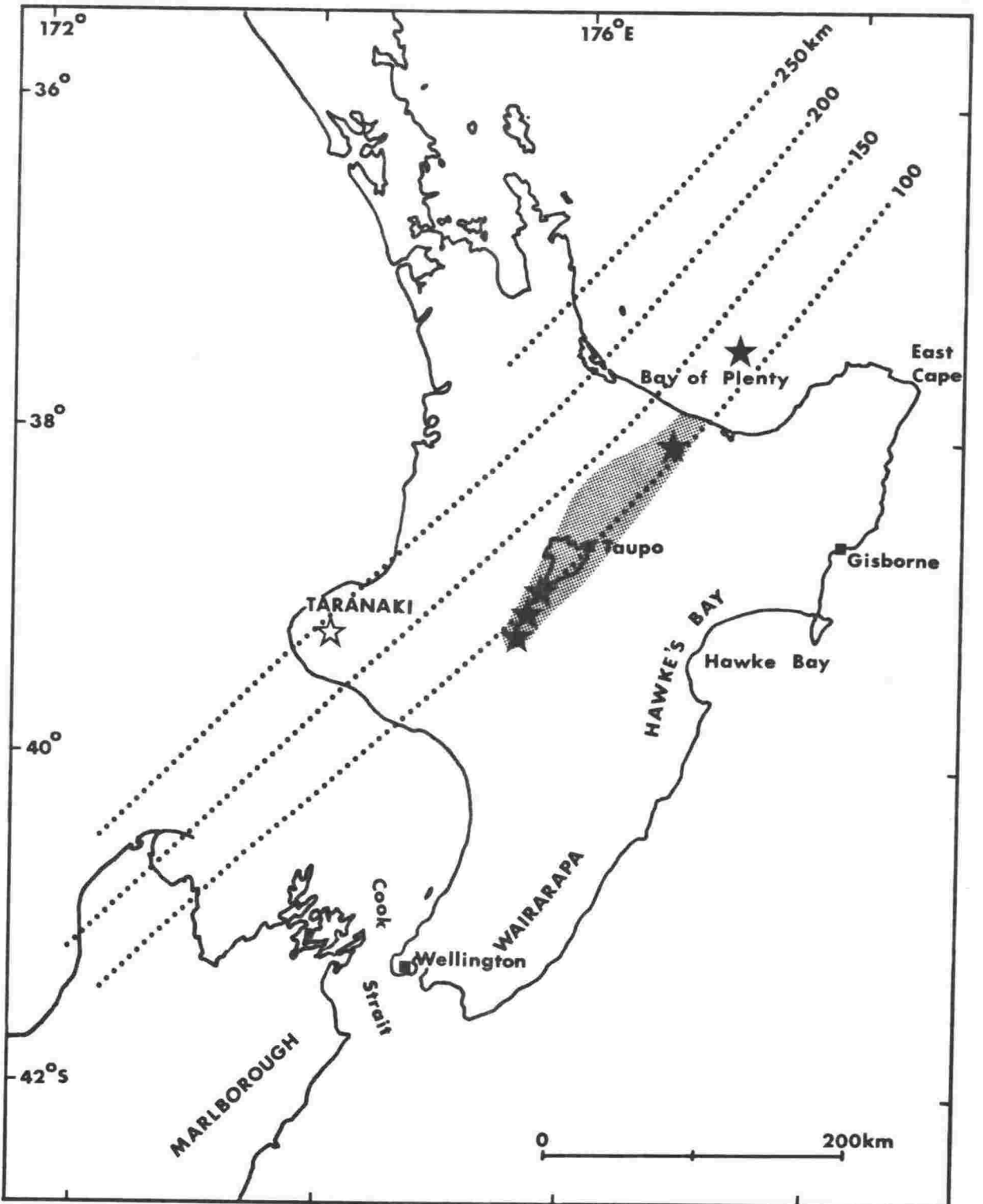
Figure 2.2   Isobaths of subcrustal earthquake activity at the Hikurangi
Margin (dotted lines), as determined by Adams & Ware (1977).   Also shown
are the Taupo Volcanic Zone (shaded), recently active andesitic volcanoes
(filled stars for low-potash andesites, open star for high-potash andesite),
and localities outside the study area referred to in the text.
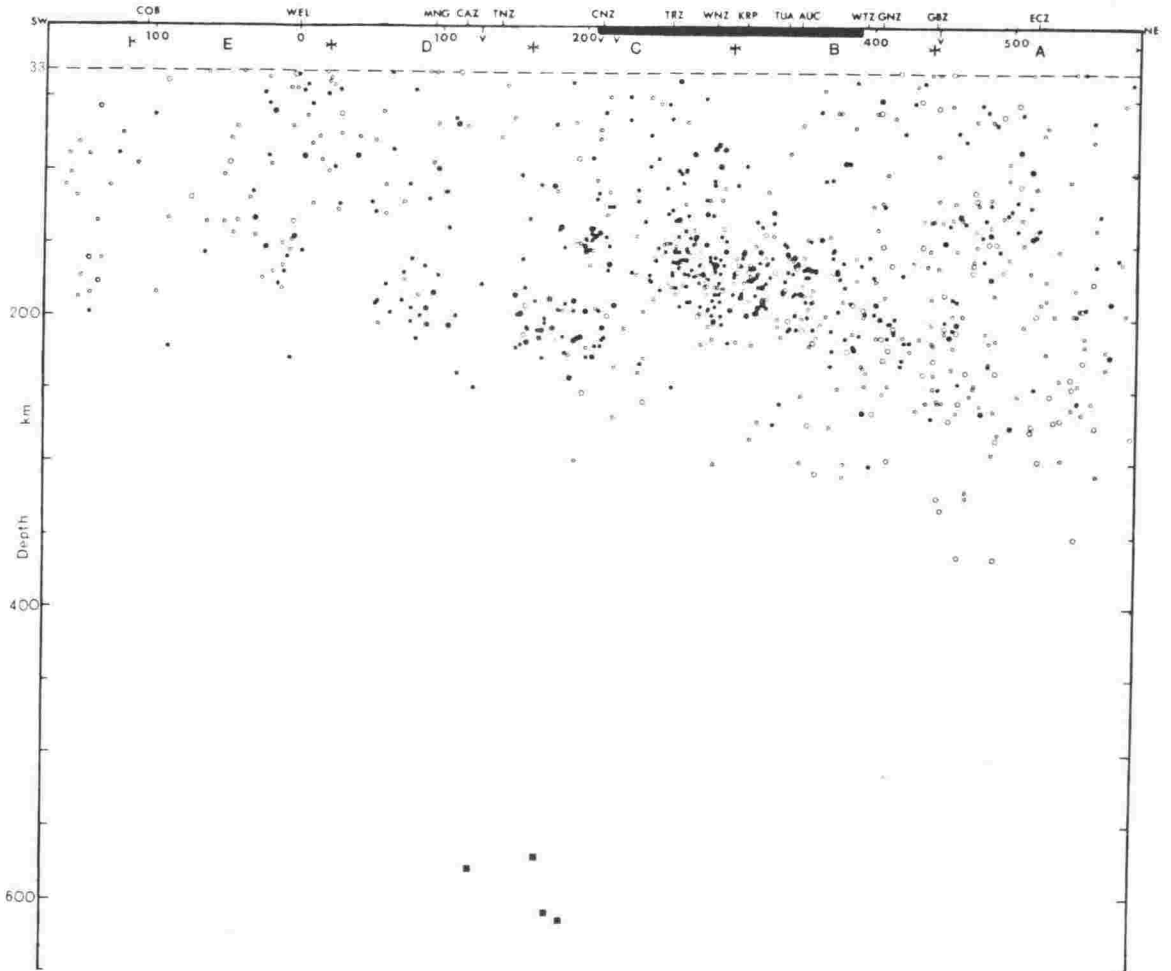
Figure 2.3   Vertical cross section of subcrustal earthquake foci along the strike of the Benioff zone, showing stations of the New Zealand seismograph network, volcanoes (V) and the Taupo Volcanic Zone (shaded) [taken from Adams & Ware (1977)]. Larger symbols represent earthquakes of magnitude 4.5 or greater, and solid symbols denote those more accurately located.

Adams & Ware (1977). To the northeast, subcrustal activity in the Main Seismic Region is separated from that in the Kermadec Seismic Region by a narrow transverse gap with few or no earthquakes, passing through 36°S, 179°E and marking a change in strike and maximum depth of the activity (Eiby, 1971, 1977).

Subduction of the Pacific plate at the Hikurangi Margin is accompanied by diffuse shallow seismicity stretching from the Hikurangi Trench to the region above the deepest part of the Benioff zone (fig. 2.4). This shallow seismicity shows no detailed relationship with surface faulting (Hatherton, 1970b; Eiby, 1971). Hatherton (1970b) has noted that the shallow shocks are symmetrically disposed about the axis of the negative isostatic gravity anomaly (fig. 2.5), and that the main belt of shallow earthquakes follows the negative gravity anomaly axis in changing direction from southwest to south-southeast through Cook Strait. A relatively aseismic corridor in the upper crust lies to the west of this main belt of activity (see fig. 2.4).

Shallow earthquakes at the Hikurangi Margin display a regular regional pattern with regard to source properties (Gibowicz & Hatherton, 1975). Average displacements across the fault plane are small for shocks between the Hikurangi Trench and the east coast of the North Island and also northwest of the recently active low-potash andesitic volcanoes (fig. 2.2). Between these two regions, and thus over most of the North Island, displacements are large. Large values of displacement imply higher strength of the source material, while low values may indicate pre-existing faults and fractures in the area or zones of major weakness.

Large shallow earthquakes that have occurred at the Hikurangi Margin since European settlement (1840) display a diffuse distribution similar to that of the smaller shallow shocks. Those that have occurred in the immediate vicinity of the microearthquake traverse are shown in fig. 2.6, together with faults thought to have been active during the Holocene. What follows are brief notes on seismological aspects of the earthquakes of magnitude seven or more shown in fig. 2.6.

SHALLOW
EARTHQUAKES
1956 – 1974

- $3.0 \leqslant M < 4.0$
- $4.0 \leqslant M < 5.0$
- $5.0 \leqslant M < 6.0$
- $M \geqslant 6.0$

—— MAJOR FAULTS

➤ ◄ Relatively aseismic
corridor of Hatherton (1970b)

0   100   200 km
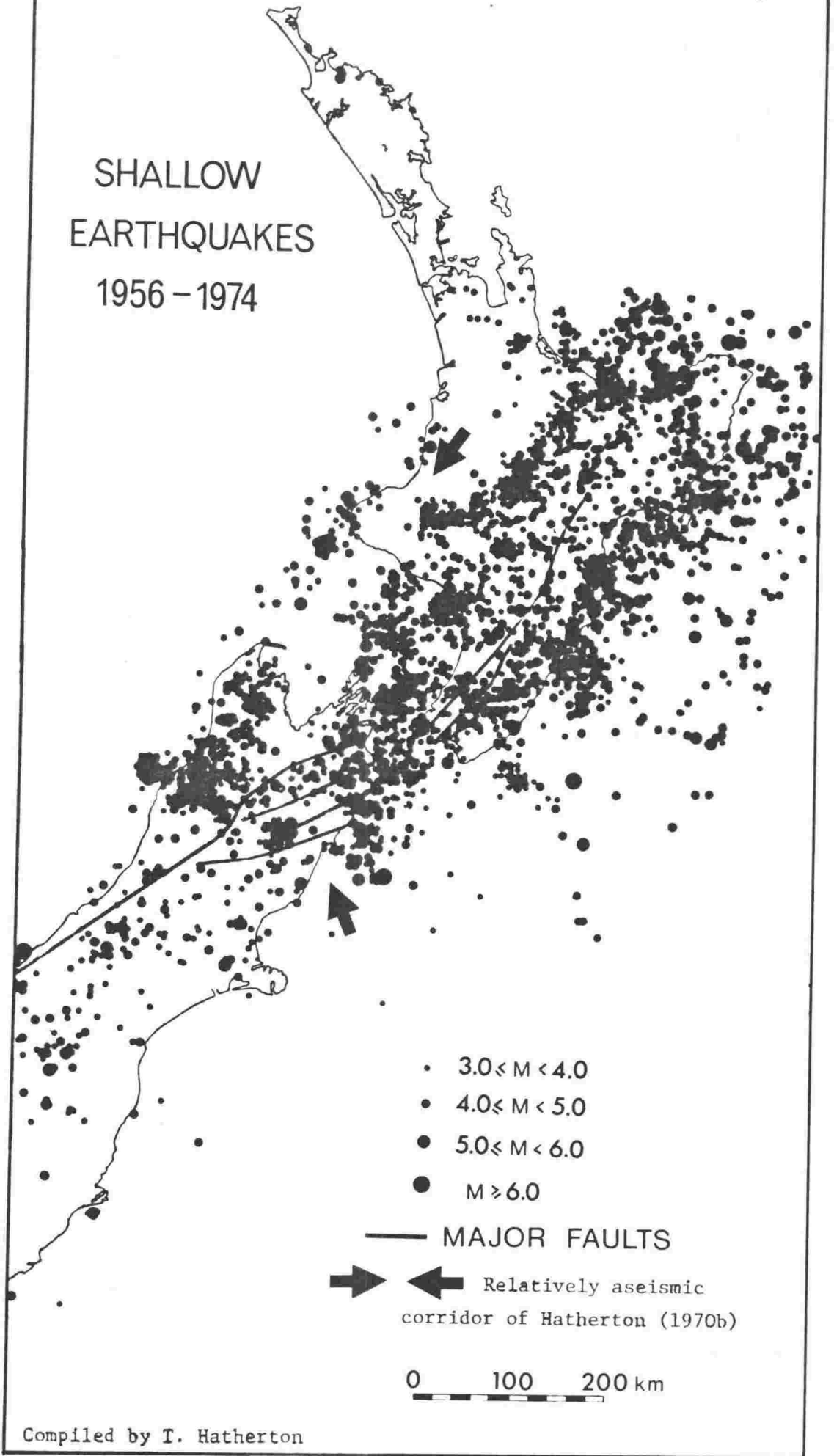
Compiled by T. Hatherton

Figure 2.4
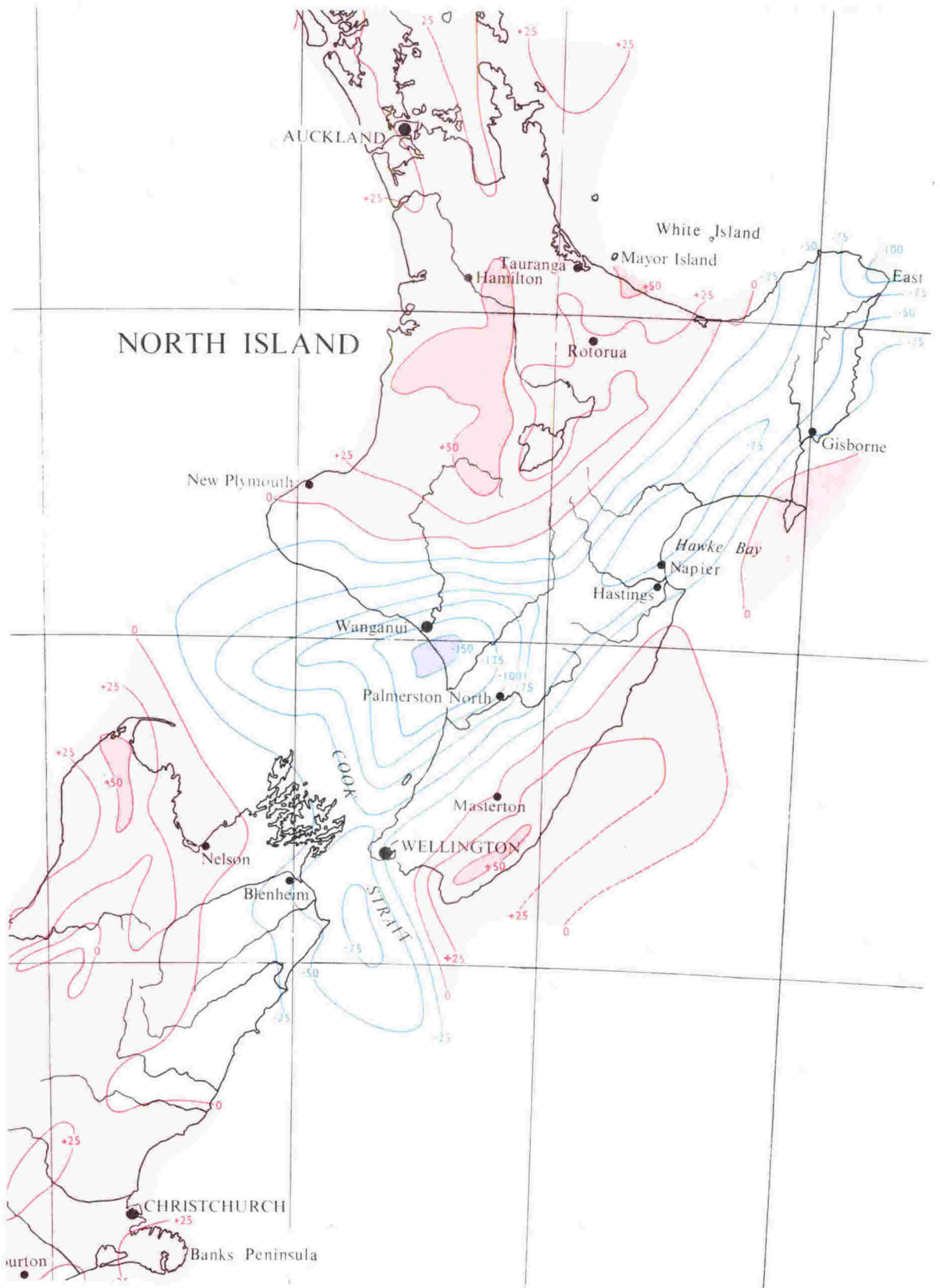
Figure 2.5   Isostatic gravity anomalies at the Hikurangi Margin
compiled by Reilly (1965).   The contour interval is 25 mgal (i.e.
250 μN/kg), and the scale is 1:4,000,000.

Earthquakes less than 100km deep

Magnitude (M_L) ≥ 7 (1840 – 1977)

" ≥ 6 (1940 – 1977)

—— Faults active during Holocene

(after N.Z. Geological Survey, 1973)
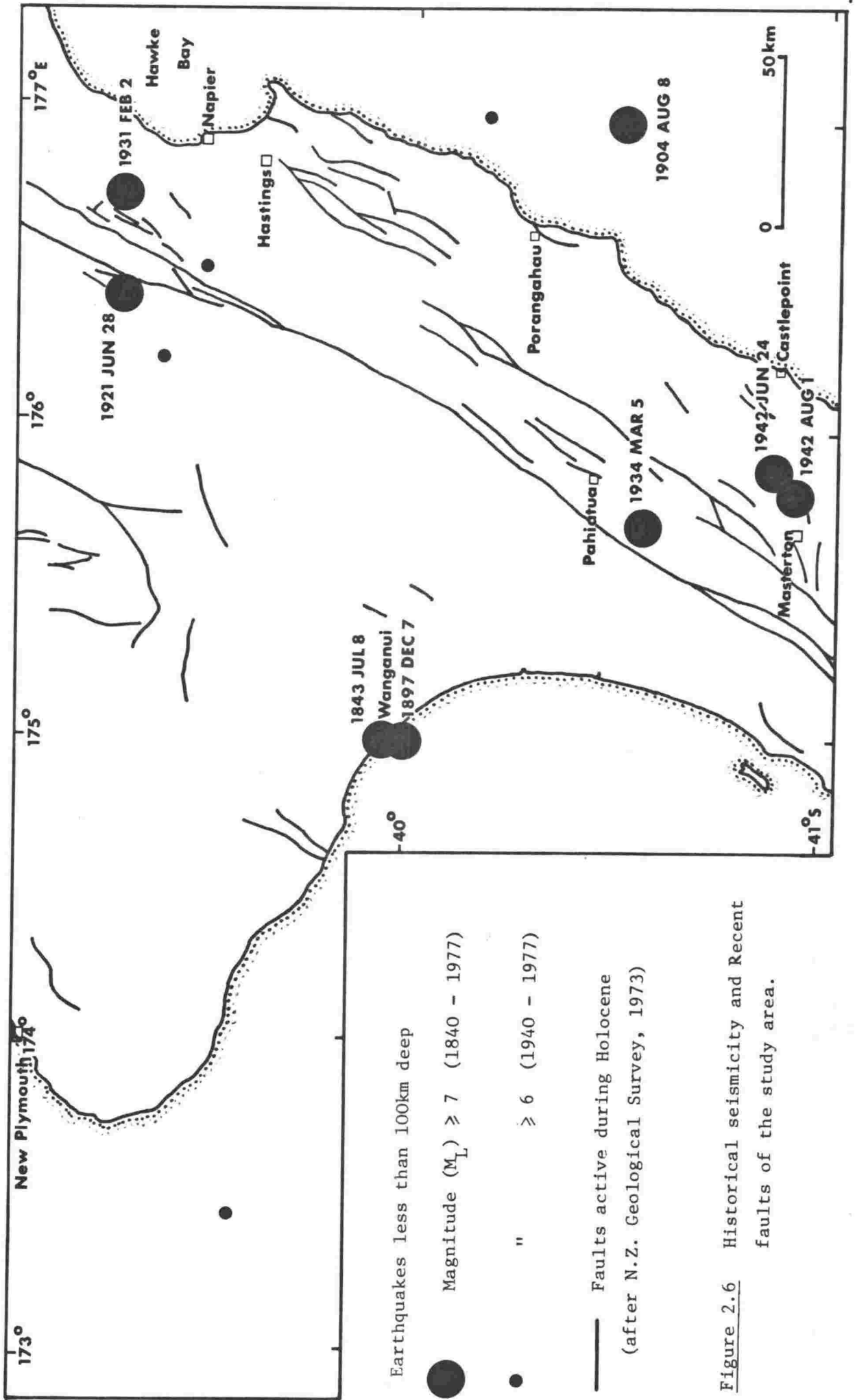
Figure 2.6   Historical seismicity and Recent faults of the study area.

1843 July 8th

Historical data on this earthquake has been studied in detail by Eiby (1968a). This was a major earthquake, with a magnitude not less than 7½ and an epicentre close to Wanganui, or within 50 km to the northeast of it. There were large landslides and conspicuous cracking of the banks of the Wanganui River, a suggestion of seiche movements in the river, and regional uplift and subsidence. Maximum intensity was certainly MM9 and probably MM10. The earthquake was most likely shallow, as it was followed by numerous aftershocks, some of the larger ones being felt in New Plymouth and Wellington.

1897 December 7th

Hayes (1953) assigns this earthquake a magnitude of 7. The epicentre calculated by Hogben (1898) at approximately 40.5°S, 174.2°E is very likely to be in error: his isoseismal map suggests an epicentre close to Wanganui. Felt reports indicate a maximum intensity of MM8 at Wanganui. A conspicuous lack of aftershocks ("at all events, not more than one very slight one" - Field, 1897) and the wide distribution of higher intensity suggest the depth of the earthquake is likely to have been greater than the 25 km deduced by Hayes (1953).

1904 August 8th

This earthquake was felt over nearly the whole country, and Hayes (1953) assigns it a magnitude of 7½. Its effects were most marked in the Hawke Bay and Wellington Districts, especially on or near the coast from Porangahau to Castlepoint, where rockfalls occurred from cliffs and fissures were observed in the ground (indicating an intensity of about MM9). Hogben (1904) calculates an epicentre at 42° 23½'S, 178° 58'E, but his isoseismal map suggests an epicentre much nearer to the coast (see fig. 2.6). The earthquake is likely to have had a shallow focus, as it was followed by at least twenty felt aftershocks.

1921 June 28th

A detailed analysis of this earthquake has been made by Bullen (1937) using data of the International Seismological Summary. He calculates an epicentre at 39.3°S, 176.4°E, with a standard error of about 0.4°. Both P and PKP observations indicate a focal depth of about 80 km. Such a depth is in agreement with the isoseismal distribution. The earthquake produced intensity MM7 or 8 over most of Hawke Bay District, and Hayes (1953) has assigned it a magnitude of 7 from the felt data.

1931 February 2nd

This magnitude $7\frac{3}{4}$ earthquake produced major destruction in Napier and Hastings and caused the loss of 256 lives. Intensity reached MM11 at Napier. Regional uplift and subsidence occurred, and extensive ruptures formed in an area of Tertiary limestones some 10 km southwest of Hastings. Taken together, ground movements indicate that the earthquake involved movement on a northwest-dipping thrust fault (Henderson, 1933). Using readings from New Zealand stations, Adams et al. (1933) place the mainshock about 20 km north of Hastings and 16-24 km deep. Bullen (1938a) finds the seismological evidence from both local and overseas stations is consistent with an epicentre some 25 km northwest of Napier. He suggests a focal depth of 15-20 km, "though the evidence for this is not precise". The mainshock was followed by numerous aftershocks, the largest having a magnitude of 7.1.

1934 March 5th

The region most severely shaken by this magnitude 7.1 earthquake was the eastern part of the North Island between Porangahau and Castlepoint. There has been some debate as to the location of this earthquake. Bullen (1936) and Hayes (1937) calculate epicentres at sea, east of Castlepoint (at 40.85°S, 176.8°E and 40.95°S, 176.8°E respectively). However, a reinterpretation of the earthquake incorporating overseas readings (Bullen, 1938b) gives an epicentre onshore near Pahiatua (at 40.6°S, 175.7°E). Both Bullen (1938b) and Hayes (1937) agree the earthquake had a fairly shallow focus. This is also suggested by the numerous aftershocks which occurred.

1942 June 24th and August 1st

The magnitude 7 earthquake of June 24th was damaging in southern Wairarapa and Wellington, reaching intensity MM9. It was followed by numerous aftershocks, and its depth has been estimated at 20 km (Hayes, 1942). The magnitude 7.1 earthquake which occurred on the 1st of August had an epicentre close to that of the earthquake of June 24th, but was appreciably deeper, its focal depth being calculated at 55 km (Eiby, 1968b). The difference in depth between these two shocks is borne out by the intensity distributions they produced (Hayes, 1943).

The earthquake of June 24th produced ground fracture close to the computed epicentre (Ongley, 1943), but since the fractures were small and of limited extent it is difficult to ascertain if true surface faulting occurred. Recently, two faults have been postulated as having moved during the August 1st earthquake. In a dendrochronological study of bent trees on a fresh fault scarp on the western flank of the Aorangi Range (southern Wairarapa), Berryman (1977) establishes faulting took place about 1942, and suggests the August 1st earthquake was responsible. Neef(1976) postulates on rather meagre evidence that a young minor bedding fault some 30 km northeast of Masterton probably moved during the same earthquake. Both these fault movements are hard to reconcile with the seismological evidence.

The tectonic significance of many of the aforementioned earthquakes will be discussed in chapter six in the light of the results of this microearthquake study.

2.3 STRUCTURE

The andesitic volcanism typically associated with lithospheric subduction is well-developed at the Hikurangi Margin. Hatherton (1969) has shown that the composition of the andesitic lavas can be related to the depth of the subjacent Benioff zone. As can be seen in fig. 2.2, recently active low-potash andesitic volcanoes in the North Island (hereafter referred to as the "volcanic front" following Adams & Hatherton (1973)) straddle the 100 km isobath of the underlying Benioff zone. The volcanic front appears to have a more northerly strike than the Benioff zone, a fact which has led Hamilton & Gale (1968) to associate the volcanism with the most intense intermediate-depth earth-quake activity, which also has a more northerly strike than the Benioff

zone by virtue of its increase in depth from southwest to northeast within the Benioff zone (see fig. 2.3). Recent high-potash andesitic volcanism has been restricted to a small area (fig. 2.2), and occurs where the underlying Benioff zone is approximately 200 km deep.

A magmatic arc has been present in northern New Zealand for about the last 20 million years, and has migrated eastwards and southwards with time (Ballance, 1976). From the apparent migration of axes of andesitic volcanism, Calhaem (1973) has proposed that asymmetrical spreading of about 3 cm per year is currently occurring within the Taupo Volcanic Zone (fig. 2.2). This zone is a region of Recent volcanism, high heat flow, shallow seismic activity (Evison et al., 1976), normal faulting (Grindley, 1960) and significant rates of strain (B. Sissons, pers. comm., 1978). It is aligned with, and is presumed to be an extension of, the Lau-Havre Trough, which Karig (1970) interprets as having formed by back-arc spreading behind the Kermadec subduction zone. Calhaem (1973) recognizes the eastern boundary of the Taupo Volcanic Zone as the proper boundary of the Indian plate, and the region between this boundary and the Hikurangi Trench as part of a separate, minor, passive plate. He maintains the Benioff zone, trench and minor plate have migrated together, relative to the Indian plate. Ballance (1976) supports the existence of such a minor plate, terming it the Hawke's Bay Microplate. In addition, Eiby (1977) invokes migration of a similar plate fragment to explain the apparent eastward displacement of seismicity shallower than about 150 km relative to deeper seismicity in the region of East Cape.

There has been some debate as to whether the Hikurangi Trench marks the commencement of subduction of the Pacific plate. The trench is rather amorphous compared with, say, the Kermadec and Tonga Trenches, and is atypically placed with respect to the negative isostatic gravity anomaly (fig. 2.5) and the intermediate-depth earthquake activity (fig. 2.2). Katz (1974) has argued that the trench does not represent a continental margin but rather a depositional basin of entirely continental affiliation, closely related to the thick Cenozoic sediments of the east coast of the North Island. Cole (1978) prefers the major fault zone separating Mesozoic greywacke/argillite and Cenozoic sediments in the east of the North Island (see fig. 2.7) as the surface expression of the plate boundary. On the other hand, Gibowicz & Hatherton (1975)
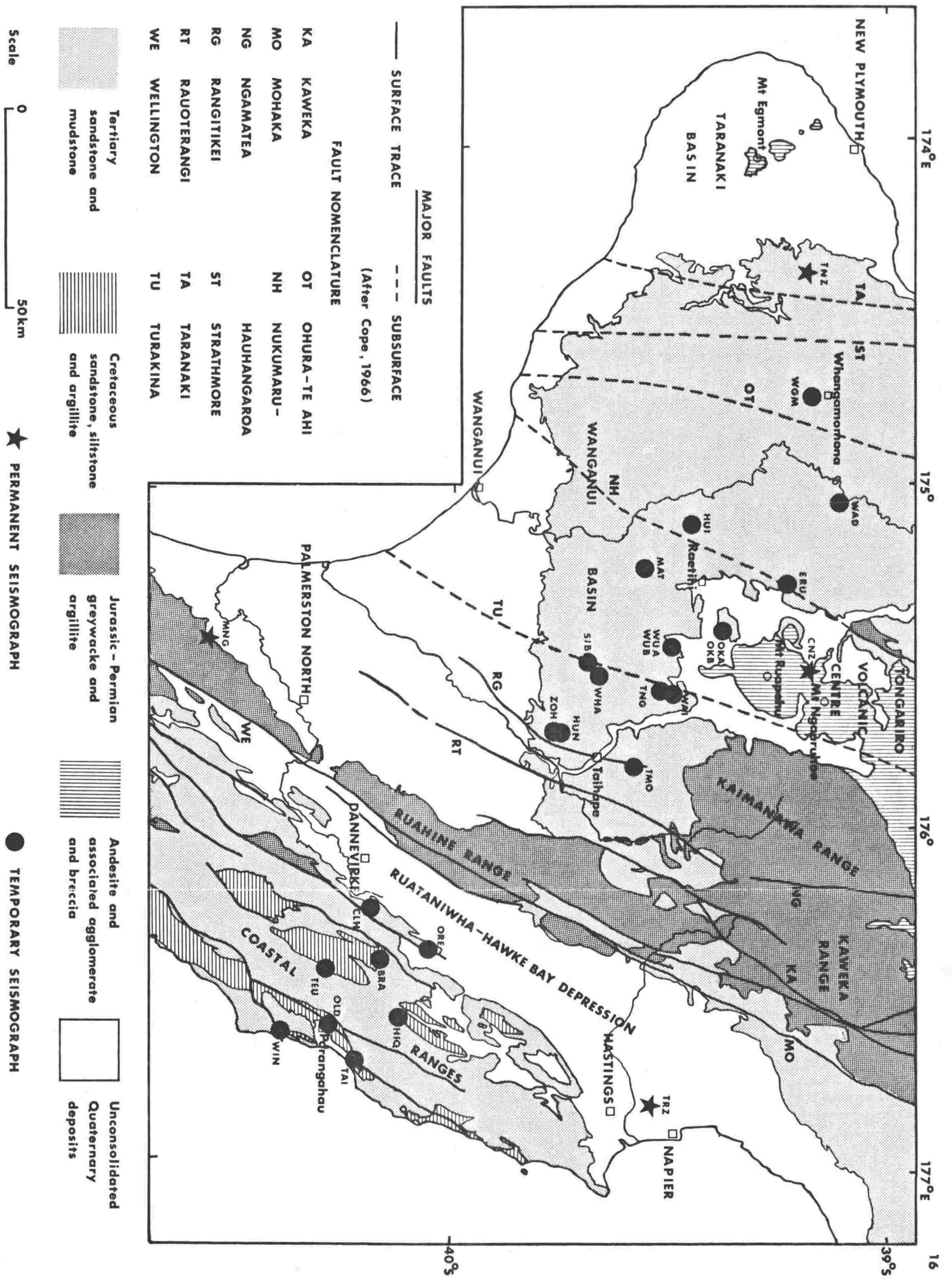
FIG. 2.7 GENERALIZED GEOLOGY OF THE TRAVERSE

(After New Zealand Geological Survey, 1972)

MAJOR FAULTS

SURFACE TRACE

- - - SUBSURFACE

(After Cope, 1966)

FAULT NOMENCLATURE

KA   KAWEKA   OT   OHURA-TE AHI
MO   MOHAKA   NH   NUKUMARU-
NG   NGAMATEA   HAUHANGAROA
RG   RANGITIKEI   ST   STRATHMORE
RT   RAUOTERANGI   TA   TARANAKI
WE   WELLINGTON   TU   TURAKINA

Tertiary
sandstone and
mudstone

Cretaceous
sandstone, siltstone
and argillite

Jurassic – Permian
greywacke and
argillite

Andesite and
associated agglomerate
and breccia

Unconsolidated
Quaternary
deposits

★ PERMANENT SEISMOGRAPH

● TEMPORARY SEISMOGRAPH

Scale

0   50km

contend that the associated shoaling of the trench and intermediate-depth seismicity, and the equivalent behaviour of the trench boundary and a line marking a change in the source properties of shallow earthquakes in the eastern North Island, indicate that the trench plays a very real tectonic role.

The generalized geology of the area of the present study is shown in fig. 2.7, together with the location of permanent stations of the New Zealand seismograph network and the temporary microearthquake stations. From southeast to northwest, salient structural features include:

a) The coastal ranges of southern Hawke's Bay

These are a region of intense faulting and folding containing shales, siltstones and minor sandstones of Cretaceous to Pliocene age. Faults strike predominantly north-northeast and show both dextral transcurrent and vertical movement. Kingma (1962) has suggested that the synclinal folding exhibited by the Tertiary strata of the ranges largely results from transcurrent drag rather than compression.

On the continental shelf to the east of the coastal ranges, actively growing folds have been recognized from tilted wave-planed surfaces (Lewis, 1971).

b) The Ruataniwha-Hawke Bay Depression

This contains mainly marine silty mudstones of Pliocene and Pleistocene age with interbedded coquina limestones in the Pleistocene and Upper Pliocene. Seismic reflection results (Leslie & Hollingsworth, 1972) indicate the depression is asymmetrical, with its deepest part lying adjacent to the Ruahine Range in the west. Numerous parallel faults trending approximately northeast traverse the area, particularly at pre-Pleistocene levels. Many of these appear to be northwest-dipping thrust faults; others appear to be wrench faults showing dextral movement (ibid.).

c) The Ruahine Range

The rugged Ruahine Range, with peaks over 1700 m, consists pre-dominantly of well dissected Mesozoic greywacke/argillite, intersected and bordered by numerous faults showing both dextral transcurrent and vertical movement. Its structure appears to be

that of a horst (Kingma, 1957). Uplift of the range is thought to
have begun in the late Tertiary (Kingma, 1962).

d)   The Wanganui Basin

In the Wanganui Basin, progressively younger strata are exposed from
north to south, from Lower Oligocene beds resting on exposed
Mesozoic basement in the north and northeast, to the thick
Pleistocene-Recent sequence near Wanganui in the south (Hay, 1967;
Kingma, 1962; Lensen, 1959). Extensive oil prospecting in the
basin, involving surface mapping, gravity surveys, seismic reflection
and refraction surveys and drilling, has indicated that block
faulting of basement is the dominant element of subsurface structure
(Cope, 1966). The most important faults are the Taranaki, Strathmore,
Ohura-Te Ahi, Nukumaru-Hauhangaroa and Turakina Faults (see fig. 2.7).
Major faults in the western part of the basin have a northerly to
north-northeasterly strike and were active in pre-Upper Miocene time,
whereas those in the eastern part have a northeasterly strike and
were active in the interval from Middle Miocene to Recent (ibid.).
Northeasterly striking faults in the extreme southeastern part of
the basin are known to have undergone dextral transcurrent movement
in Recent time (Kingma, 1962). Normal faults are also known in
the basin (for example the Ohura Fault (Hay, 1967)).

e)   The Tongariro volcanic centre

The Tongariro volcanic centre (Cole, 1978) lies at the southwestern
end of the Taupo Volcanic Zone (fig. 2.2), and contains the presently
active Mt. Ruapehu and Mt. Ngauruhoe volcanoes. Mt. Ruapehu is
a composite andesitic stratovolcano which has been in existence
since early Quaternary times (Fleming & Steiner, 1951), while the
smaller Mt. Ngauruhoe is thought to have begun eruption about
2500 years ago (Topping, 1974).

f)   The Taranaki Basin

Seismic surveys and deep drilling have revealed that the subsurface
Taranaki Fault is a major structural line, separating a 6 km deep
Cenozoic basin to the west (the Taranaki Basin) from the much
shallower Wanganui Basin to the east (Cope, 1965). The surface
geology of the Taranaki Basin is dominated by the Egmont chain of

andesitic volcanoes (Kaitake, Pouakai and Egmont) and their
associated ring plains of laharic agglomerate. Volcanic activity
commenced at Kaitake in the early Quaternary and has moved progressively
south-southeastwards (Hay, 1967). Mt. Egmont has been recently active,
its most recent identified ash eruption being dated at 1755 A.D.
(Druce, 1966).

CHAPTER 3

INSTRUMENTATION AND FIELD WORK

3.1 INSTRUMENTATION

Three types of portable microearthquake recorder were used in this study. Victoria University of Wellington provided five Sprengnether smoked-paper microearthquake recorders and two slow-motion magnetic tape seismographs, while the Geophysics Division of the DSIR supplied five Kinemetrics smoked-paper microearthquake recorders.

Four of the Sprengnether recorders were identical models (MEQ-600) which record unattended for 26 hours at a drum speed of 60 mm/minute. These recorders have a nominal peak displacement magnification (at 23 Hz) of 5.2×10^7. In the field, the recorders were usually operated 36 dB below full gain, resulting in a displacement magnification of about 8×10^5. The remaining Sprengnether recorder (model MEQ-800) is capable of 50 hours unattended operation at a drum speed of 60 mm/minute. Average displacement magnifications achieved in the field with this recorder were also about 8×10^5, peaking at 14 Hz. All Sprengnether recorders incorporate a quartz clock which provides a timing accuracy within 0.1 sec when used in conjunction with radio time-signals. During the Dannevirke survey (the first microearthquake survey of this study), radio time-signals were recorded daily on the MEQ-600 recorders. However, in order to achieve more efficient operation of the microearthquake array these recorders were modified for the Ruapehu survey (the second survey of the study) so that they automatically recorded time-signals broadcast on the hour by the New Zealand Time Service. In both surveys radio time-signals were recorded on the MEQ-800 recorder every two days; the drift of the quartz clock of this recorder (0.04 sec/week) was such that timing accuracy was still well within 0.1 sec.

Two model PS-1 and three model PS-1A Kinemetrics micro-earthquake recorders were used in the study. Both models have similar magnifications and filter settings. In the field filter setting 4 (20 Hz peak) was usually used, but in times of high wind noise it was found beneficial to use filter setting 2 (5 Hz peak). Displacement

magnifications achieved in the field averaged 7.5×10^5. Daily
calibration of the internal clocks of the recorders revealed that
four of the clock drifts were <0.03 sec/day while the fifth clock
drifted 0.12 sec/day.

All Sprengnether and Kinemetrics recorders were operated with
identical 1 Hz vertical seismometers (Mark Products model L4). Except
for a few occasions when MEQ-600 recorders were run at a drum speed of
30 mm/minute (2-day recording), all recorders were run at a drum speed
of 60 mm/minute. This speed is necessary if microearthquake first
motions are to be clearly read from the records. Filter settings adopted
in the study ensured all recorders gave good amplification in the
10-20 Hz range, into which the predominant microearthquake frequencies
are observed to fall (Oliver et al., 1966).

The two portable slow-motion magnetic tape recorders used in
the study are similar and have been described in detail by Dibble
(1964). Each recorder was used with a Willmore Mark 1 vertical
seismometer (T = 1 sec). The four-channel recording head of the
instruments enables the following to be recorded simultaneously:

1)   High-gain signal from the seismometer
2)   Low-gain signal from the seismometer
3)   Internal time-marks generated by a crystal oscillator
4)   Radio time-signals broadcast by the New Zealand Time Service

A tape speed of 0.4 mm/sec produces a recording frequency range
of 0.1-20 Hz when playback heads similar to the recording heads are
used. At this speed a 550 m magnetic tape lasts 16 days. These
recorders were installed at the most inaccessible sites of the Ruapehu
survey because of this advantage of a long period of unattended
recording.

The magnetic tapes were played back on a four-channel tape
recorder with heads similar to the slow-motion recorders. The output
from this tape recorder was filtered at 1-20 Hz and displayed on a dual-
beam digital storage oscilloscope. Microearthquake arrivals and time
corrections were then read directly off the oscilloscope. The overall
timing accuracy of the recording and playback system is better than
0.1 sec.

Typical low-noise records produced by the various micro-
earthquake recorders are shown in figs. 3.1 and 3.2.

Stations CNZ, MNG and TNZ of the national network of permanent
seismographs (New Zealand Seismological Observatory, 1978a) provided
valuable information on larger microearthquakes recorded during the
Ruapehu survey. Because of its proximity to the microearthquake array
and its high magnification (44,980 at 0.3 sec), coupled with an absence
of volcanic tremor from nearby active volcanoes during the Ruapehu
survey, CNZ clearly recorded almost all microearthquakes selected for
analysis on the basis of arrivals at the microearthquake recorders.
TNZ, although a low magnification station, provided useful information
on larger Taranaki microearthquakes, while MNG provided important
control on the numerous earthquakes occurring at sea immediately south
of the city of Wanganui.

For the study of microearthquake first motions, it is essential
that the polarity of all seismographs with respect to ground motion
is known. Laboratory tests on the Sprengnether and Kinemetrics recorders
have established that they are all of normal polarity (i.e. upward
trace movement for upward ground motion). As the polarity of the tape
seismographs used in the Ruapehu survey can vary according to the mode
of connection of the seismometer to the tape recorder, the polarities of
all seismographs of the Ruapehu array, including permanent stations
CNZ, MNG and TNZ, were tested in situ by reading first motions of earth-
quakes well outside the array. The use of these earthquakes ensures
arrivals at the array cover a small area on the focal sphere; they
often lie in the same quadrant of an earthquake's radiation pattern.
Analysis of the first motions of twelve such earthquakes revealed all
seismographs to be of normal polarity except for the two tape
seismographs and the permanent station CNZ, which were of reversed
polarity. Corroborating evidence on the polarity of CNZ comes from
an explosion detonated in the Crater Lake of Mount Ruapehu during
Easter, 1974. This produced a downward trace motion on the CNZ
seismograph, indicating reversed polarity.
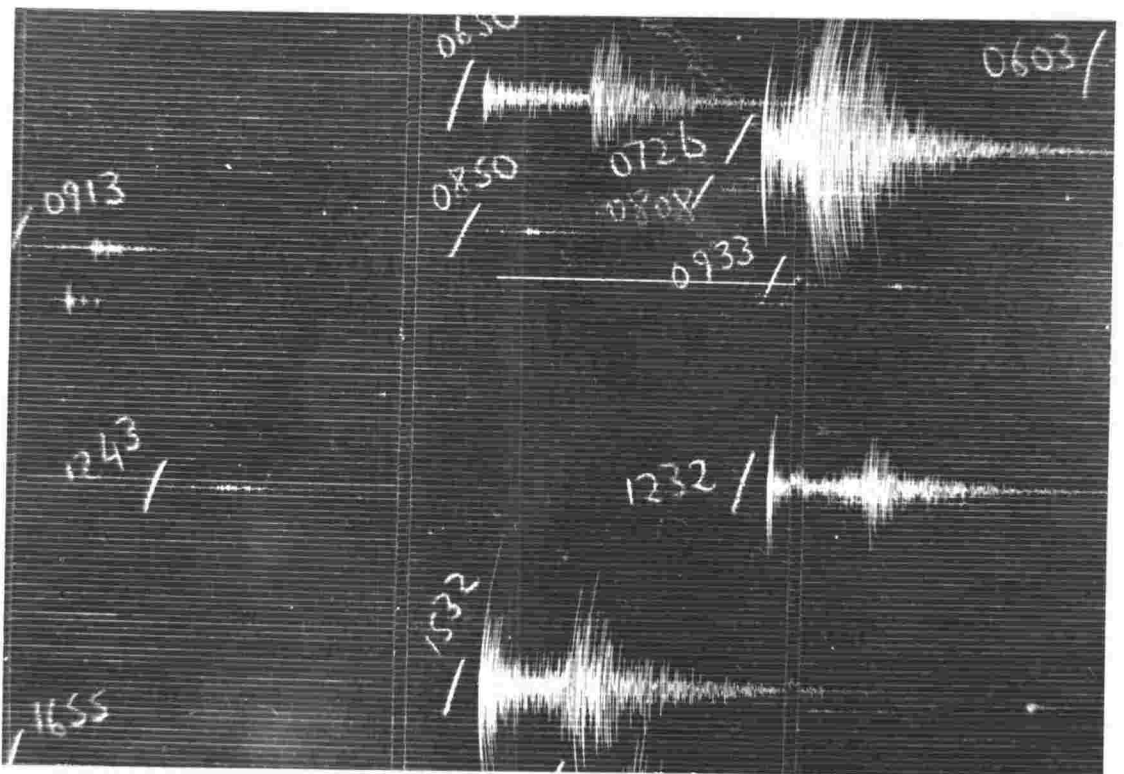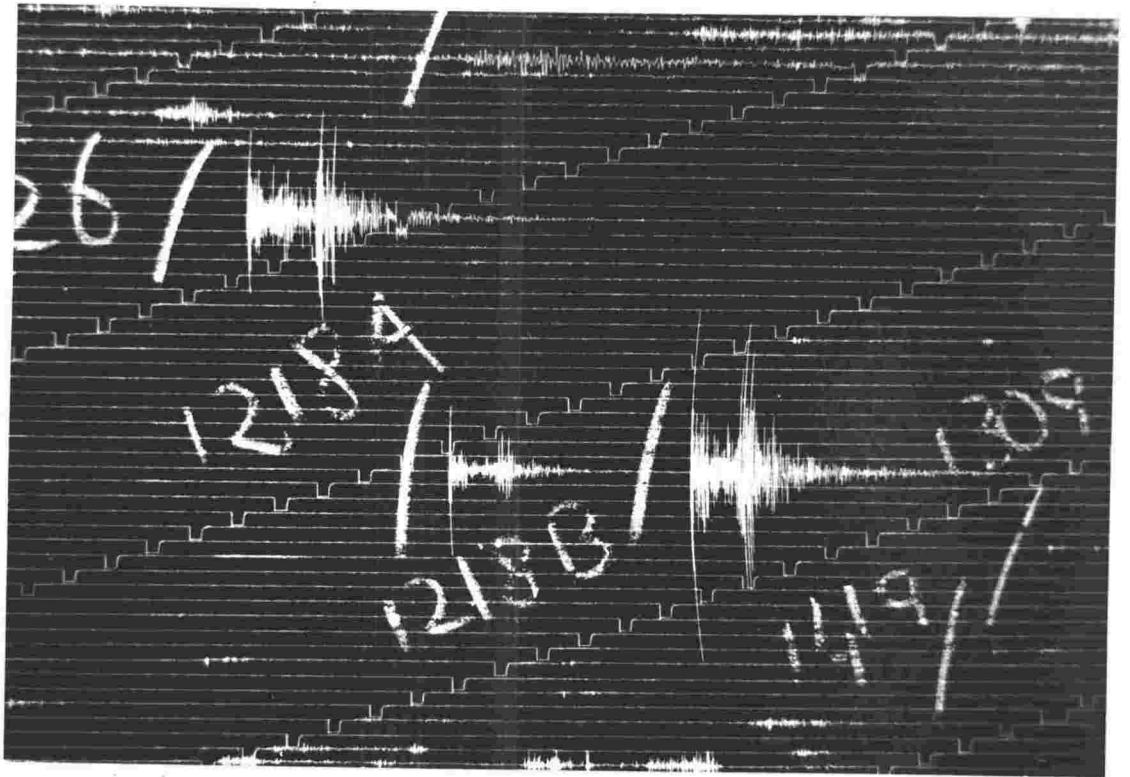
Figure 3.1 Typical low-noise records produced by a
Sprengnether MEQ-600 (top) and a Kinemetrics PS-1A micro-
earthquake recorder (bottom). On both records, time marks
are one minute apart, and microearthquakes have been
annotated.
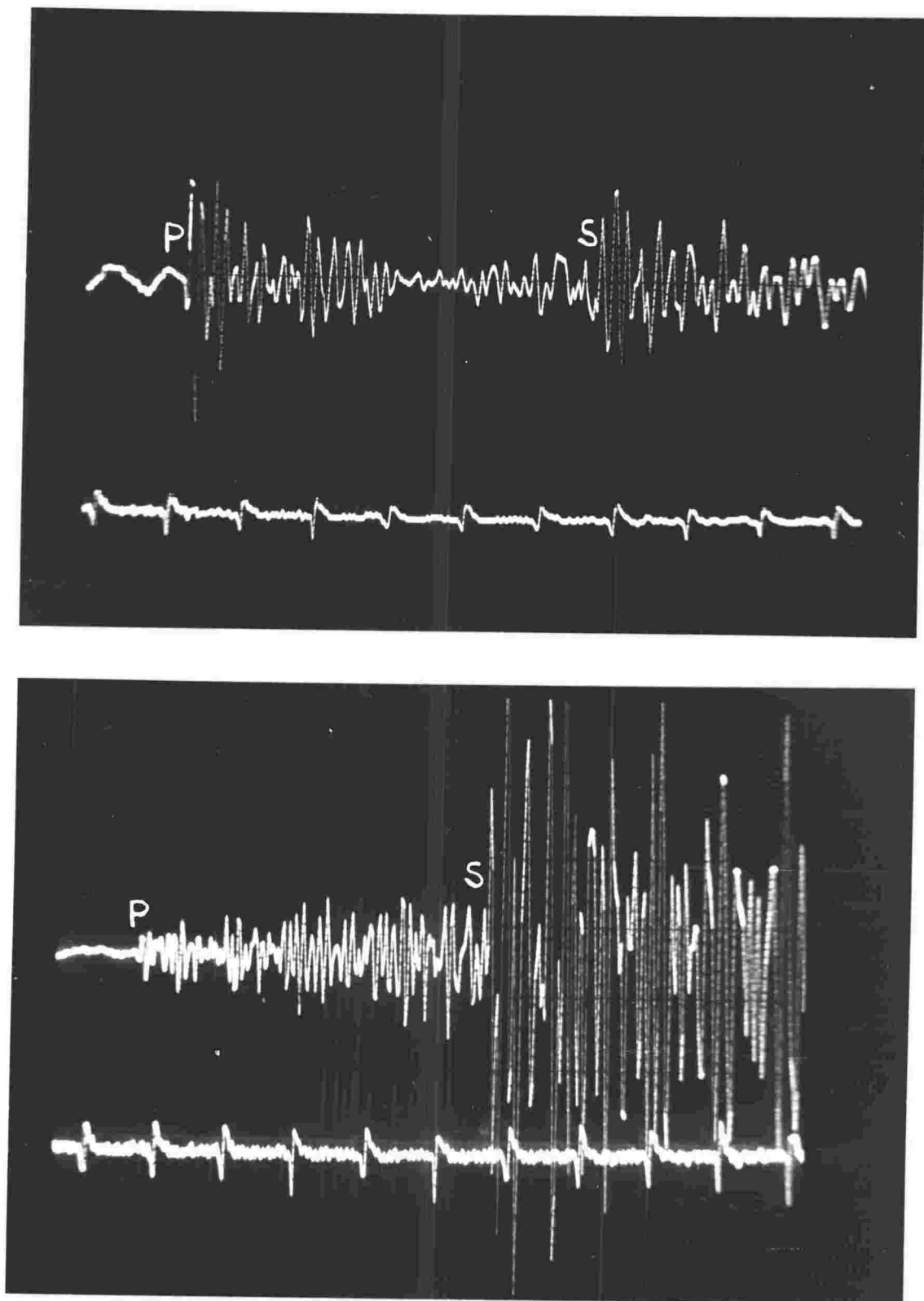
Figure 3.2   Two examples of microearthquakes recorded by a slow-motion tape recorder.   In both pictures, the top trace is the high-gain signal from the seismometer, while the bottom trace shows second pulses generated by an internal crystal oscillator.

3.2 FIELD WORK

In a microearthquake survey, ideally one would place the microearthquake recorders in an array of aperture comparable with the expected average depth of microearthquake activity. However, the distribution of recorders in the field depends on the following factors:

1) Ease of access. The records of the Sprengnether and Kinemetrics recorders and the 12-volt lead-acid battery power source of the Sprengnethers require daily replacement.

2) Outcrops of bedrock. The recorders must be placed on competent rock to ensure a minimum of noise during the high-gain recording necessary to detect microearthquakes.

3) Distance from major noise sources. The extreme sensitivity of the recorders necessitates placing them at least one kilometre from vehicular traffic. Since wind in trees causes ground roll (which has a predominant frequency of about 20 Hz, i.e. near the frequency of peak response of the recorders), seismometers must be kept away from trees as much as possible. Wandering stock must also not be in the vicinity of a seismometer as, apart from causing noise, they revel in chewing seismometer cables.

4) The logistics of servicing the recorders with the personnel and vehicles available.

3.2.1 The Dannevirke survey

This survey was carried out between February 6th and March 3rd 1974, with a maximum of five Sprengnether recorders operating at any one time. Details of the microearthquake stations occupied are shown in tables 3.1 and 3.3, and the station positions are mapped in fig. 2.7.

Almost all earthquakes located by the New Zealand Seismological Observatory in the Dannevirke region during the ten year period prior to this survey had been interpreted as crustal and restricted to depths of either 12 or 33 km (N.Z. Seis. Obs. Bulletins E-145 to E-154). In order to obtain good control on this crustal activity, the microearthquake recorders were placed in an array with a diameter of approximately 25 km. For the first half of the survey, such a five-station array (TAI, WIN, HIQ, OLD and TEU) was operated, the eastern-most stations of the array being as close to the coast as possible. By leapfrogging the three

Table 3.1   Details of the microearthquake stations of the Dannevirke survey.

Station	Code	Latitude S	Longitude E	Elevation (m ASL)	Lithology		
Taikura	TAI	40°13.50'	176°42.45'	105	Upper	Cretaceous	Siltstone
Windy	WIN	40 24.12	176 37.21	135	Miocene		Siltstone
Hiranui Quarry	HIQ	40 07.60	176 34.56	245	Upper	Cretaceous	Siltstone
Te Uri Stream	TEU	40 17.55	176 26.78	170	"	"	"
Old Hill	OLD	40 16.57	176 36.38	260	"	"	Argillite
Ore Ore	ORE	40 03.55	176 22.53	395	Lower	"	Sandstone
Brays	BRA	40 10.56	176 23.91	215	Upper	"	Siltstone
Clear Hills	CLH	40 11.80	176 15.55	410	Lower	"	Sandstone

eastern-most stations of the first array to the north-west, another five-station array of approximately 25 km diameter (HIQ, TEU, BRA, ORE and CLH) was operated for the second half of the survey.

Because of an abundance of farm tracks and good outcrops of bedrock in the region of the survey, good sites for microearthquake recording away from vehicular traffic could be found. Magnifications achieved averaged 8×10^5. However the region is heavily stocked, and it was difficult to find sites which were not affected by stock noise. As weather was favourable for most of the survey, wind noise was no great problem until the last week, when two gales played havoc with the recording of microearthquakes and upended two tents housing micro-earthquake recorders. Owing to the nature and distribution of roads in the area, it was found difficult to service the array with the single vehicle available. Thus when it became apparent during the survey that a large amount of subcrustal activity was being recorded, it was not feasible to increase the diameter of the array to get a better fix on this activity.

3.2.2 The Ruapehu survey

This survey, which lasted from September 30th to October 30th 1974, was a co-operative effort involving Victoria University of Wellington (VUW) and the Seismological Observatory of the DSIR. VUW provided five Sprengnether recorders, two tape seismographs, two vehicles and two personnel, while the Seismological Observatory supplied five Kinemetrics recorders together with a vehicle and a technician. As a result of this co-operation an extensive microearthquake array stretching from Taihape in the southeast to Whangamomona in the northwest was established, with a maximum of eleven recorders operating at any one time. Details of the microearthquake stations (and permanent stations used to supplement their results) are shown in tables 3.2 and 3.3, and station positions are mapped in fig. 2.7.

As well as crustal earthquakes, subcrustal earthquakes associated with the North Island Benioff zone occur in the region of the Ruapehu survey, and the microearthquake array was designed to be effective in locating both types of activity. The array was approximately 100 km long and elongated in a SE-NW direction, the dip direction of the underlying Benioff zone. Its width averaged 25 km. Such a configuration

Table 3.2 Stations of the Ruapehu survey

Station	Code	Latitude S	Longitude E	Elevation (m ASL)	Instrument*	Lithology
Whangamomona	WGM	39°10.63'	174°44.76'	135	TS	Miocene Sandstone
Wades Landing	WAD	39 07.29	175 03.62	135	TS	"
Erua	ERU	39 14.44	175 17.43	685	K PS-1	"
Huikumu	HUI	39 27.03	175 07.76	505	K PS-1A	Pliocene "
Ohakune A	OKA	39 23.31	175 25.90	715	K PS-1	"
Ohakune B	OKB	39 23.17	175 25.97	730	K PS-1	"
Matahiwi	MAT	39 33.66	175 14.42	305	K PS-1A	Mudstone
Whangaehu A	WUA	39 32.14	175 27.24	595	S MEQ-600	"
Whangaehu B	WUB	39 32.11	175 27.23	580	K PS-1A	"
Waione	WAI	39 29.65	175 36.51	715	S MEQ-600	Sandstone
Tangiwai	TNG	39 31.42	175 36.47	730	S MEQ-600	"
Siberia	SIB	39 41.96	175 31.26	305	S MEQ-800	Mudstone
Wharenui	WHA	39 40.86	175 33.26	410	S MEQ-800	"
Te Moehau	TMO	39 35.66	175 49.61	600	S MEQ-600	Sandstone
Zoh's Road	ZOH	39 47.39	175 43.84	425	S MEQ-600	Mudstone
Hunka	HUN	39 45.78	175 43.78	440	S MEQ-600	"
Chateau	CNZ	39 12.00	175 32.85	1116	Willmore I	Volcanic ash and lava
Tarata	TNZ	39 11.23	174 22.82	123	Willmore II	Pleistocene Mudstone
Mangahao	MNG	40 37.12	175 28.92	396	Willmore II	Jurassic Greywacke

(* TS = Tape Seismograph; K = Kinemetrics Recorder; S = Sprengnether Recorder)

Station	Date (Universal Time)	
	Installed	Removed
	d h	d h

DANNEVIRKE SURVEY 1974

Station	Installed	Removed
TAI	Feb 06 23	Feb 18 23
WIN	Feb 07 07	Feb 14 06
HIQ	Feb 08 04	Mar 02 21
TEU	Feb 10 06	Mar 03 07
OLD	Feb 12 02	Feb 20 00
ORE	Feb 15 07	Mar 02 14
BRA	Feb 21 04	Mar 02 15
CLH	Feb 22 06	Mar 03 06

RUAPEHU SURVEY 1974

Station	Installed	Removed
WGM	Oct 01 02	Oct 28 04
WAD	Oct 01 23	Oct 29 23
ERU	Sep 30 22	Oct 29 22
HUI	Oct 02 03	Oct 30 03
OKA	Sep 30 04	Oct 18 03
OKB	Oct 18 03	Oct 27 20
MAT	Oct 01 22	Oct 30 05
WUA	Oct 01 05	Oct 09 21
WUB	Oct 09 23	Oct 30 01
WAI	Sep 30 06	Oct 02 22
TNG	Oct 03 03	Oct 28 23
SIB	Oct 02 05	Oct 13 05
WHA	Oct 15 06	Oct 28 04
TMO	Oct 03 02	Oct 29 02
ZOH	Oct 05 04	Oct 06 13
HUN	Oct 07 04	Oct 27 05
CNZ	Recording continuously	
TNZ	Recording continuously	
MNG	Recording continuously	

Table 3.3 Recording periods of microearthquake stations

of microearthquake recorders enables accurate location of earthquakes
in the direction of dip of the Benioff zone down to at least 150 km
depth. Location accuracy along the strike of the Benioff zone is
naturally poorer, but this was not considered crucial, since structure
along the strike of the Benioff zone can be expected to be more uniform
than that in the direction of dip. The 20-25 km station spacing proved
very effective in locating crustal microearthquakes, the bulk of which
were found to lie in the lower half of the crust. However, the
stations were too far apart to provide good depth control on low
magnitude,very shallow microearthquakes associated with Mt. Ruapehu.

All stations were located on Pliocene-Miocene sandstones and
mudstones, locally known as 'papa'. This papa proved surprisingly
good for microearthquake recording, especially when a massive outcrop
well removed from trees was selected. Magnifications achieved averaged
8×10^5 during favourable weather, 4×10^5 during periods of high winds.
The major difficulty of the survey was the uniformly bad weather. High
winds, rain and even snow were encountered. High winds caused a large
tree to fall onto one of the microearthquake recorders; fortunately it
sustained only superficial damage. Persistent rain made off-road access
to the microearthquake stations difficult, and vehicles became bogged
on numerous occasions.

Notwithstanding the weather, the array operated successfully
for the duration of the survey, an abundance of microearthquakes
compensating for the poor recording conditions. The shape of the array
was not changed significantly during the survey. Poor recording
conditions at some sites required only minor changes in station location.

CHAPTER 4

MICROEARTHQUAKE ANALYSIS

4.1 MICROEARTHQUAKE IDENTIFICATION AND LOCATION CRITERIA

Initially, all microearthquake records were scanned and the
approximate arrival times of all possible microearthquakes noted.
Microearthquakes can be recognized by their sharp P-wave onset,
distinctive S-wave train and gradually decaying coda (see figs. 3.1
and 3.2).

In both the Dannevirke and Ruapehu surveys a large number of
microearthquakes with a wide range of S-wave arrival time minus P-wave
arrival time (S-P) were recorded, and microearthquakes for which hypo-
centres were determined were restricted to those which were both well
recorded and close to the array. In the analysis of Dannevirke survey
data, only those microearthquakes which had an S-P time at the nearest
station of 10.0 sec or less and produced at least four readable phases
at a minimum of three stations were considered for hypocentre determination.
The S-P time restriction delimits a volume inside which microearthquakes
can be reasonably located by the 25 km-diameter array, while the phase
restriction represents the smallest number of readings needed to
determine the location and origin time of a hypocentre. Of the
625 microearthquakes recorded during the Dannevirke survey, 267
satisfied the above location criteria.

For Ruapehu survey microearthquakes, a location criterion of
S-P <17.5 sec at stations ERU or HUI was imposed. This restriction
delimits a volume within which the resolving power of the 25 km × 100 km
array is good. A microearthquake 150 km deep and 75 km outside the array
lies near the boundary of this volume. Earthquakes deeper than 150 km are
better studied using the permanent seismograph network of the Seismological
Observatory. The phase restriction used for Ruapehu survey data was based
on the records of the Sprengnether and Kinemetrics instruments. Initially,
only those microearthquakes which were well recorded at nine of these
instruments were located. This restriction was then progressively
relaxed until sufficient microearthquakes to define the seismicity of
the area had been located. Ten or more phases were used for all but

four hypocentre determinations. The above procedure results in the location of only the larger magnitude activity, and for this reason significant low-magnitude activity close to Mt. Ruapehu has not been located. Hypocentres were determined for 133 of the 805 microearthquakes recorded during the Ruapehu survey.

4.2 HYPOCENTRE DETERMINATION

The data read from seismograms of microearthquakes selected for location consist of:

Direction of P-wave first motion.

P-wave arrival time.

S-wave arrival time.

The arrival time of prominent phases other than P and S.

Microearthquake duration, i.e. the time when the microearthquake coda becomes indistinguishable from the background noise minus the P-wave arrival time.

The nodal character of the microearthquake record.

A 10x magnifier was used for all readings, and a 60 mm graticule was used to divide minute lengths (which varied by up to 1%) into sixty equal seconds. Although the best overall accuracy that can be achieved with the recorders is ±0.1 sec, P and S arrivals were read to the nearest 0.01 sec to minimise the effect of subsequent roundoff error. Micro-earthquake duration times were read to the nearest second.

The reading of seismograms was the most time-consuming part of this study.

4.2.1 The HYPO71 computer program

Hypocentres, magnitudes and first motion patterns of microearthquakes were determined using the HYPO71 program on the Burroughs 6700 computer of Victoria University of Wellington. This program employs an iterative least-squares method of hypocentre determination and has been described in detail by Lee & Lahr (1975). The program incorporates the following advantageous features:

a) Both P and S readings can be weighted according to quality. Well-determined P readings were given full weight. S onsets were

invariably difficult to determine as they occur during the P coda; they were rarely given more than one quarter weight.

b)   Azimuthal weighting of stations by quadrant can be applied in order to minimise the effect of stations being unevenly distributed about a hypocentre.

c)   Auxiliary values of the root mean square error of the time residuals, i.e. RMS, can be calculated at ten points on a sphere centred on the hypocentre. This feature indicates whether the solution is at the RMS minimum.

Care must be exercised in the use of HYPO71. If a trial hypocentre is not specified, HYPO71 uses the location of the nearest station as the trial hypocentre (with the addition of 0.1 minute to both latitude and longitude to avoid ARCTAN(0/0) in calculating the azimuth between epicentre and station). This procedure can result in a solution converging to a local minimum in the time residual surface near the array, rather than to the global minimum. The presence of relative minima in the time residual surface is a manifestation of the lack of variable independence inherent in a four-parameter least-squares hypocentre location method (James et al.,1969). Focal depth can be traded for origin time, even when an earthquake is recorded at many stations and azimuthal and range control is good. The inclusion of as many S readings as possible in a hypocentre location is crucial in combating this solution instability, since S readings serve to fix the origin time of an event. In the present study hypocentres based on P readings only were considered unreliable, even if their formal errors of location were acceptable.

HYPO71 also experiences difficulty in moving trial hypocentres across large velocity discontinuities (e.g. the Mohorovičić Discontinuity). This shortcoming is best remedied by experimenting with two trial hypo-centres, one above and the other below the discontinuity.

4.2.2   The P-wave velocity model adopted for the Dannevirke array

Little direct information is available on the velocity structure beneath the Dannevirke array, as no deep seismic sounding experiments have been carried out in the area. The velocity structure will be complicated by the subducted Pacific plate, and it is therefore necessary to obtain an estimate of the depth of this plate below the array.

To this end, all microearthquakes satisfying the location criteria of sect. 4.1 were first located using the standard New Zealand crustal model (Hamilton, 1966; table 4.1). A vertical cross section along the traverse of the resulting hypocentres is shown in fig. 4.1. Below the Ruapehu array subcrustal hypocentres define a thin, dipping band of activity. Below the Dannevirke array, the distribution of hypocentres is rather diffuse, though two groupings are apparent, one comprising shocks shallower than 35 km, the other comprising shocks 40-63 km deep. Microearthquakes of the group labelled A in fig. 4.1 have been located with their first arrivals interpreted as head waves refracted along the horizontal Mohorovičić discontinuity of the standard New Zealand crustal model. The northwesterly dip of the upper limit of activity below the Dannevirke array suggests structure in the region has a similar dip. Consequently, the microearthquakes of group A are likely to be shallower than shown in fig. 4.1. A shallower location for these microearthquakes would enhance the dipping trend evident in the shallower grouping of hypocentres below the Dannevirke array. The dipping trend suggests these hypocentres form a shallow extension of the band of subcrustal activity below the Ruapehu array.

Dipping bands of subcrustal earthquakes have been related to either the oceanic crust capping the subducted plate (Oliver & Isacks, 1967; Wyss, 1973), or some colder, more brittle region in the upper half of the subducted plate (Engdahl, 1973). The extension of such a band of activity to shallow depths below the Dannevirke array suggests that the question of where in the subducted plate this activity is occurring might be resolved by deep seismic sounding.

A dipping band of high microearthquake activity at shallow depth, similar to that present below the Dannevirke array, has recently been revealed by a telemetered microearthquake array in the Wellington region (Robinson, in press). Also, the Wellington crustal structure project (Eiby, 1957) has provided information on deep structure in this region. A reinterpretation of the refracted arrivals of this study has revealed an 8.04 km/sec refractor at a depth of 36 km below Wellington Province (Garrick, 1968). As this refractor lies near the lower boundary of the dipping band of high microearthquake activity, it appears plausible to associate it with the Mohorovičić discontinuity of the oceanic crust

THE STANDARD NEW ZEALAND CRUSTAL MODEL

(after Hamilton, 1966)

P-wave velocity of layer (km/sec)	Depth to top of layer (km)
5.50	0.0
6.50	12.0
8.10	33.0

A Poisson's ratio of 0.25 was adopted for all layers.

THE VELOCITY MODEL ADOPTED FOR THE DANNEVIRKE ARRAY

P-wave velocity of layer (km/sec)	Depth to top of layer (km)
4.40	0.00
5.43	1.00
6.21	4.56
6.46	12.93
8.04	30.00
8.50	35.00

A Poisson's ratio of 0.25 was adopted for all layers

(see section 4.2.6).

Table 4.1
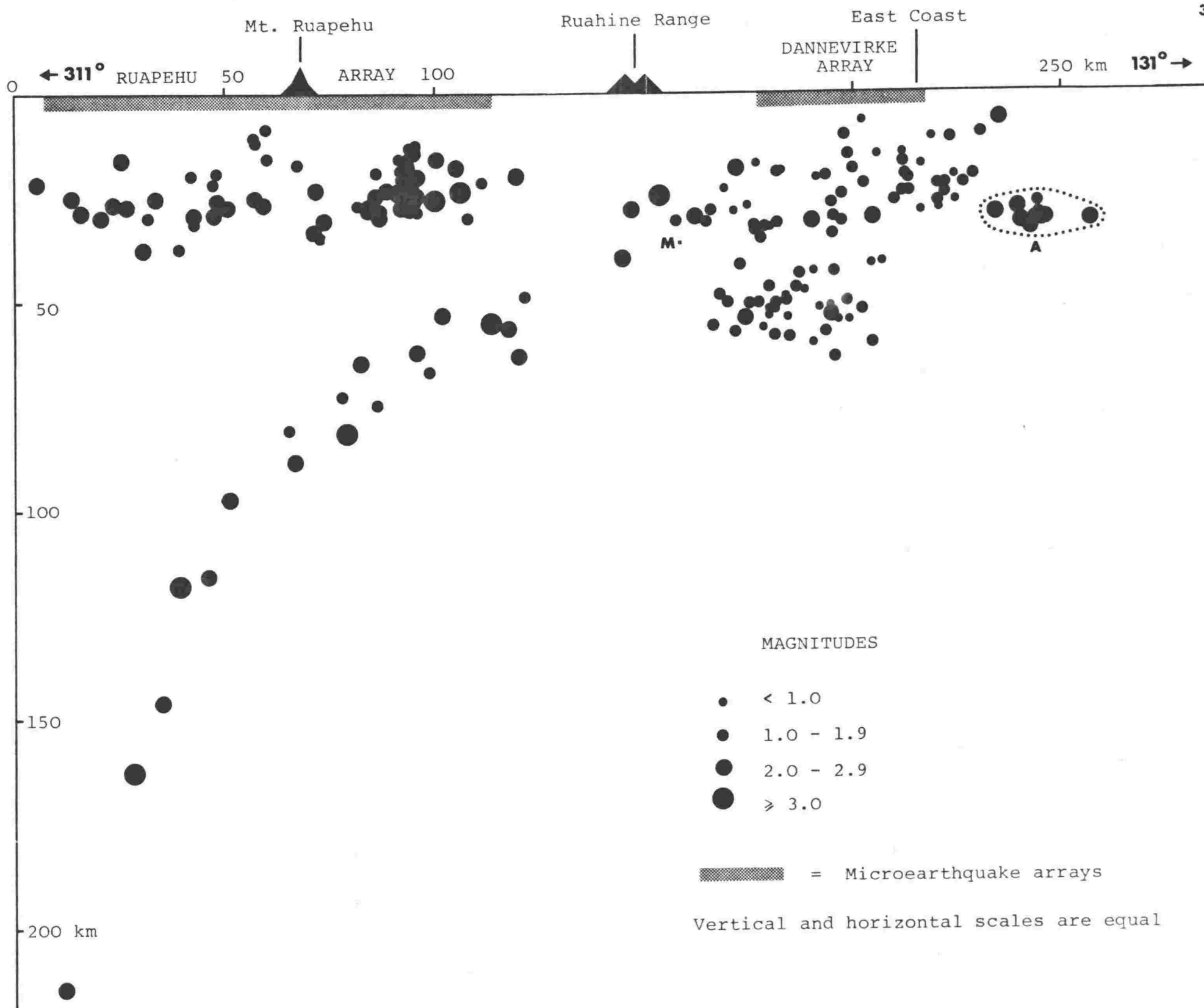
Figure 4.1 Vertical cross section along the traverse showing microearthquakes located using the standard New Zealand crustal model. Only those hypocentres with epicentral and depth standard errors of less than 5 km are plotted. An explanation of labels 'A' and 'M' is given in sect. 4.2.2.

of the subducted Pacific plate. The band of high microearthquake activity is thus associated with the oceanic crust of the subducted plate. Such an interpretation is supported by observations of strong P-wave reflections from quarry blasts in the Wellington region. These indicate the existence of a seismic interface near the top of the band of high microearthquake activity,which may be related to the top surface of the subducted Pacific plate (E.G.C. Smith, pers. comm., 1978).

These results from the Wellington region suggest that the shallower grouping of activity below the Dannevirke array is likely to be largely confined to the oceanic crust of the subducted Pacific plate. Projection of the 8.04 km/sec refractor underlying Wellington Province along the strike of the Benioff zone in the southern North Island (fig. 2.2) and onto the line of the microearthquake traverse places it at the point marked M in fig. 4.1. This point lies near the lower boundary of the shallower grouping of microearthquakes below the Dannevirke array, again suggesting that this refractor can be associated with the Mohorovičić discontinuity of the oceanic crust of the subducted Pacific plate. The dip of this shallower grouping of activity indicates this Mohorovičić discontinuity will be approximately 30 km deep below the centre of the Dannevirke array.

A 30 km crustal column in the centre of the Dannevirke array, comprising both continental and oceanic crust, appears consistent with gravity in the area. The Bouguer anomaly there is close to zero (Whiteford & Woodward, 1975) and can be interpreted as indicating a continental crustal thickness of 30-35 km. (A summary of formulae relating crustal thickness to Bouguer anomaly is given by Reilly (1962)). The gravity effect of the crustal column below the array is similar to that of a purely continental crust, since the average density of the oceanic crust, excluding sediments, is close to that of the continental crust (e.g. Worzel, 1974).

The above deduction of the location of the subducted Pacific plate below the Dannevirke array facilitates the specification of a P-wave velocity model for the array. The model adopted is listed in table 4.1 and explained below.

Layer 1 P-wave velocity (α) = 4.40 km/sec. Layer thickness (H) = 1.00 km.

It is very difficult to assign a near-surface P-wave velocity to the Dannevirke region because of the complicated geology (see sect. 2.3). The velocity and thickness chosen for this layer represent an attempt to model both an indeterminate thickness of Cretaceous sediments ($\alpha \simeq 4.0$ km/sec (Garrick, 1969)) and uppermost basement (the "unconsolidated greywackes" of Garrick (1968)).

Layer 2 α = 5.43 km/sec   H = 3.56 km

Layer 3 α = 6.21 km/sec   H = 8.37 km

Layer 4 α = 6.46 km/sec   H =17.07 km

These three layers have been interpreted from the Wellington crustal structure project by Garrick (1968).   Because of a small mistake in the calculations of Garrick, layer thicknesses given here are those recalculated by Dibble (pers. comm., 1977). Layer 4 incorporates the subducted oceanic crust. A standard model of the oceanic crust (Worzel, 1974) gives an average P-wave velocity for the crust (excluding sediments) of approximately 6.2 km/sec, close to the 6.46 km/sec of layer 4. Any subducted oceanic sediment present below the Dannevirke array will form a relatively thin layer of velocity reversal, and the effect of neglecting it in a velocity model will be small.

Layer 5 α = 8.04 km/sec   H = 5.00 km

This layer corresponds to the mantle of Garrick (1968) and is here identified with the uppermost mantle of the subducted plate. The velocity of this layer is very similar to the standard oceanic mantle velocity of 8.08 km/sec calculated on a world-wide basis by Worzel (1974).

Layer 6 α = 8.50 km/sec

In his determination of upper mantle velocities beneath New Zealand, Haines (1976) has found a high value of P-wave velocity (8.5 km/sec) and a similarly high value of S-wave velocity (4.75 km/sec) in the region of the Dannevirke array. A high P-wave velocity of 8.60 km/sec, at a depth of 5 km below the oceanic Mohorovičić discontinuity has also been determined from a deep seismic sounding experiment northeast of the Kurile Islands (an area of active subduction). This high-velocity layer has been considered definite enough to be included in a generalized seismic model of the typical oceanic crust of the Pacific (Kosminskaya & Kapustian, 1976).

Both these results suggest the inclusion of layer 6 in a velocity model for the Dannevirke array.

Station corrections were not used in the analysis of Dannevirke survey microearthquakes. The coastal ranges in the area of the array are geologically complex, with intense faulting and folding common (see sect. 2.3), and any downward extrapolation of surface geology, or correlation of isolated boreholes, is highly speculative. Moreover, except for ORE and CLH, stations of the array vary in elevation by only 150 m, and relative elevation corrections will be small (<0.05 sec). Stations ORE and CLH, though at a higher elevation than other stations of the array (see table 3.1), lie on inliers of Lower Cretaceous sandstone, which is older than the rock underlying other stations of the array. It is likely that higher seismic velocities in this older rock will at least partially compensate for the longer paths to these stations.

The P-wave velocity model for the Dannevirke array determined in this section includes certain simplifications. A major simplification is that of horizontal layering, which is required by the HYPO71 program. As discussed previously, structure below the array appears to be dipping towards the northwest, rather than horizontal. Consequently, micro-earthquakes occurring to the southeast and northwest of the array are likely to be mislocated, especially in depth. The assumption of lateral homogeneity in seismic velocity is also a simplification in a region of subduction (cf. Haines, 1976). However, the distribution of microearth-quakes located using the present velocity model should provide a structural picture from which more detailed velocity models can be constructed for use with more advanced location techniques, such as ray tracing.

4.2.3 Explanation of prominent phases other than P and S shown by Dannevirke survey microearthquakes

The often complicated nature of seismograms produced by Dannevirke survey microearthquakes reflects the complicated crustal structure of the region. Many seismograms display phases other than direct and critically-refracted P and S; examples of these are shown in figs. 4.2 and 4.3. An attempt was made to explain the more prominent of these anomalous phases
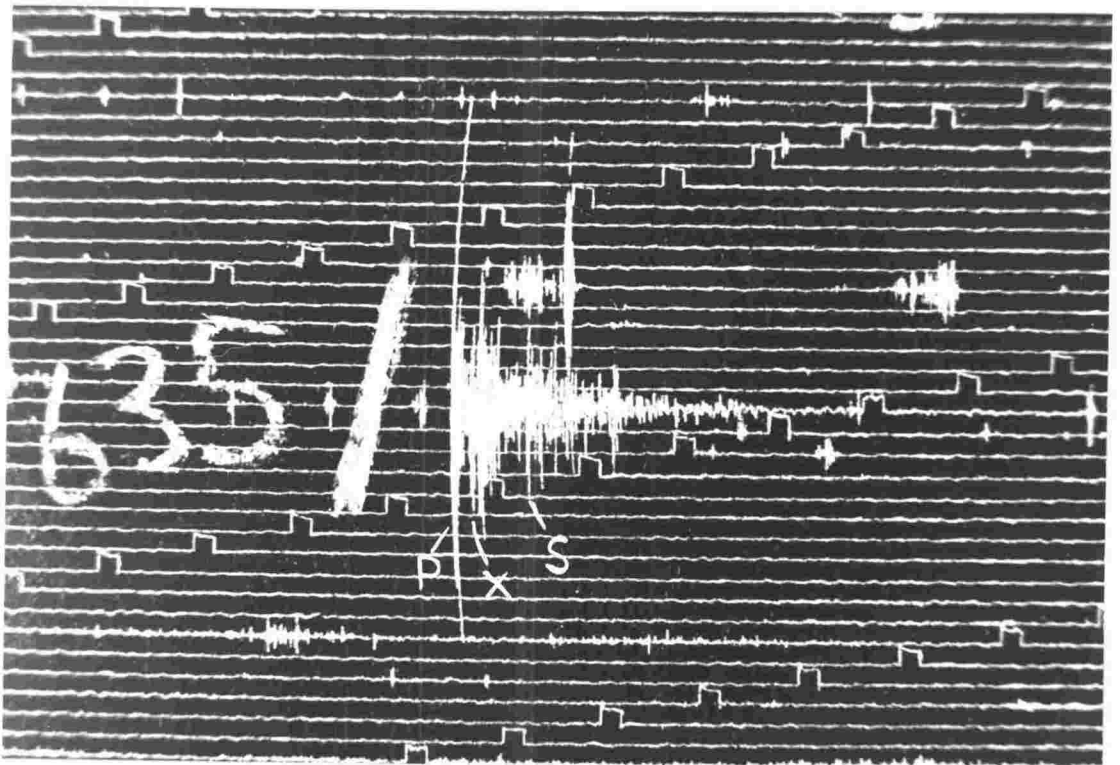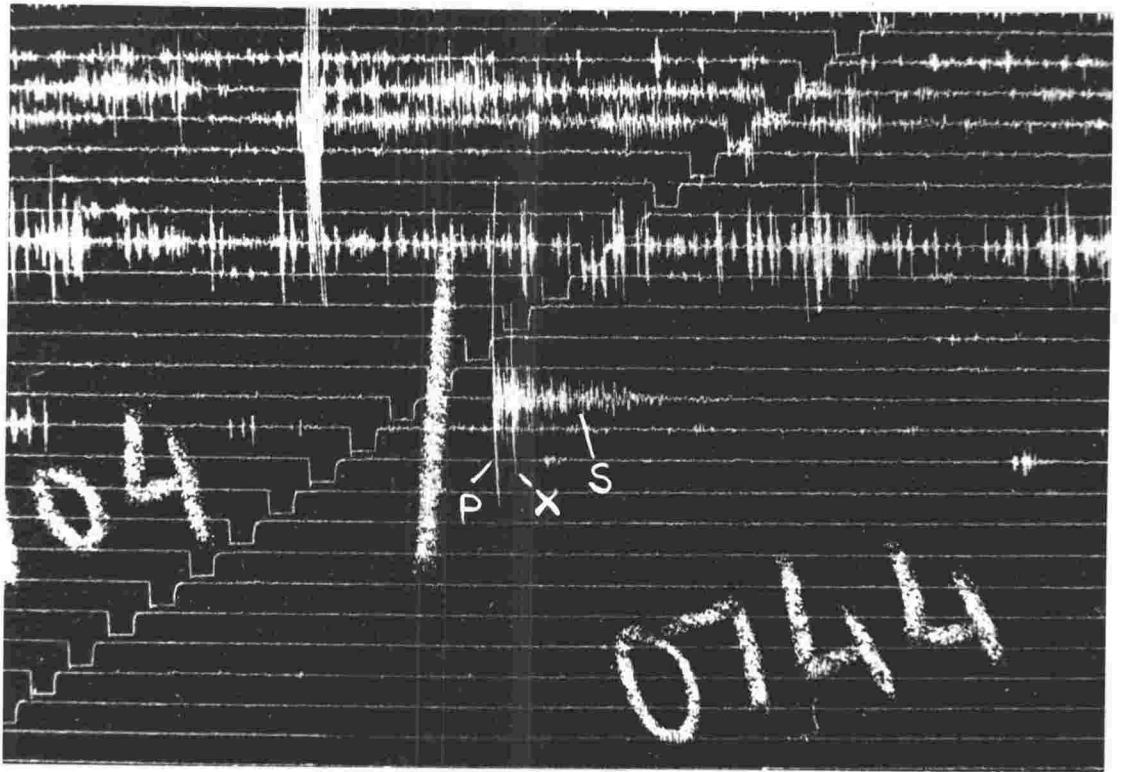
Figure 4.2   Seismograms of microearthquakes recorded during the
Dannevirke survey showing phases other than P-phases and S-phases.
The phases in these seismograms marked with an X were interpreted
as reflected P-phases.
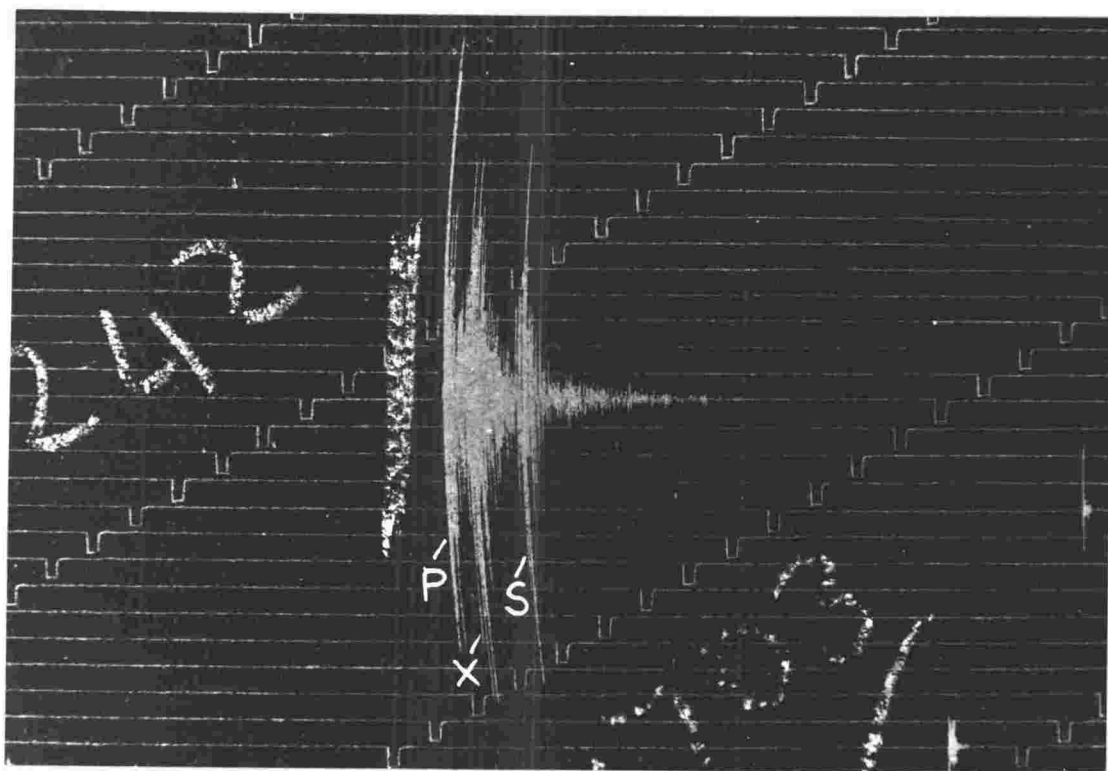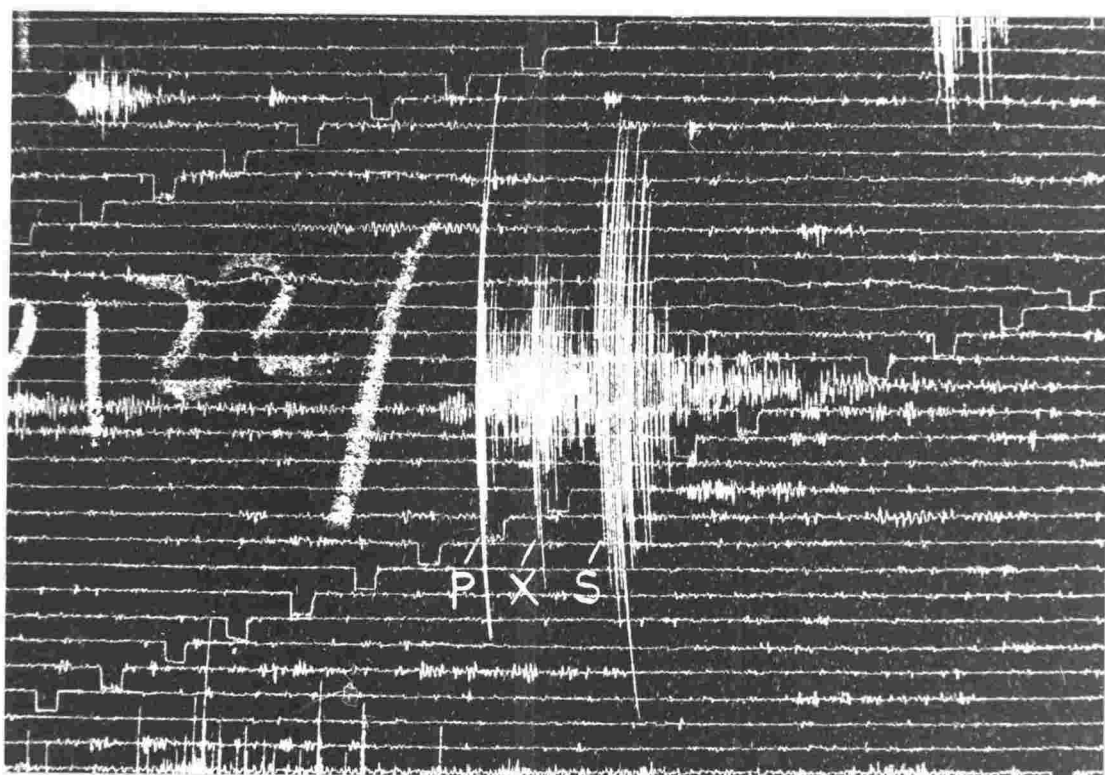
Figure 4.3   Seismograms of microearthquakes recorded during the Dannevirke survey showing phases other than P-phases and S-phases. The phases in these seismograms marked with an X were interpreted as S to P converted phases.

as reflections or conversions at suitable discontinuities within the crust and upper mantle, with a view to testing and possibly refining the velocity structure discussed in the previous section.

For microearthquakes shallower than 20 km, the interpretation of anomalous phases as reflections from a discontinuity below the hypocentre proved inconclusive. Determinations of the depth of such a reflector centred on 20 km, but control was poor, largely because there are few well-located microearthquakes shallower than 20 km in the Dannevirke region (see fig. 5.3). The most likely reflector present at this depth is the top of the subducted Pacific plate.

Interpretation of anomalous phases of microearthquakes in the 45-60 km depth range in terms of S to P conversion at an overlying discontinuity proved more successful. Only those microearthquakes which produced definite anomalous phases correlateable at three or more stations were studied. The method involved calculating model travel times for S to P (Sp) converted phases produced at suitable discontinuities in the velocity model determined in the previous section, and comparing these with observed travel times for the anomalous phases. As no three-component instruments were used in the Dannevirke survey, there is no direct way of testing the validity of the interpretation of the anomalous phases as Sp. However, for the six microearthquakes studied, the slowness of the anomalous phases across the array was consistent with the phase Sp, and the microearthquakes were so positioned that the angles of incidence of S-waves at suitable conversion interfaces lay in a range from which energetic Sp phases would be expected (Ewing et al., 1957).

Generally speaking, S to P conversion is best developed for the strongest and sharpest discontinuities in a given crustal column (e.g. Burdick & Langston, 1977). Interestingly, the anomalous phases of all six microearthquakes studied were incompatible with conversion at the interface identified with the Mohorovičić discontinuity of the subducted plate, even when the model depth of this was varied. One microearthquake indicated conversion at the 8.04/8.50 km/sec discontinuity, while all the others indicated conversion at an interface above the Mohorovičić discontinuity. The lack of conversions at the Mohorovičić discontinuity might be explained by recent results of Kosminskaya & Kapustian (1976), who have determined that this discontinuity is not as sharp as first thought, and that a layer of intermediate velocity

(7.55 km/sec) 1-2½ km thick separates the mantle and layer II of the oceanic crust. Similarly, synthetic modelling of a seismic profile in the Bering Sea has revealed a 2 km thick oceanic crust - mantle transition zone (Helmberger, 1977). The conversion apparent at the 8.04/8.50 km/sec interface suggests this may be a sharp discontinuity.

Conversions interpreted as occurring above the Mohorovičić discontinuity of the subducted plate were modelled as being produced at the interface between layers I and II of the subducted oceanic crust. Before subduction, the velocity contrast across this discontinuity is large (1.6 km/sec - e.g. Worzel, 1974), and it is likely that a sizeable contrast still exists under the Dannevirke array. The discontinuity can also be expected to be sharp (e.g. Helmberger, 1977). Another possible conversion interface is the boundary between layer I of the subducted oceanic crust and subducted sediment. However, this was not modelled because of uncertainty as to whether a significant amount of sediment is subducted, and if so, the level of induration of such sediment below the Dannevirke array. The aforementioned modelling indicated that the anomalous phases were consistent with layer II of the subducted oceanic crust having a thickness of approximately 5 km. This thickness is indistinguishable from a standard thickness for this layer of 4.8 km (Worzel, 1974). The Sp conversion interface determined by Smith (1970) to lie 24 ± 3 km below Wellington may similarly represent the interface between layers I and II of the oceanic crust of the subducted plate.

Thus information yielded by phases other than P and S broadly corroborates the velocity model adopted for the Dannevirke array. Although these phases emphasise the importance of the layer I/layer II interface in the subducted oceanic crust as a region of conversion, layers representing the subducted oceanic crust were not added to the velocity model as they are relatively thin and have an average velocity close to that of layer 4, which incorporates the subducted oceanic crust.

4.2.4 The P-wave velocity model adopted for the Ruapehu array

Since a large number of microearthquake stations were used in the Ruapehu survey, it might have been possible to determine simultaneously both hypocentre and velocity model parameters using a properly formulated

least-squares estimation procedure (Crosson, 1976). However, such an approach was not adopted, since the assumptions of lateral homogeneity and horizontal layering required by the method appear invalid for the region underlying the Ruapehu array (e.g. Adams & Ware, 1977; Haines, 1976). In the absence of any deep seismic sounding results, the standard New Zealand crustal model (table 4.1) was used as a basis for structure below the array. Extensive prospecting for oil, involving gravity surveys, seismic reflection and refraction surveys and drilling, has resulted in a detailed determination of basement structure in the region of the array (e.g. Cope, 1966). This has permitted the addition of a low-velocity surface layer to the velocity model and the calculation of relative station corrections.

The adopted velocity model and station corrections are shown in table 4.2. The low velocity layer chosen is based on seismic refraction carried out by Watson & Allen (1964) near Raetihi, which is close to the centre of the Ruapehu array. Here sediments with an average P-wave velocity of 3.4 km/sec overlie 5.3-5.5 km/sec basement interpreted as lying approximately 1.7 km below mean sea level. The datum of the velocity model for the Ruapehu array was taken as mean sea level, and elevation corrections were incorporated in the station corrections. The near-surface crustal structure under each station was determined from nearby geophysical data, and station corrections relative to the adopted velocity model were calculated assuming vertical paths for seismic waves. The assumption of vertical paths is justifiable since the majority of microearthquakes recorded during the Ruapehu survey were lower crustal or subcrustal (see fig. 4.1).

In the determination of station corrections, extensive use was made of a time-depth curve for the Raetihi area obtained by Watson & Allen (1964) through reflection shooting. Near-surface Tertiary sediments were modelled as having a velocity of 2.3 km/sec (cf. Ingham , 1971; Watson & Allen, 1964). Basement depths below stations were interpolated from the tentative basement contour map of Cope (1966). The large station correction of CNZ (+0.35 sec) reflects the 1116 m elevation of this station; this is the least reliable of all the station corrections since structure below the station will be complicated by lava flows, which have not been modelled. The very large station correction of TNZ (+0.55 sec)

THE VELOCITY MODEL ADOPTED FOR THE RUAPEHU ARRAY

P-wave velocity of layer (km/sec)	Depth to top of layer (km)
3.40	0.0
5.50	1.7
6.50	12.0
7.60	33.0

Different values of the ratio of P-wave velocity to S-wave velocity were adopted for crustal and subcrustal microearthquakes, as described in sect. 4.2.6.

STATION CORRECTIONS ADOPTED FOR THE RUAPEHU ARRAY

STATION	DELAY (sec)	STATION	DELAY (sec)
WGM	0.02	TNG	0.18
WAD	0.01	SIB	0.05
ERU	0.20	WHA	0.09
HUI	0.14	TMO	0.00
OKA	0.24	ZOH	0.06
OKB	0.24	HUN	0.06
MAT	0.06	CNZ	0.35
WUA	0.19	TNZ	0.55
WUB	0.18	MNG	-0.08
WAI	0.16		

Table 4.2

is well determined from seismic surveys (Kaan, 1960); it reflects the great depth to basement (c. 6.25 km) under the station.

The determination of the velocity structure of the upper mantle below the Ruapehu array is problematical, as the subducting Pacific plate is likely to produce both vertical and lateral variations in mantle properties. A detailed study of velocities at the top of the upper mantle in New Zealand has been made by Haines (1976). He has approximated the distribution of velocities using a simple model consisting of regions within which the velocities were assumed to be constant. His regions of assumed constant velocity in the area of this study are shown in fig. 4.9. Boundaries to these regions could not be defined to better than 30 km.

It is possible to determine the velocity at the top of the upper mantle below an array by measuring the variation in arrival time across the array of the phase Pn from local crustal earthquakes. To this end, ten earthquakes which occurred during the Ruapehu survey and were determined to be crustal by the Seismological Observatory were studied. Of the earthquakes chosen, five occurred to the northeast of the array, the other five to the southwest (see table 4.3). It was hoped that by using arrivals from both directions a reversed section of the top of the upper mantle beneath the array could be determined, and hence the dip of the Mohorovičić discontinuity could be calculated.

On studying these earthquakes, the following facts emerged:

1) The first-arriving phase at stations of the array is invariably of much lower amplitude than the following P-phases, and precedes them by up to 2.75 seconds. Examples of these low amplitude phases are shown in fig. 4.4.

2) Comparison of the arrival times of these low amplitude phases reveals that they arrive at the array from an azimuth which is often significantly different to that defined by straight-line propagation between the epicentre determined by the Seismological Observatory and the array. For earthquakes to the northeast of the array the phase appears to arrive from an azimuth east of that expected, while for earthquakes to the southwest it appears to arrive from an azimuth south of that expected.

These observations suggest that the initial low amplitude phases have been laterally refracted through a region of higher velocity than

Date Oct. 1974	Latitude (deg)	Longitude (deg)	Depth (km)
01 2331	37.90 S	177.62 E	33 R
02 0400	37.77 S	178.09 E	33 R
03 0320	33.19 S	178.95 W	33 R
04 0445	42.62 S	172.86 E	12 R
04 1602	42.41 S	172.13 E	12 R
12 1746	43.20 S	172.42 E	12 R
17 2333	41.93 S	172.22 E	12 R
20 1639	41.52 S	174.38 E	12 R
22 1446	37.95 S	177.45 E	33 R
24 2300	38.34 S	177.22 E	12 R

Table 4.3   Earthquakes used to study Pn velocity below the Ruapehu array.   Hypocentres are those determined by the Seismological Observatory (Bulletin E-155).   R denotes a restricted depth.
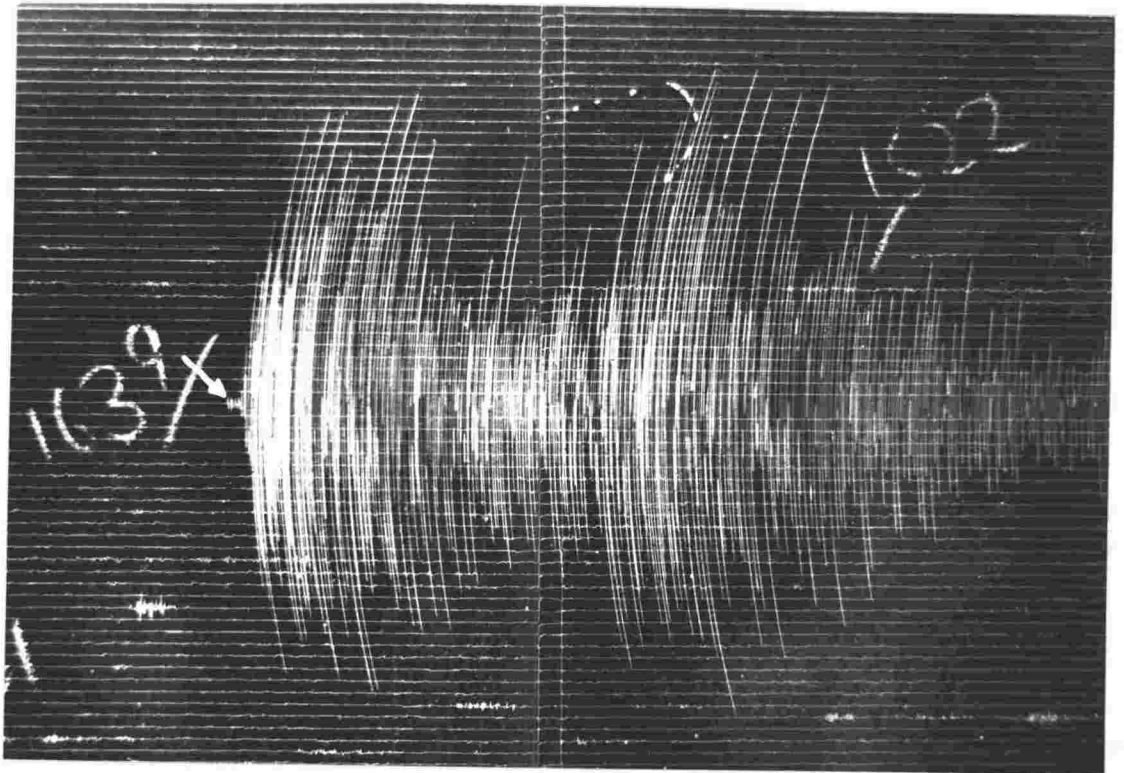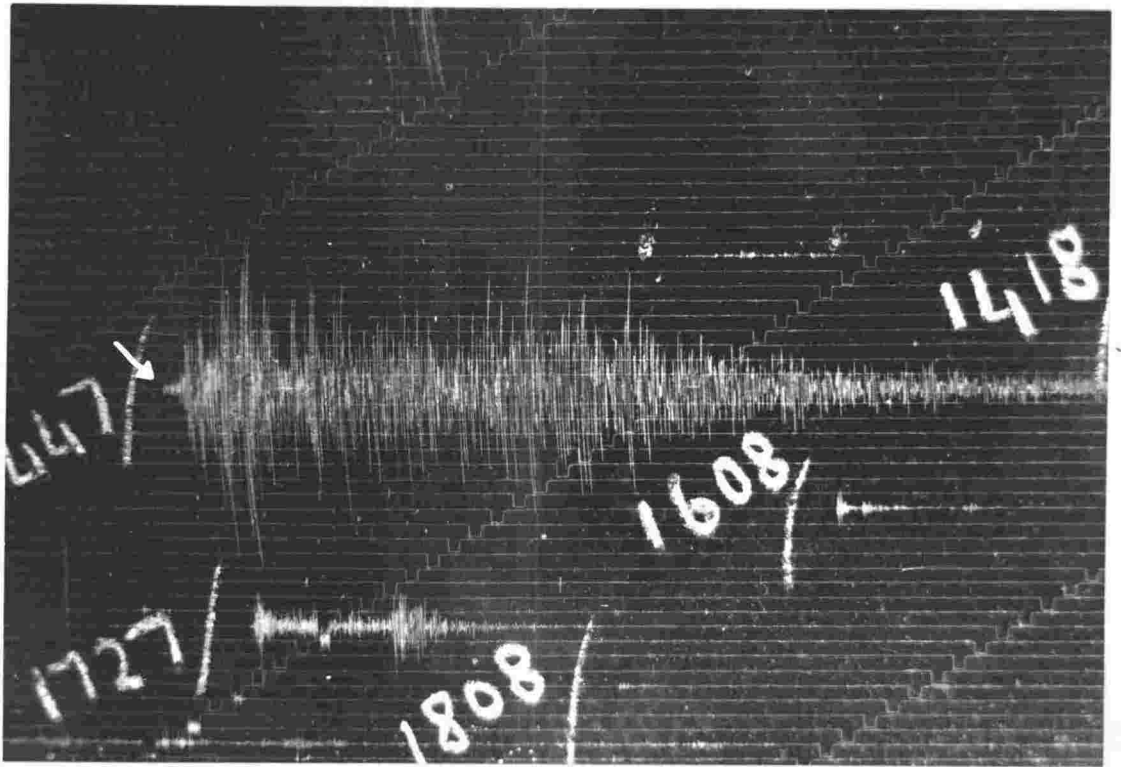
Figure 4.4   Seismograms of local crustal earthquakes showing a
low amplitude first-arriving phase.

that traversed by the later P-phases. From joint hypocentre determinations of subcrustal North Island earthquakes, Smith (1977) has deduced a velocity contrast for both P- and S-waves of 6-10% between paths in and entirely out of the subducted Pacific plate. He attributes a calculated 8.6 ± 0.1 km/sec P-wave velocity in the subducted plate to oceanic crust transformed to eclogite. Thus a logical high-velocity refractor for the observed low amplitude phases is the crust of the subducted plate; the later-arriving P-phases have presumably travelled above the subducted plate.

It is thus clear that an analysis of first arrivals of the above earthquakes will not yield the velocity at the top of the upper mantle below the Ruapehu array. However, such an analysis might give the P-wave velocity in the crust of the subducted plate. This was not pursued since the configuration of the top of the subducted plate in the region of the array is not sufficiently well-known for the accurate determination of path differences. If one interprets the larger amplitude phase following the first-arriving phase as a true Pn phase, the calculation of a velocity at the top of the upper mantle might be possible. This was attempted, but without success, since it is difficult to read accurately the arrival time of this phase as its commencement is often masked by the coda of the first-arriving phase.

The upper mantle P-wave velocity finally adopted for the Ruapehu array is based on the work of Haines (1976). Stations of the array straddle boundaries of his regions of assumed constant velocity, especially that between regions 2 and 5 (fig. 4.9). Consequently, an average upper mantle P-wave velocity between that of regions 2 and 5 was chosen, namely 7.6 km/sec. This velocity, although low compared with the 8.1 km/sec of the standard New Zealand crustal model (table 4.1), is similar to that measured above subduction zones in other parts of the world. Using large explosions at sea, the Research Group for Explosion Seismology (1977) have determined, with good accuracy, a Pn velocity of 7.5 km/sec beneath northeastern Japan. Above the subducted plate in Kamchatka, the average P-wave velocity in the mantle has been calculated as 7.7 km/sec, decreasing to 7.2 km/sec in regions containing basaltic magma (Fedotov, 1968).

Adoption of a single upper mantle velocity of 7.6 km/sec for the location of all subcrustal microearthquakes recorded by the Ruapehu array

is an obvious simplification of upper mantle structure. Different velocity models change a hypocentral depth more than they do an epicentre (e.g. Ward et al., 1974). Thus a different choice of upper mantle velocity will primarily change the dip of the Benioff zone as defined by the micro-earthquake hypocentres. It should be noted that one cannot use the root mean square error of the time residuals of a hypocentre to discriminate between different velocity models,as this is very insensitive to structure (e.g. Hashizume, 1970).

4.2.5 Explanation of prominent phases other than P and S shown by Ruapehu survey microearthquakes

As in the Dannevirke survey, prominent anomalous phases are present in many seismograms of microearthquakes recorded during the Ruapehu survey. These phases can be classified into five groups:

1) Low amplitude first arrivals (see fig. 4.5). These have been discussed earlier, and were interpreted as phases laterally refracted along the top of the subducted plate. The phases are recorded from earthquakes well outside the array; they are especially well-defined for earth-quakes in the Benioff zone below the Kaweka Range. A rough estimate of the velocity of the phase is provided by the earthquake of 1974 Oct. 22nd 09^h05^m. This earthquake occurred along the strike of the Benioff zone from stations TMO and HUN, and thus the difference in epicentral distance between TMO and HUN should not be greatly different from the difference in distance waves to these stations have travelled in the inferred refractor. Hence the velocity of the phase can be obtained by simply dividing this difference in epicentral distance by the arrival time difference of the phase at TMO and HUN, corrected for station terms. The 8.7 km/sec obtained must be considered rather approximate, since both the configuration of the top of the subducted plate and the station terms of TMO and HUN are not well known. Nevertheless, the fact that this velocity is indistinguishable from the 8.6 ± 0.1 km/sec attributed by Smith (1977) to the crust of the subducted plate lends weight to the interpretation of the low amplitude first arrivals as phases laterally refracted along the top of the subducted plate.
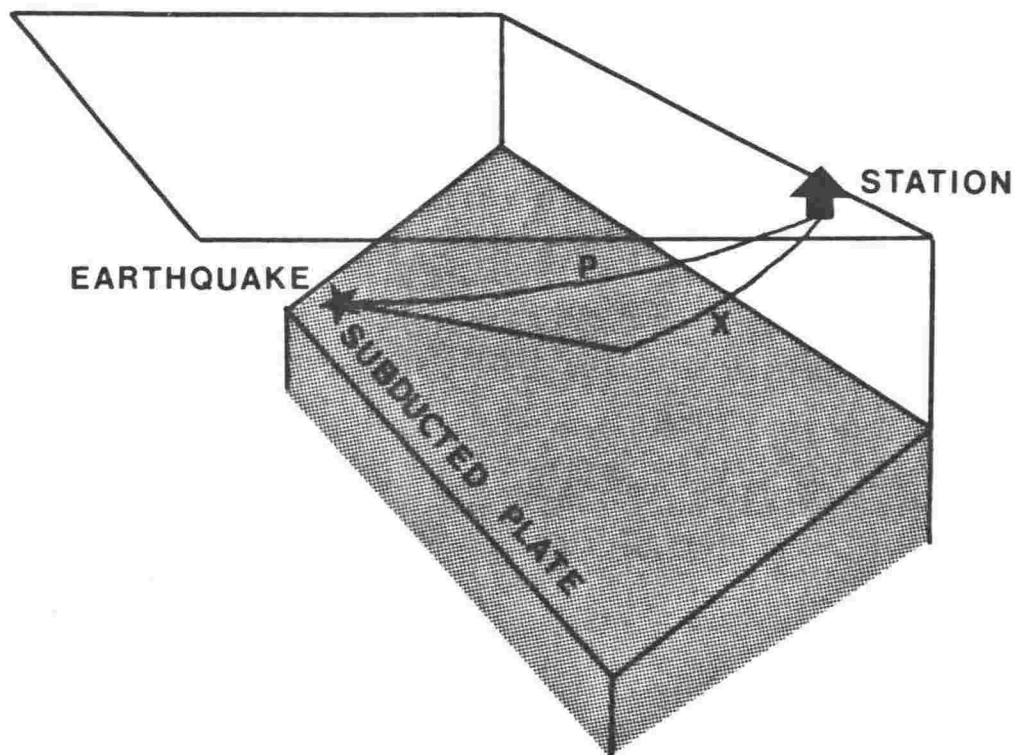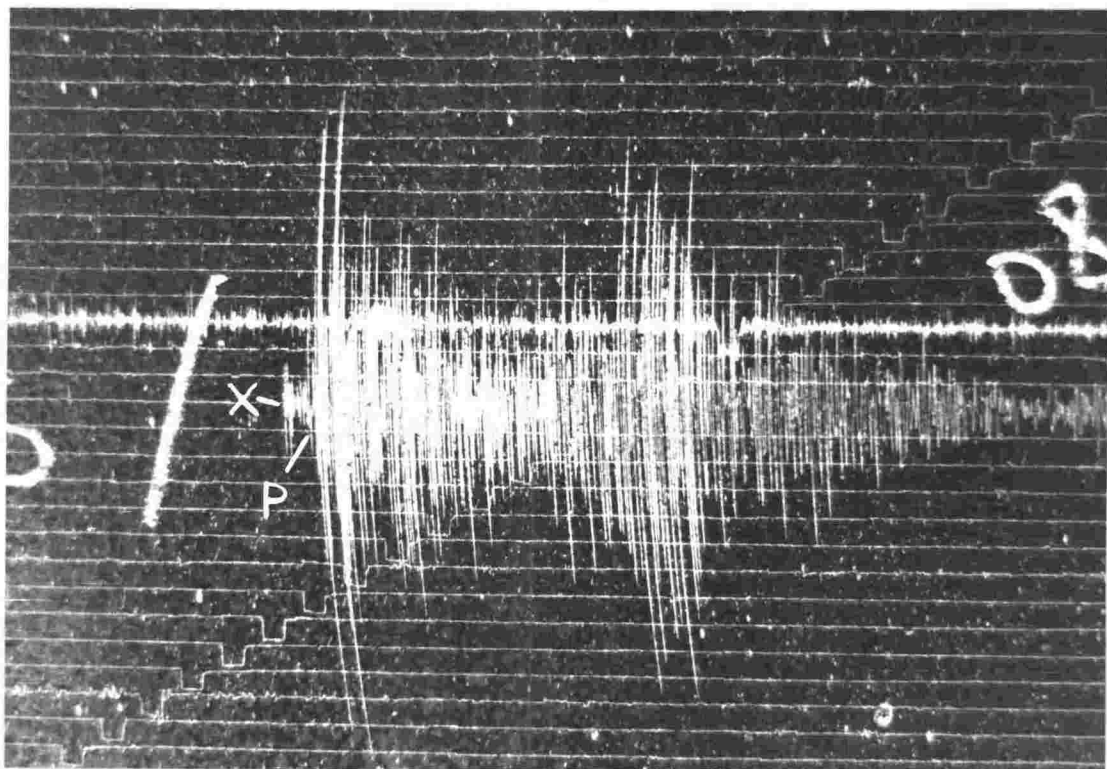
Figure 4.5   A seismogram exhibiting a low amplitude first-arriving
phase and a diagram indicating an interpretation of the phase.

2) A strong phase closely following the first-arriving energetic P-phase (see fig. 4.6). This phase is produced by subcrustal earthquakes well outside the array. Its explanation is difficult, but the tendency of earthquakes showing this phase to lie below the top of the Benioff zone suggests it could be an Sp phase generated near the top of the subducted plate. The effectiveness of this region as a conversion interface has been demonstrated in the Dannevirke survey.

3) A strong phase between P and S for earthquakes in the Dannevirke region (see fig. 4.7). During the Ruapehu survey, significant activity was recorded from the Dannevirke region. Depth control on this activity was obviously poor; RMS errors of the time residuals of these earthquakes were abnormally large, reflecting complicated structure between these earthquakes and the Ruapehu array. The results of the Dannevirke survey suggest that the great majority of these earthquakes occur in the subducted Pacific plate. Consequently, a ready explanation of the strong phases seen between P and S in these earthquakes is that of converted phases generated near the top of the subducted plate. The large error in location of the earthquakes precludes any calculation of the location of the top of the subducted plate interpreting the phases as conversions.

4) A definite phase between P and S for some earthquakes in the Benioff zone near the Ruapehu array (see fig. 4.8). This phase is difficult to explain, especially in the absence of three-component seismographs. An attempt to model it as a conversion at the Mohorovičić discontinuity of the Indian plate, taken as horizontal, met with little success.

5) Phases between P and S from 33-42 km deep microearthquakes in the upper basin of the Wanganui river (see fig. 4.8). These are generally poorly developed. Interpretation of the phases as conversions at the Mohorovičić discontinuity of the Indian plate proved inconclusive. Although one microearthquake (1974 Oct. 3rd 18^{h}49^m) indicated a Mohorovičić discontinuity at approximately 26 km depth, control was poor and the question of whether the shallow activity in the upper basin of the Wanganui River below the 33 km deep Mohorovičić discontinuity of the velocity model adopted for the Ruapehu array reflects a greater than normal crustal thickness remains unresolved.
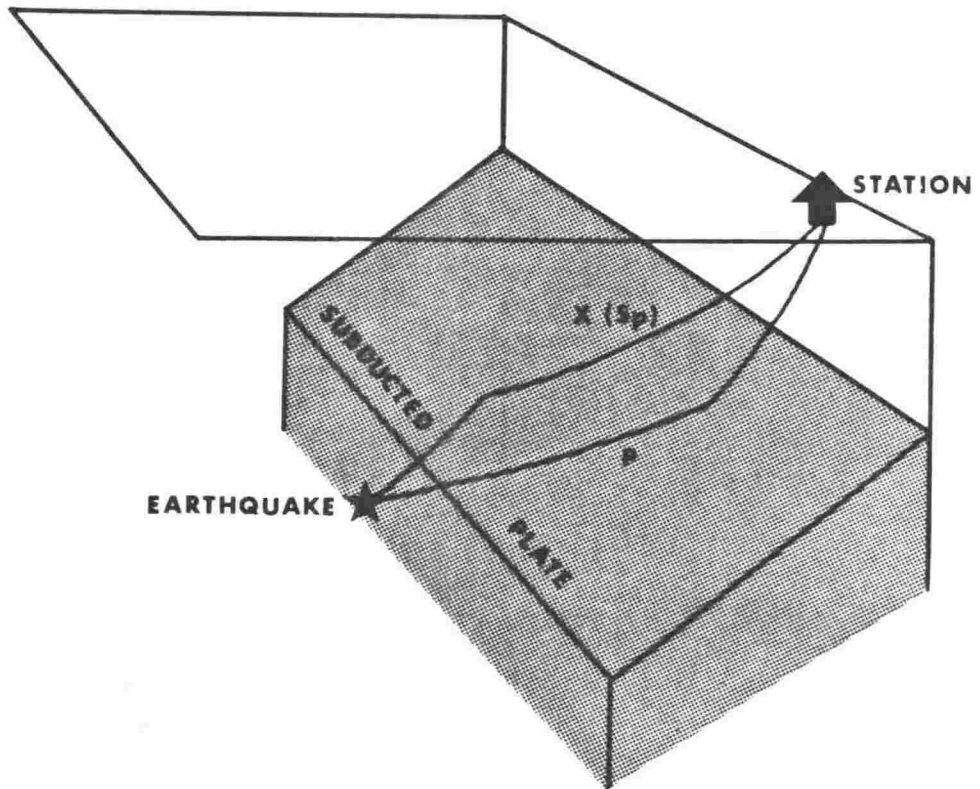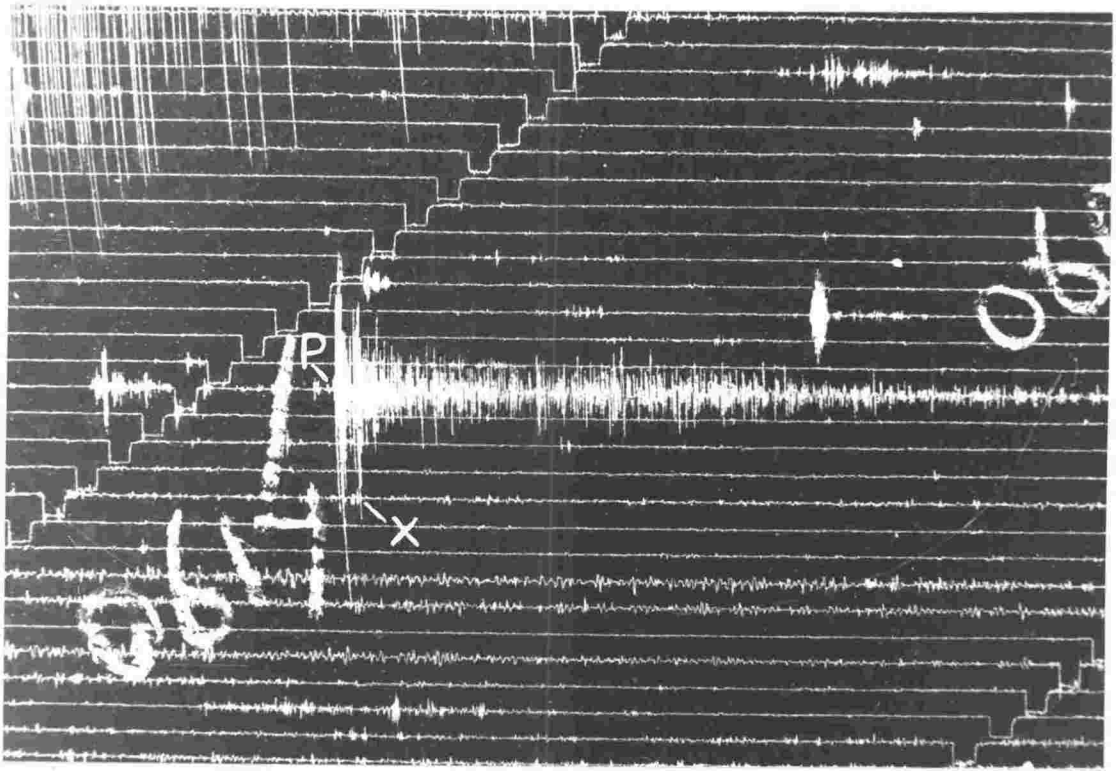
Figure 4.6   A seismogram showing a strong phase closely following the first-arriving P-phase and a diagram illustrating the interpretation of this phase as Sp generated near the top of the subducted plate.
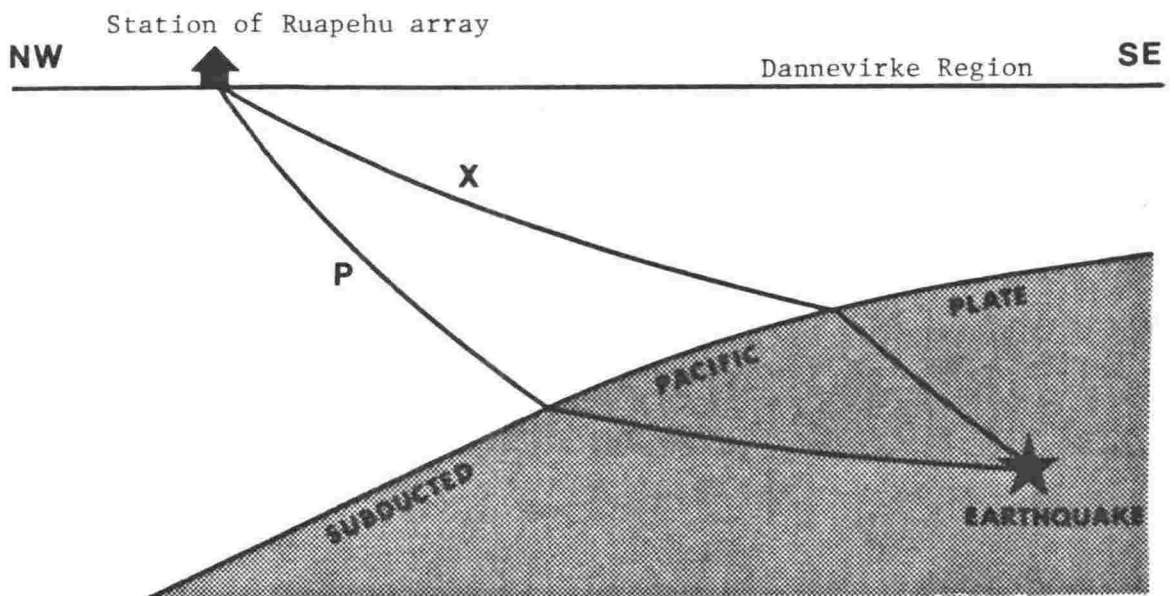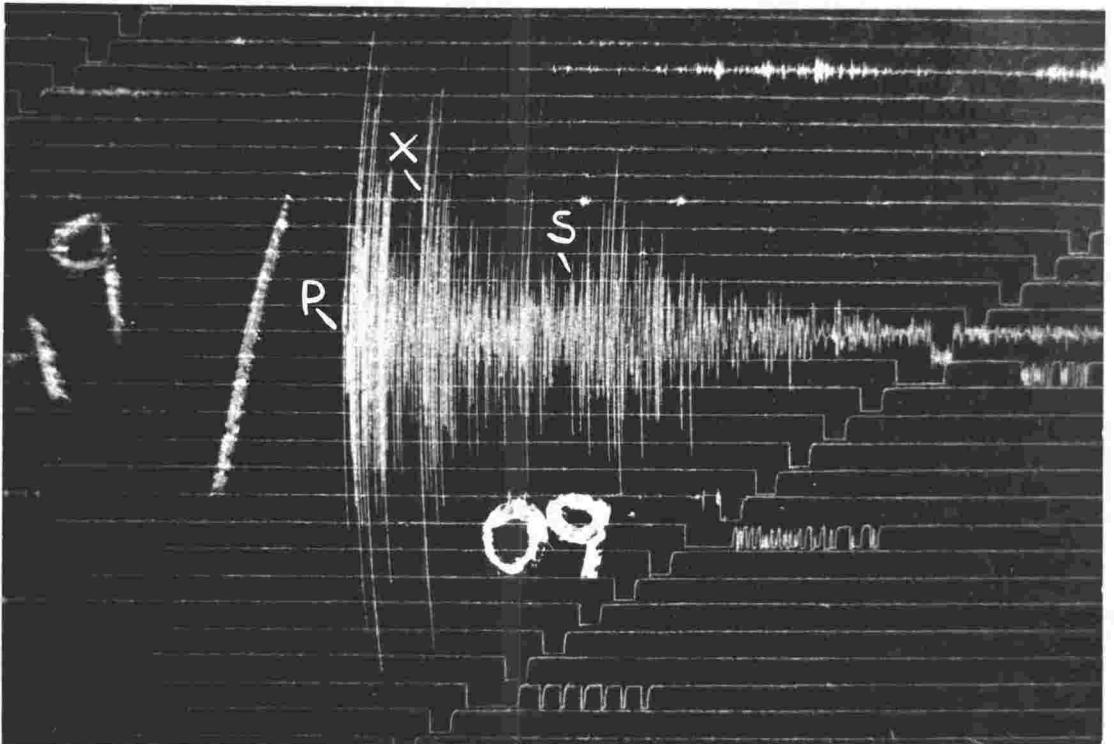
Figure 4.7   A seismogram of an earthquake in the Dannevirke region
recorded by the Ruapehu array and a diagram illustrating the inter-
pretation of the strong phase between the P- and S-phases as Sp generated
near the top of the subducted plate.
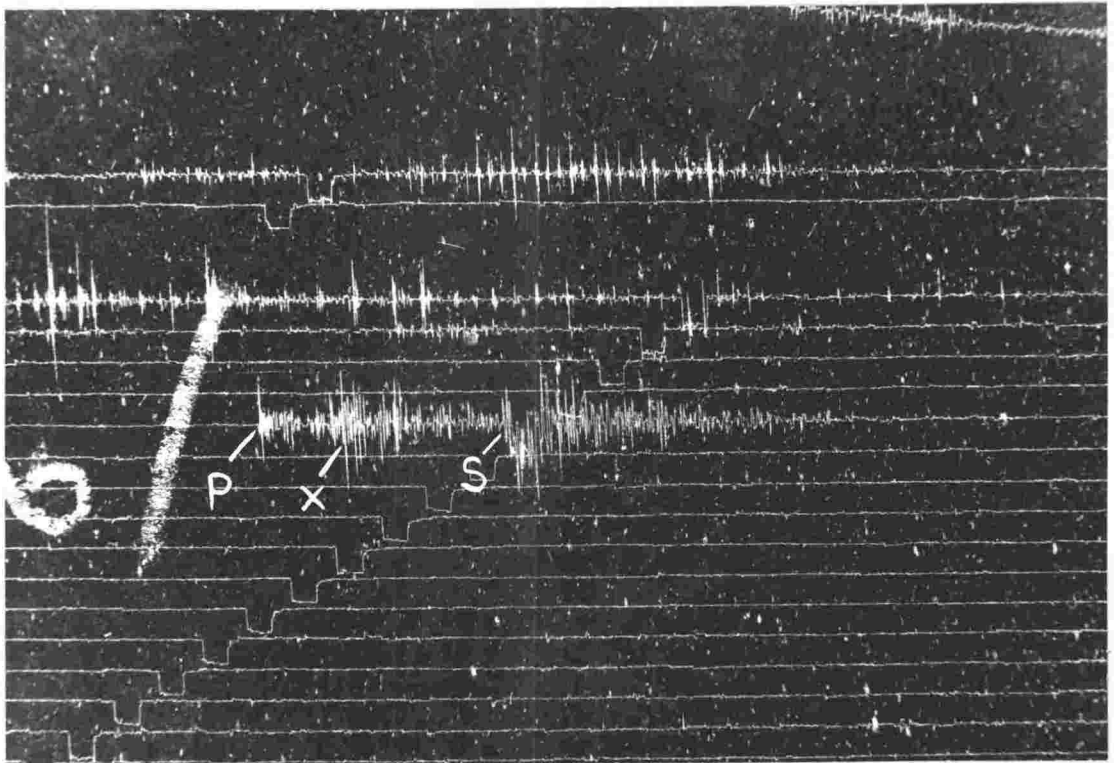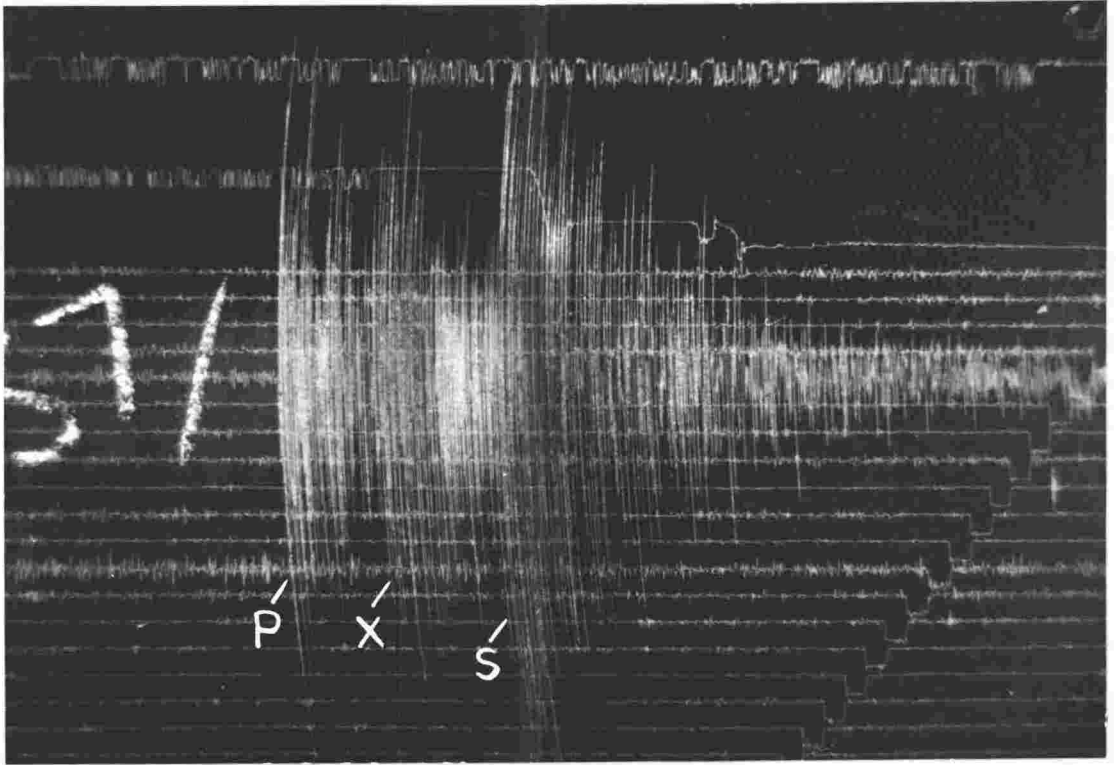
Figure 4.8   Seismograms showing definite phases between P and S, recorded from an earthquake in the Benioff zone near the Ruapehu array (top) and a microearthquake 39km below the upper basin of the Wanganui River (bottom).

4.2.6 Determination of the ratio of P-wave velocity to S-wave velocity

If one assumes that Poisson's ratio is the same in all layers traversed by the waves of an earthquake, it can be shown that the plot of S-P against P, where P is the P-wave arrival time and S is the S-wave arrival time, is a straight line (Wadati, 1933). In such a plot, known as a Wadati diagram, the ratio of P-wave velocity to S-wave velocity (γ) can be obtained from the slope of the line, and the intercept of the line on the P-axis corresponds to the origin time of the earthquake. In addition to giving an estimate of the origin time, the Wadati diagram is useful because it yields important information about γ without requiring the development of travel-time curves or the location of the source event.

Caldwell & Frohlich (1975) have attempted to determine γ by means of the Wadati diagram using data obtained in an eight-instrument micro-earthquake survey near Haast in the South Island of New Zealand. They conclude that because of scatter in the data, errors in the reading of S and errors in clock-time corrections, γ values have an error of 10%, and thus nothing can be said about the γ variation found, namely 1.62-1.76, as this could be due solely to errors in the data. In contrast, Rynn & Scholz (1978), using data from two microearthquake surveys in the South Island (one utilizing ten instruments, the other eight), find meaningful γ values can be obtained from the Wadati diagram. By restricting the data set used for the calculation of γ to those micro-earthquakes which

a) are "locatable from four or more stations" and

b) have a range of P-wave arrival time greater than four seconds, these authors find the average uncertainty of individual γ values is approximately 1-2%.

During the Ruapehu survey a large number of stations (up to 14 including permanent stations of the Seismological Observatory) were operating in a well-distributed array, and the effect of different restrictions on the number of (P,S) pairs and the range of P-arrival time used in the Wadati diagram could be studied. It was found that meaningful γ values could only be obtained from the Wadati diagram for those microearthquakes with seven or more (P,S) pairs and a range of P-arrival time of seven seconds or greater. Hereafter these micro-earthquakes will be referred to as (7,7) microearthquakes.

Errors inherent in the calculation of γ from a Wadati diagram include:

a) errors in reading P- and S-arrivals, particularly errors due to misidentification of the S phase, and

b) errors due to a differing Poisson's ratio in the various layers traversed by the waves of an earthquake.

The use of a large number of (P,S) pairs in a Wadati diagram often reveals badly misidentified S phases, and the use of as large a range of P-arrival time as possible gives a good indication of the linearity of the diagram and hence the validity of the constant Poisson's ratio assumption.

For all (7,7) microearthquakes, γ values and their standard deviations were obtained by least squares fitting of a straight line to the data of Wadati diagrams. Correlation coefficients obtained range from 0.96 to 1.00, suggesting that a straight line is a good model for the data, and that variation in Poisson's ratio in the layers underlying the Ruapehu array is likely to be small.

In fig. 4.9, the γ values obtained are plotted at the epicentres of the microearthquakes used to determine them. The standard New Zealand crustal model (table 4.1) was used for the location of the microearthquakes and the interpretation of their first arrivals at stations of the Ruapehu array. γ values determined mainly from crustal g- and *-phases are distinguished from those determined mainly from n-phases and subcrustal phases. Fig. 4.9 shows a weighted mean γ value for a tight cluster of 7 crustal (7,7) microearthquakes immediately south of Wanganui. A weighted mean γ is also shown for a group of three subcrustal earthquakes beneath the Kaweka Range. These earthquakes had seven or more (P,S) pairs and a P-arrival time range of five seconds or greater; they were included to obtain an estimate of γ in the upper mantle in the region of the Ruapehu array. Upper mantle γs determined by Haines (1976) are included in fig. 4.9.

Fig. 4.9 has several interesting features:

1) γ values for crustal (7,7) microearthquakes determined mainly from g- and *-phases, excluding those of the tight cluster of micro-earthquakes immediately south of Wanganui, show good consistency, their weighted mean being 1.67 ±0.04. γ values determined from a Wadati diagram give a measure of the average crustal structure between a microearthquake and the stations recording it. The distribution
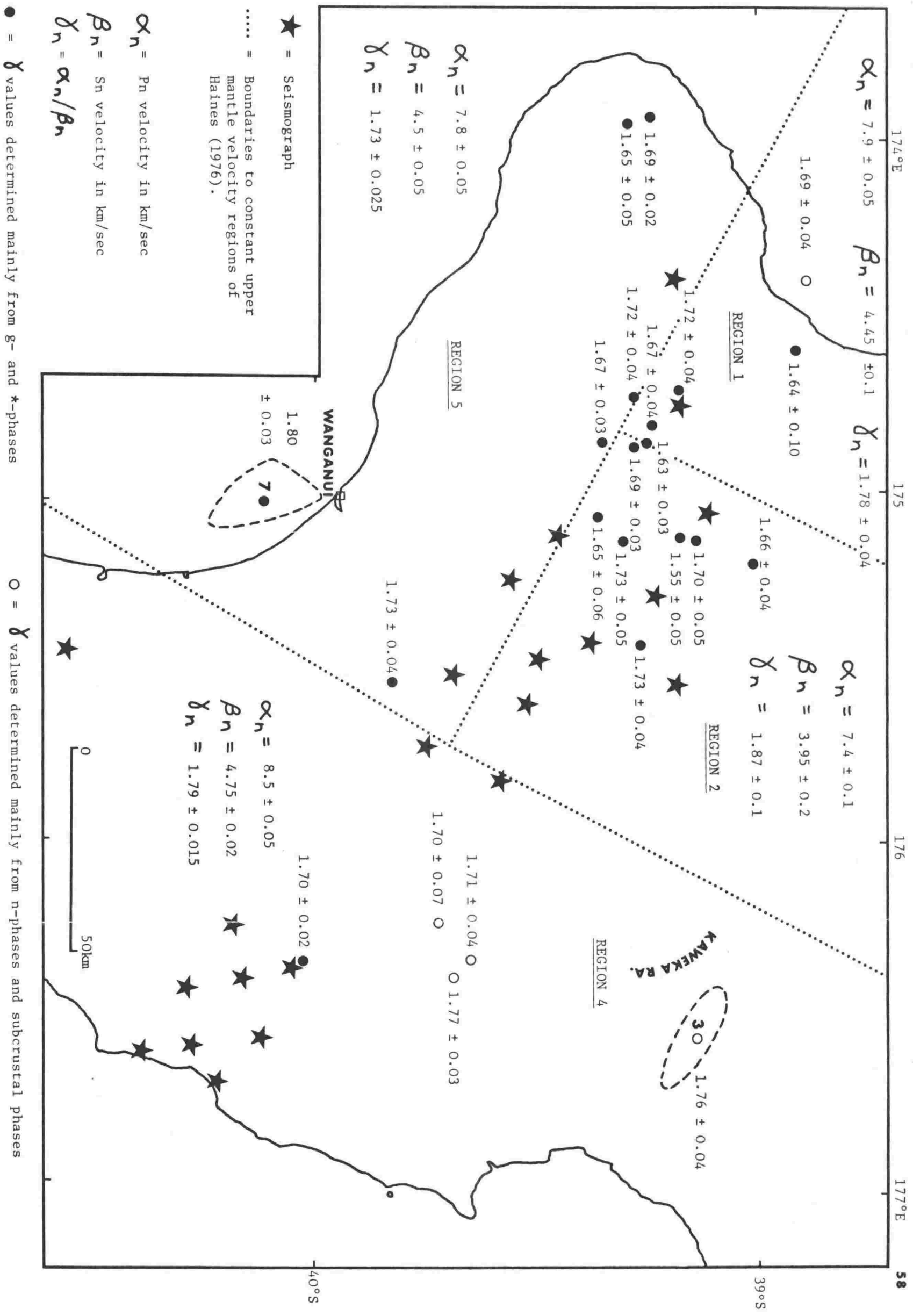
Figure 4.9. γ values determined from Wadati diagrams for microearthquakes with seven or more (P,S) pairs and a P- arrival time range of seven seconds or greater. Values are plotted at the epicentre of the microearthquake used to determine them. Also shown are the regions of constant upper mantle velocity determined by Haines (1976).

★ = Seismograph

⋯ = Boundaries to constant upper mantle velocity regions of Haines (1976).

α_n = Pn velocity in km/sec

β_n = Sn velocity in km/sec

$\gamma_n = \alpha_n / \beta_n$

● = γ values determined mainly from g- and *-phases

O = γ values determined mainly from n-phases and subcrustal phases

of (7,7) microearthquakes shown in fig. 4.9 indicates that the γ values of these microearthquakes will largely reflect the average crustal structure beneath the Ruapehu array, and thus some consistency in γ determinations is to be expected.

A crustal γ of 1.67 is somewhat lower than that found in other parts of the world, where normal crustal γ values range from 1.71 to 1.77 (e.g. Aggarwal et al., 1973, 1975; Brown, 1973; Feng et al., 1974; Nersesov et al., 1971). In a microearthquake study of a 600 km long section of the Alpine Fault zone in the South Island of New Zealand, Rynn & Scholz (1978) have found the region to be characterised by crustal γ values of 1.70-1.74, except for a 75 km long section near Arthur's Pass, where γ is 1.63. Explosions recorded by a telemetered microearthquake array around Lake Pukaki in the South Island have yielded a preliminary crustal γ value of 1.71 (I. M. Calhaem, pers. comm.,1978).

γ values of the order of 1.67 have been considered anomalously low, and indicative of an impending large earthquake (e.g. Nersesov et al., 1971). As a physical basis for temporal and spatial γ variations prior to earthquakes, a dilatancy model has been proposed (Nur, 1972; Scholz et al., 1973b). However, the present γ does not warrant an explanation in terms of dilatancy, as there is no way of knowing from only one month of recording whether its low value of 1.67 is of a temporary or permanent nature. Laboratory results indicate that quartzose sedimentary rocks have a lower γ than metamorphic or igneous rocks (Anderson & Liebermann, 1966). Thus the present γ, if a permanent feature, may show the effect of Tertiary sediments, which reach a thickness of over 2 km beneath the Ruapehu array (Cope, 1966).

2) γ values for (7,7) microearthquakes determined mainly from n-phases and subcrustal phases also show good consistency, their weighted mean being 1.72 ±0.04. n-phases and phases from subcrustal microearthquakes sample both the upper mantle and the crust on their way to recording stations. Consequently, the present result indicates that γ in the upper mantle is higher than that in the crust in the region of the Ruapehu array. Owing to the lack of control on crustal structure, it is difficult to separate the upper mantle

and crustal contributions to γ, but it is likely that γ in the upper mantle lies in the range of 1.73-1.87 determined by Haines (1976) (see fig. 4.9). The weighted mean γ of 1.76 ± 0.04 for the three (7,5) microearthquakes occurring at depths of 44-59 km below the Kaweka Range supports this conclusion.

3) The weighted mean γ of 1.80 ± 0.03 determined for the cluster of seven crustal (7,7) microearthquakes immediately south of Wanganui is unusually high. Owing to poor depth control for these micro-earthquakes, as they are over 50 km outside the Ruapehu array, and meagre control of crustal structure in the Wanganui region, it is difficult to determine if this high γ is a feature of the crust or upper mantle or both. Microearthquake activity immediately south of Wanganui is also unusual in other respects, and its geophysical significance will be discussed later.

The HYPO71 location program requires the specification of a model γ value if S-readings are used. The following model γ values were adopted in the present study:

a) Ruapehu survey (7,7) microearthquakes:- γ values determined from Wadati diagrams were used.

b) Other crustal Ruapehu survey microearthquakes:- the average crustal γ of 1.67 determined above was used.

c) Other subcrustal Ruapehu survey microearthquakes:- appropriate γ values were estimated, taking into account the average crustal γ, the upper mantle γ values of Haines (1976) and the depth of the microearthquake.

d) All Dannevirke survey microearthquakes:- the Wadati diagram could not be used to determine γ values for these microearthquakes as too few recording stations were available. A γ of 1.73 was adopted for these microearthquakes. This value represents the average γ of the layers of the standard New Zealand crustal model (table 4.1). It also lies between the average crustal γ of 1.67 determined for the Ruapehu array and the upper mantle γ of 1.79 determined for the Dannevirke region by Haines (1976). The appropriateness of this choice is difficult to test since hypocentre quality is rather insensitive to γ.

4.3 HYPOCENTRE QUALITY

Hypocentres of microearthquakes recorded in both the Dannevirke
and Ruapehu surveys have been divided into the following quality classes:

Quality class	NO	RMS (sec)	ERH (km)	ERZ (km)	DM (km)
A	≥ 8*	≤ 0.20	≤ 2.5	≤ 2.5	$\leq 2z$
B	≥ 7*	≤ 0.30	≤ 5.0	≤ 5.0	$\leq 2z$
C	≥ 5*	≤ 0.30	≤ 5.0	≤ 5.0	$\leq 2z$
D	Other microearthquakes with convergent solutions				

* including 2 S-readings

Where

NO = Number of phases (both P and S) used in locating a microearthquake

RMS = The root mean square error of the time residuals

ERH = The standard error of the epicentre

ERZ = The standard error of the focal depth

DM = The epicentral distance to the nearest station

z = The focal depth in km

The adopted limits on the number of phases were dictated by
microearthquakes of the Dannevirke survey, for which never more than
10 phases were recorded. In contrast, the large number of stations
operating during the Ruapehu survey, coupled with the location criteria
adopted (see sect. 4.1), result in from 7 to 22 phases being used to
locate Ruapehu survey microearthquakes. The use of two or more S-readings
in all A, B and C quality events serves to fix the origin time of the
event, thereby combating the solution instability discussed in sect. 4.2.1.

RMS, ERH and ERZ together give a statistical measure of the
goodness of fit of the data to the adopted velocity model. It should be
noted that HYPO71 uses a biased estimate of the error of the time residuals,
namely RMS = $\sqrt{\Sigma R_i^2 / NO}$ (where R_i is the time residual of the ith station),
rather than the unbiased estimate of $\sqrt{\Sigma R_i^2 / (NO - 4)}$. This causes the
RMS of a solution to increase, while ERH and ERZ decrease, as more
readings are added. Consequently, the RMS limits of A, B and C quality
events have been set rather widely. It should also be noted that ERH
and ERZ may not represent the actual error limits of a hypocentre, as

the statistical interpretation of standard errors involves assumptions which may not be met in earthquake locations. Nevertheless, they do provide a relative measure of the consistency of the data.

The DM criterion adopted for A, B and C quality events ensures that good depth control is maintained. Accuracy in the determination of focal depth depends critically on the rate of change of travel time with focal depth. For direct arrivals, this rate of change becomes unacceptably small beyond DM = 2z. This need not be the case with critically refracted arrivals, but since the dip and depth of refractors below both arrays are poorly known, the same DM criterion has been adopted for all microearthquakes, irrespective of the interpreted nature of their arrivals.

4.4 ESTIMATION OF MICROEARTHQUAKE MAGNITUDE

Two methods of estimating microearthquake magnitude are in common use, one utilizing the amplitude of the waves of a microearthquake (e.g. Brune & Allen, 1967; Eaton et al., 1970), the other event duration (e.g. Lee et al., 1972). As both the Sprengnether and Kinemetrics recorders used in this study clip large amplitudes, a small range of observable amplitude results. Consequently, event duration has been routinely used to estimate microearthquake magnitude.

The event duration-magnitude relationship used in this study is that empirically determined by Robinson et al. (1975) from earthquakes within 1.0° of Wellington recorded on both the Wood-Anderson seismograph at Wellington and the Sprengnether MEQ-600 microearthquake recorders, namely

$$M_d = -1.51 + 1.74 \log \tau + 0.019 R$$

where M_d = duration magnitude

τ = event duration (the time in seconds from the onset of the first P-arrival to the point where the microearthquake becomes indistinguishable from the background noise)

and R = the radial distance in km from the hypocentre to the station.

As the analysis of magnitude distribution was not a primary goal of this study, the calculation of a similar duration-magnitude relationship for the region of the microearthquake traverse was not attempted. The use

of the above relationship is justifiable since the constants in it
appear to be a function of the instruments and criteria used to measure
event duration, rather than of the geology or tectonic regime of the
region where the data were acquired (Langenkamp & Combs, 1974). To
achieve uniformity in magnitude determination, duration magnitudes were
calculated from only the Sprengnether MEQ-600 recorders in both the
Dannevirke and Ruapehu surveys. In the few instances when duration
magnitude could not be calculated because the coda of a microearthquake
was obscured by a closely-following event, the magnitude adopted was
the mean of the P-wave and S-wave amplitude magnitudes calculated using
the formulae of Robinson et al. (1975).

Larger earthquakes located both by the microearthquake arrays and
the permanent network of the Seismological Observatory provide information
on how duration magnitude compares with local magnitude determined from
Willmore and Wood-Anderson seismographs. Results of the analysis of
the four earthquakes in this category are shown in table 4.4. Hypocentres
determined by the microearthquake array and the permanent network differ
significantly, especially in depth. However, this difference does not
significantly affect M_l and M_h. The M_h magnitude of table 4.4 is based
on a modified definition of Richter local magnitude, incorporating
amplitude-distance relations determined directly from New Zealand earth-
quakes (Haines, 1978); it differs only slightly from M_l. The scant data
of table 4.4 reveal that for earthquakes nearer to the array, M_d agrees
well with M_l and M_h, but as the hypocentral distance of an earthquake
from the array increases, M_d grossly overestimates magnitude compared
with M_l and M_h. Clearly, the duration magnitude scale used in this
study is inappropriate for earthquakes at hypocentral distances of $1.0°$
or more.

4.5 CONSTRUCTION OF COMPOSITE FOCAL MECHANISM DIAGRAMS

For individual microearthquakes of this study, insufficient P-wave
first motions were recorded to enable the unambiguous determination of
a nodal pattern. Hence the composite focal mechanism technique
(e.g. Scholz et al., 1969), in which the first motions of closely related
earthquakes are superposed as if they originate from a single focus, was

Earthquake Oct. 1974	Z_m (km)	Z_o (km)	Δ_e (km)	R (km)	M_d	M_l	M_h
03 1517	33	12R	15	110	4.6	3.9	3.7
15 0654	42	93	10	56	3.5	4.0	3.7
18 1139	59	33R	21	76	3.5	3.6	3.5
24 1632	92	12R	14	166	5.6	4.1	4.1

where

Z_m = The hypocentral depth calculated in this study.

Z_o = The hypocentral depth calculated by the Seismological Observatory (Bulletin E-155). R denotes a restricted depth.

Δ_e = Difference between the epicentre determined in this study and that determined by the Seismological Observatory (ibid.).

R = Hypocentral distance to the nearest station for which M_d was determined.

M_d = Duration magnitude determined in this study.

M_l = Richter local magnitude determined by the Seismological Observatory (ibid.).

M_h = Modified Richter local magnitude determined by the method of Haines (1978), using the hypocentres determined in this study.

Table 4.4   Comparison of magnitudes

employed. If a consistent focal mechanism results from this technique, it is the orientations of the stress axes defined by the mechanism that are significant, as they reflect the regional stress field.

For groups of closely related microearthquakes first motion observations were plotted on an equal-area stereographic projection of the upper focal hemisphere. A double-couple model was adopted for the focal mechanisms, and orthogonal nodal planes were fitted to the first motion data by inspection, having regard to the following:

a) First motion quality. Clear first motions were distinguished from those which were more uncertain (e.g. because of their low amplitude).

b) Near-nodal arrivals. These were interpreted on the basis of the relative amplitudes of P and S waves (Honda, 1957). A microearthquake record was considered definitely near-nodal when $S_z > 10 \, P_z$ and less definite but worth noting when $S_z > 5 \, P_z$ (where P_z and S_z are the maximum amplitudes of the P and S waves respectively).

c) Arrivals interpreted as head waves or as leaving the focus at less than 10° from the horizontal. These arrivals were considered less reliable, even when clear first motions were read, because small changes in velocity model and/or hypocentral depth critically affect the interpretation of the arrivals (cf. Adams et al., 1974).

CHAPTER 5

MICROEARTHQUAKE RESULTS

5.1 GENERAL FEATURES OF THE MICROSEISMICITY

Microearthquakes located in this study, using the location
criteria of sect. 4.1 and the velocity models described in sect. 4.2,
are listed in the appendix and plotted in figs 5.1, 5.2 and 5.3.
Quality D hypocentres have not been included in fig. 5.3 as depth
control for these is invariably very poor. It should be noted that
the microearthquakes shown in figs 5.1, 5.2 and 5.3 do not represent
a sample of the microseismicity which is homogeneous in time. Although
the Dannevirke and Ruapehu surveys both lasted approximately one month,
the region between the arrays was sampled in both surveys and thus
the activity recorded there represents a two-month sample of the
microseismicity. Furthermore, the microearthquake sample is not
homogeneous in magnitude,as the minimum magnitude required by a
microearthquake before it is capable of location increases with
increasing distance from an array. This is illustrated by the concen-
tration of the lower magnitude activity near the arrays evident in
figs 5.1, 5.2 and 5.3. These figures also show the lack of located
activity of magnitude less than 1.0 near the Ruapehu array resulting
from the location criteria adopted.

There has been some debate as to whether microearthquake surveys
of short duration give a representative picture of longer term
seismicity. Udias & Rice (1975) maintain that conclusions concerning
seismicity based on microearthquakes recorded by temporary stations
running for a few days or even months may be erroneous owing to the
inhomogeneity of microearthquake activity in time. In contrast,
Crompton & Butler (1976) suggest that a good statistical estimate of
seismicity can be obtained from surveys whose length is measured in
tens of days. The degree to which the present microearthquake sample
is representative of longer term seismicity can be ascertained by
comparing it with macroseismicity located by the Seismological Observatory
in the region of the traverse. Comparison of figs 2.4 and 5.1 reveals
that the main features of the macroseismicity evident in a 19-year
compilation of shallow earthquakes are reproduced by the microearthquake
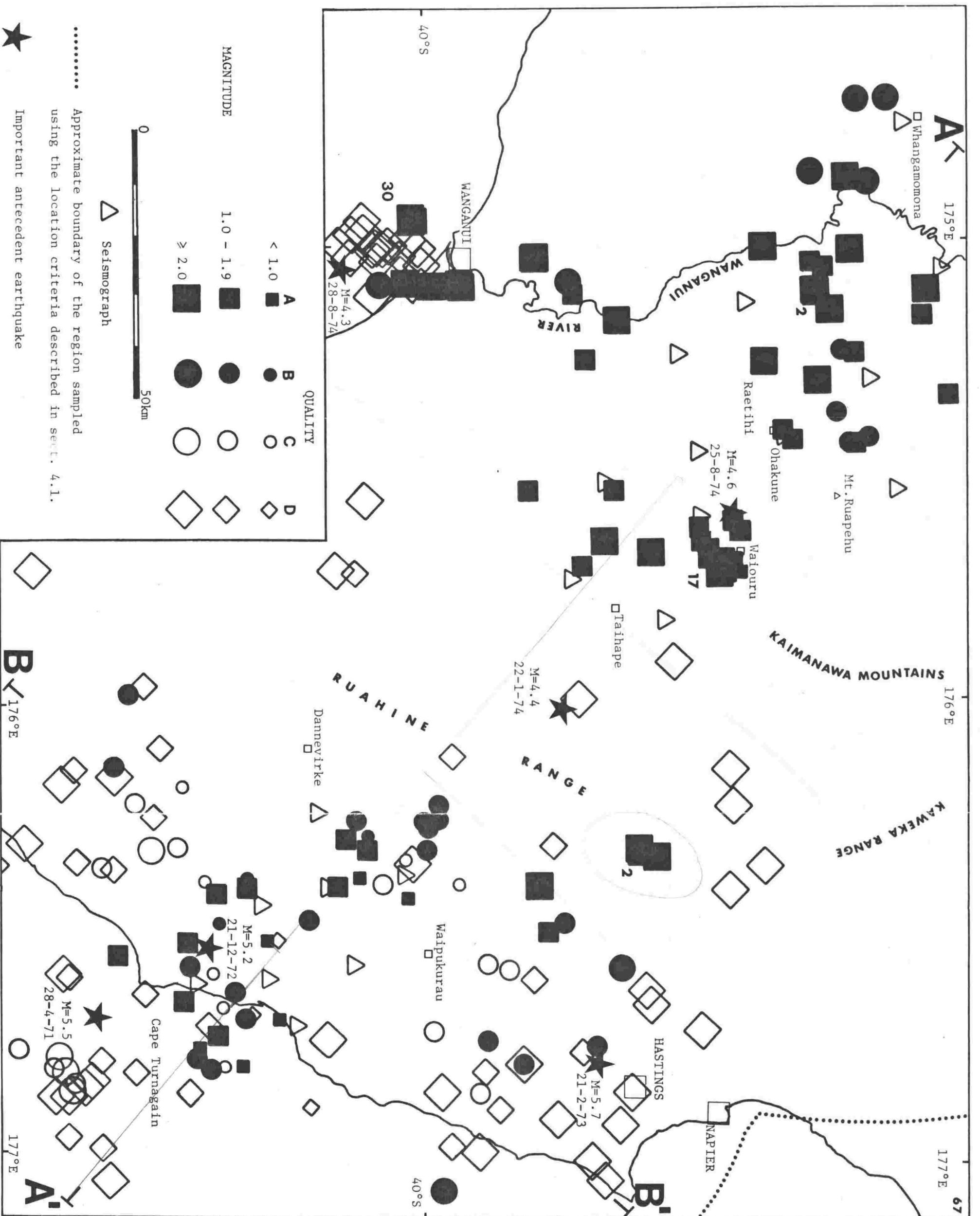
Figure 5.1   Epicentres of microearthquakes with focal depth less than 40km located using the velocity models described in sect. 4.2.
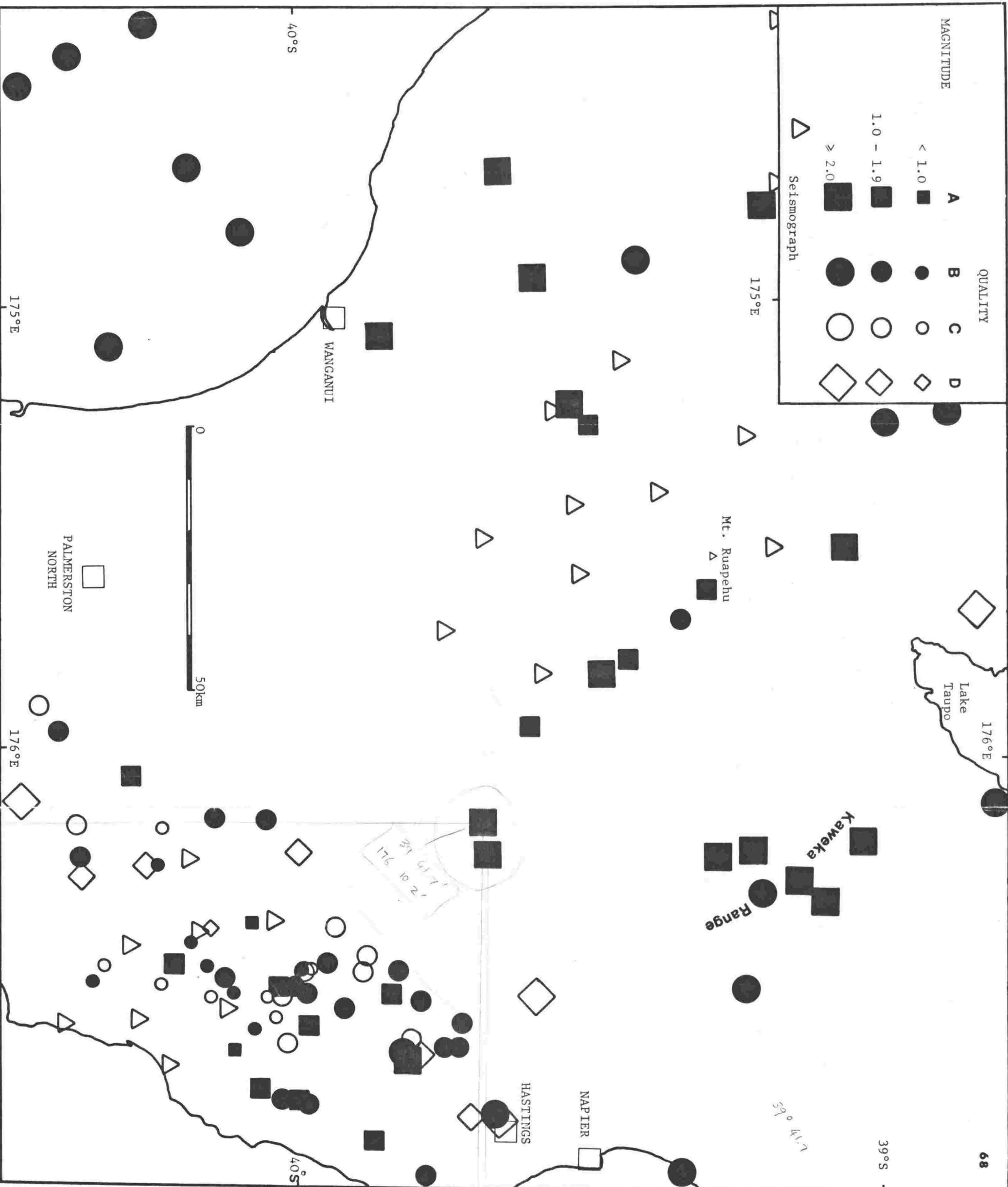
Figure 5.2 Epicentres of microearthquakes deeper than 40 km located using the velocity models described in sect. 4.2.

A ←311°

DEPTH (km)

50

100

150

A' 1131→ 250km

RUAPEHU   Mt. Ruapehu   ARRAY

Ruahine Range

DANNEVIRKE   East Coast   ARRAY

0   50   100   150   200
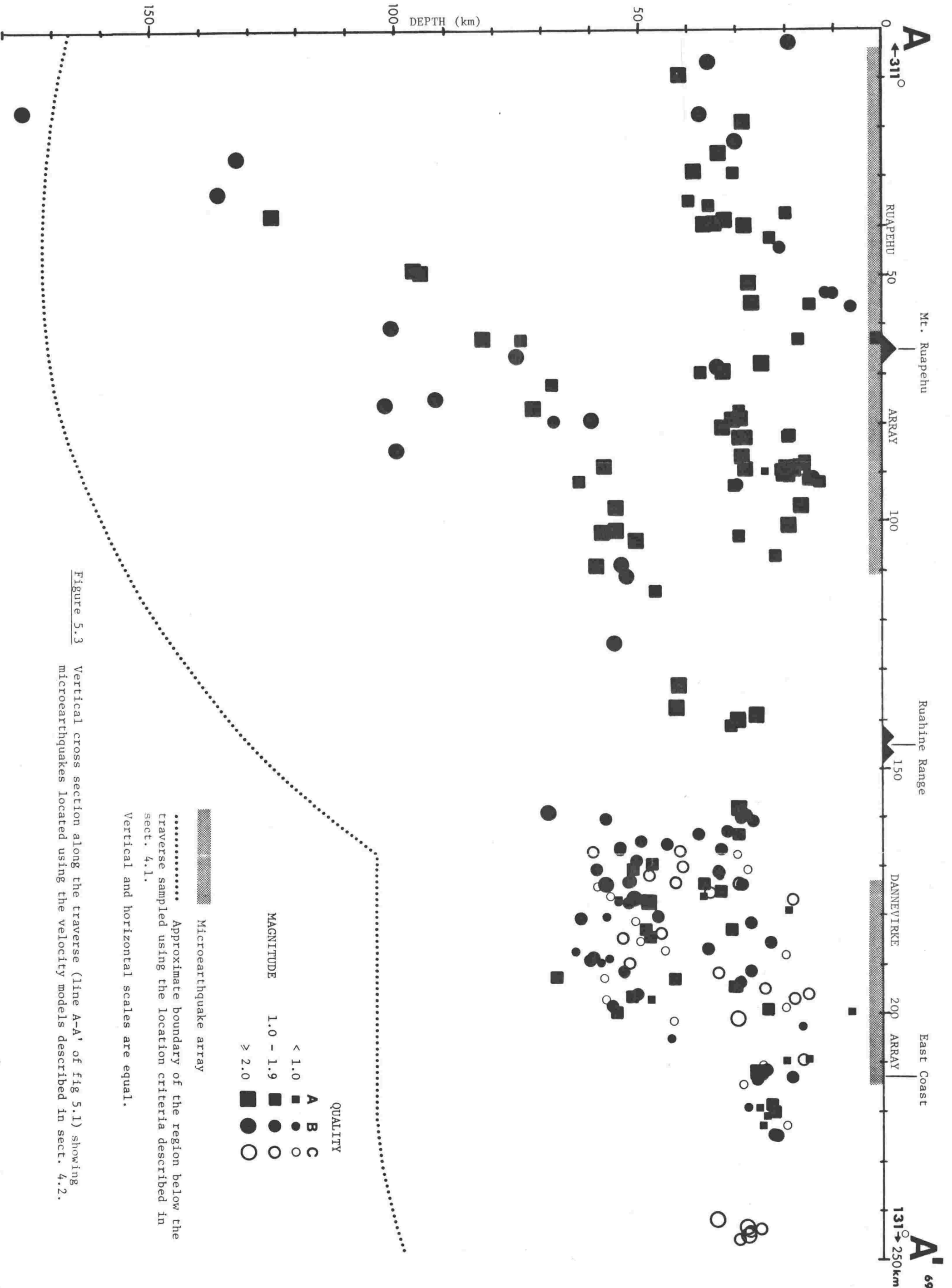
Figure 5.3   Vertical cross section along the traverse (line A-A' of fig 5.1) showing
microearthquakes located using the velocity models described in sect. 4.2.

·········   Microearthquake array

·········   Approximate boundary of the region below the
traverse sampled using the location criteria described in
sect. 4.1.

Vertical and horizontal scales are equal.

MAGNITUDE   QUALITY

< 1.0   A B C

1.0 - 1.9

≥ 2.0

69

sample. Both figures show seismicity is high along the east coast, in the upper basin of the Wanganui River and near the city of Wanganui, while it is relatively low in the Ruahine Range. Similar correspondence between short-term microseismicity and longer-term macroseismicity has been observed in the central North Island (Evison et al., 1976).

5.2   DETAILED STUDY OF GROUPINGS OF MICROEARTHQUAKES

5.2.1 Microearthquakes shallower than 40 km located with the Dannevirke array

Microearthquakes in the region of the Dannevirke array less than 40 km deep have been grouped separately from those at greater depth because of the break in microseismicity at about 40 km depth apparent in fig. 5.3. Epicentres of these microearthquakes show significant clustering (see fig. 5.1), and it is important to determine whether this clustering identifies microaftershocks of previous large earthquakes or is a feature of the background microseismicity. A survey of past seismicity suggests the Dannevirke array may have recorded micro-aftershocks from four prior earthquakes. These are plotted in fig. 5.1.

The greatest amount of microaftershock activity expected is from the magnitude 5.7 earthquake of 1973 February 21st, which the Seismological Observatory located near Hastings at a restricted depth of 12 km. Arabasz & Robinson (1976) have derived an expression for an estimate of t_1, the time after a mainshock, in days, when aftershocks of magnitude M_{min} or greater occur at a rate of one per day. This is a function of M_L, the mainshock magnitude, namely:

$$\log t_1 = (1.87 - M_{min}) + 0.98 (M_L - 4.0)$$

This expression assumes that b = 1.0 in the Gutenberg and Richter frequency-magnitude relation and that aftershock rate decays hyperbolically with time. It indicates residual aftershock activity of the earthquake of 1973 February 21st of about one shock per day of magnitude 1.0 or more during the Dannevirke survey. Thus microaftershocks of this earthquake are likely to contribute to the significant microearthquake activity near Hastings shown in fig. 5.1.

Aftershock activity of one shock per day of magnitude 0.8 or more can have been expected during the Dannevirke survey from the magnitude 4.4 crustal earthquake which occurred below the western flank of the Ruahine Range 15 days before the beginning of the survey. One microearthquake has been located near the epicentre of this earthquake. A low level of aftershock activity can also have been expected from the magnitude 5.2 crustal earthquake of 1972 December 21st and the magnitude 5.5 crustal earthquake of 1971 April 28th. For these earthquakes, M_{min} = 0.4 and 0.3 respectively. It is possible microaftershocks of these earthquakes have been located, as the mainshocks occurred close to the Dannevirke array.

Much of the clustering shown by microearthquakes located with the Dannevirke array cannot be accounted for by the above large earthquakes. Some of the clusters represent microearthquake mainshock-aftershock sequences. The best developed sequence of this kind is that of the magnitude 1.9 microearthquake of 1974 February 17th $00^h 35^m$, which occurred 20 km northeast of Dannevirke at a depth of 33.1 km. Three microaftershocks of this event, with magnitudes 1.2, 1.0 and 1.0, were located by virtue of their proximity to stations of the array. Other clusters of microearthquakes represent intermittent activity occurring in a localized area. The cluster 25 km west of Waipukurau is a good example of this. Microearthquakes comprising the concentration of activity 20 km southeast of Cape Turnagain are part of a sequence of 17 microearthquakes, ranging in magnitude from 1.3 to 2.9, which occurred in less than 12 hours on February 20th, 1974. Eight of the microearthquakes of this sequence were insufficiently recorded to be located, though S-P intervals suggest they occurred in the same region as the located microearthquakes of the sequence. The sequence resembles a swarm insofar as it does not include an outstanding, principal event. Earthquake swarms are not unknown along the east coast of the North Island, a recent good example being that which occurred some 60 km northeast of Napier during March and April of 1976. This swarm included 37 earthquakes between magnitudes 4.0 and 5.6, with no single event being outstanding (N.Z. Seismological Observatory, 1978b).

A feature of the vertical cross section of microearthquakes located with the Dannevirke array, shown in fig. 5.3, is the marked lack of activity shallower than 15 km. This precludes correlation

of microseismicity with surface faults. It is also in contrast with
the Wellington region, 200 km to the southwest, where diffuse activity
occurs above 15 km depth (Robinson, in press).

Microearthquakes shallower than 40 km, especially those of A
and B quality, define a band of activity which dips towards the northwest.
As discussed in sect. 4.2.2, this band of activity can be identified
with the crust of the subducted Pacific plate. It should be noted that
the group of three microearthquakes at about 30 km depth below the
Ruahine Range and the southeastern-most group of six microearthquakes
in fig. 5.3 have been located with some of their arrivals interpreted
as head waves refracted along horizontal discontinuities of the adopted
velocity model. As refractors below the Dannevirke array can be
expected to be dipping towards the northwest rather than horizontal,
these two groups of microearthquakes are likely to be deeper and
shallower, respectively, than shown in fig. 5.3, and may form extensions
of the dipping band of activity defined by other microearthquakes
shallower than 40 km.

While activity in the dipping band is fairly uniform below the
Dannevirke array in the direction of the microearthquake traverse,
this is not the case normal to the traverse. Fig. 5.4 illustrates
an abrupt decrease in activity of the band immediately northeast of
the Dannevirke array, which is underlain by a similarly abrupt increase
in deeper activity.

For the purpose of constructing a composite focal mechanism
diagram, all quality A and B microearthquakes were grouped together.
The first motion pattern produced, shown in fig. 5.5, is rather
consistent. A mixture of normal and strike-slip faulting is indicated.
Relative to the surface of the subducted plate below the array, normal
faulting predominates. Which nodal plane is to be preferred as the
fault plane is difficult to decide. Surface faulting in the region of
the Dannevirke array strikes predominantly north-northeast and shows
both dextral strike-slip and vertical movement (Kingma, 1962),
suggesting that the nodal plane striking at 45° is to be preferred
as the fault plane. On the other hand, the abrupt decrease in micro-
earthquake activity shallower than 40 km along the northeast edge of
the Dannevirke array, and the submarine Madden Canyon southeast of the
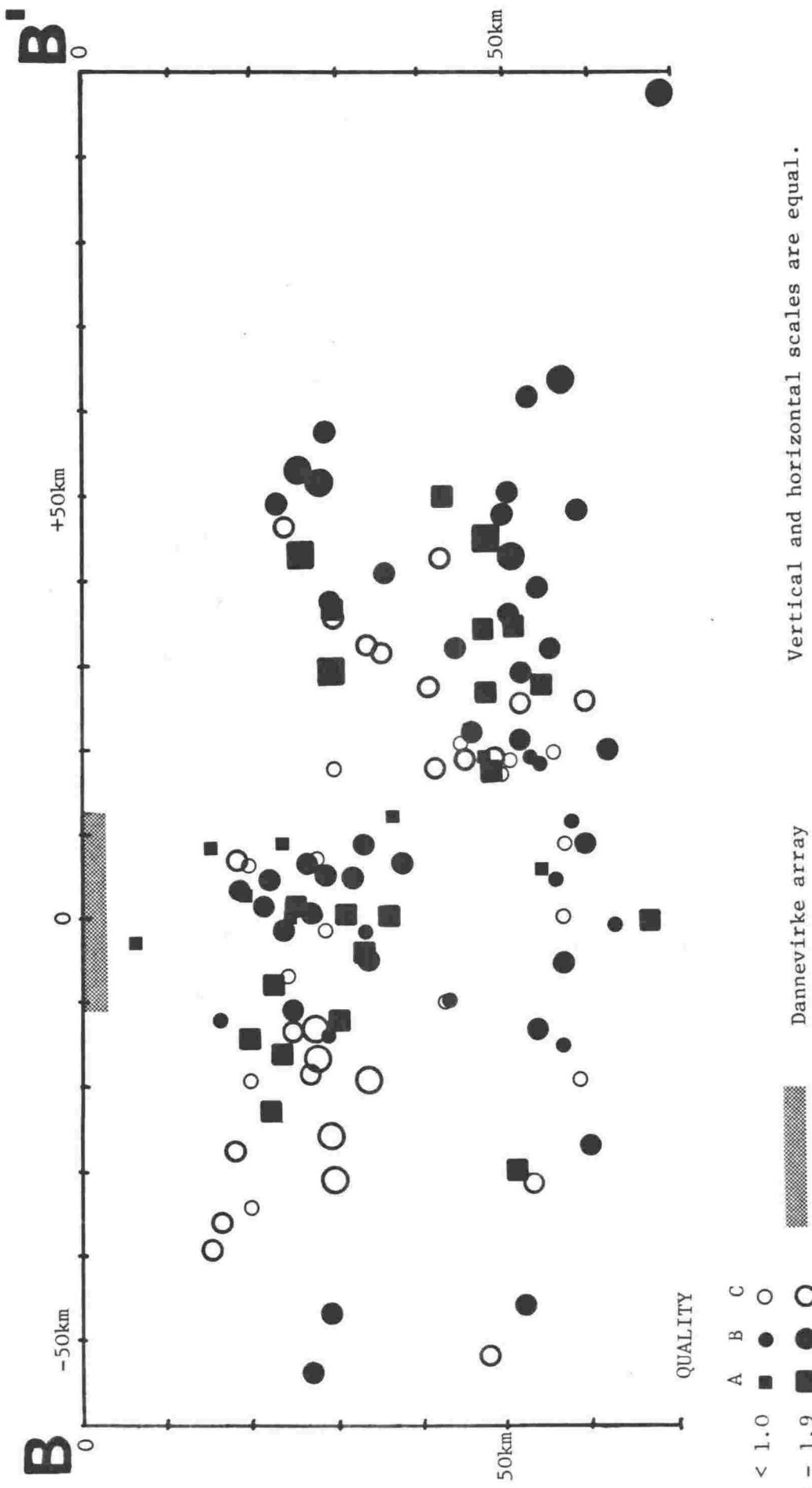
73

Figure 5.4 Vertical cross section along line B – B' of fig. 5.1 showing microearthquakes located with the Dannevirke array.
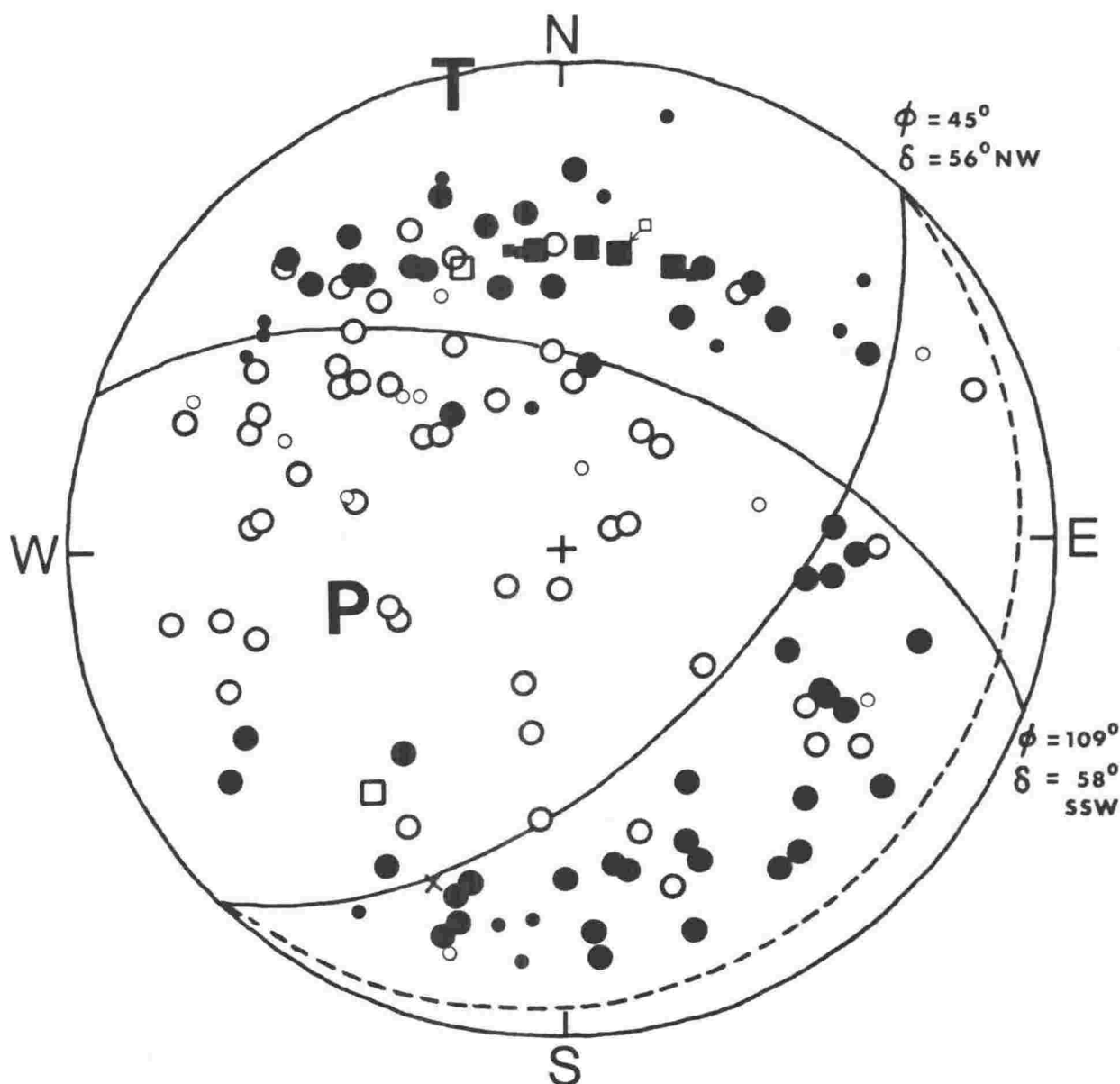
Figure 5.5 A composite focal mechanism for all quality A and B micro-earthquakes less than 40 km deep located with the Dannevirke array.

The diagram is an equal-area projection of the upper focal hemisphere. Open symbols represent dilatational P-wave first motions, solid symbols are compressions. Circles signify arrivals leaving the focus in an upward direction; squares are critically refracted arrivals projected from the lower hemisphere. Smaller symbols represent less reliable readings. X's denote near-nodal arrivals. For large X's, $S_z \geq 10 P_z$, while for small X's $S_z \geq 5 P_z$, where S_z and P_z are the maximum amplitudes of the S-wave and P-wave respectively. ϕ and δ are the strike and dip of the nodal planes, and P and T denote the axes of compression and tension respectively. The dashed curve shows the approximate orientation of the subducted plate below the Dannevirke array.

array (fig. 6.5), which both strike at approximately 130°, suggest the nodal plane striking at 109° may represent the fault plane.

5.2.2 Microearthquakes deeper than 40 km located with the Dannevirke array

The significant subcrustal microearthquake activity down to 70 km in depth located with the Dannevirke array was unexpected. Compared with crustal activity, very few subcrustal earthquakes have been routinely located in the region of the array by the Seismological Observatory (e.g. N.Z. Seis. Obs. Bulletins E145-E154). One possible reason for this is that the subcrustal activity seldom reaches a large enough magnitude to be well recorded by the national network of permanent seismographs. A more likely explanation is that subcrustal activity has been misinterpreted as crustal, as a consequence of deficiencies in the standard New Zealand crustal model and the poor azimuthal control provided by the permanent network in the region of the Dannevirke array, there being no stations to the southeast apart from Chatham Island, some 700 km away.

Other microearthquake studies of regions where a subducted plate lies at shallow depth have similarly revealed the existence of significant activity throughout much of the thickness of the subducted plate. A telemetered array in the Wellington region, New Zealand,has located microearthquakes up to 40 km below the surface of the subducted plate (Robinson, in press), while microearthquakes in the subducted Pacific plate in the region of the Japan Trench reach depths of about 70 km (Hasegawa et al., 1978).

The 40-70 km deep microseismicity below the Dannevirke array appears confined in the direction of dip of the subducted plate (fig. 5.3). Its southeastern boundary is likely to be real, since the resolving power of the array is good in this region, whereas its northwestern boundary may reflect a limit of detectability of the array. As can be seen from fig. 5.4, this microseismicity is continuous but non-uniform along the strike of the subducted plate, a sharp increase in activity in the 40-55 km depth range occurring northeast of the array.

The composite focal mechanism diagram produced when all 38 quality A and B microearthquakes deeper than 40 km located with the Dannevirke

array are grouped together is shown in fig. 5.6. Clearly these
microearthquakes do not share a common focal mechanism. Attempts were
made to define composite focal mechanisms for subsets of the micro-
earthquakes. For example, all events to the northeast of the array
were grouped separately from those below and to the southwest of the
array. Interpretation of the resulting composite focal mechanism
diagrams proved difficult, largely because of the small number of
first motions recorded from each microearthquake and the small spread
of data on the focal sphere, and no unambiguous focal mechanisms
were obtained.

5.2.3 Microearthquakes deeper than 40 km located with the Ruapehu
array

Apart from one event 42 km below the upper basin of the Wanganui
river, which will be discussed later together with shallower shocks
in the same region, these microearthquakes define a northwest-dipping
Benioff zone. Adoption of the velocity model for the Ruapehu array
described in sect. 4.2.4 has resulted in a greater number of well-
located hypocentres than that determined using the standard New Zealand
crustal model, as can be seen by comparing figs 5.3 and 4.1. Hypocentres
in fig. 5.3 are also shallower than those in fig. 4.1, because of the
lower velocity adopted for the upper mantle.

A conspicuous feature of the Benioff zone below the Ruapehu array
is the thin band of concentrated activity at the top of the zone.
Between the Ruahine Range and Mt Ruapehu, this band dips towards the
northwest at about 20°. When location errors are taken into account,
it appears likely that microearthquakes in this section of the band
originate in a zone about 10 km thick. This thickness, and correlation
of the band with the similar dipping band of activity below the Dannevirke
array identified with the crust of the subducted plate, both suggest
microearthquakes in the band originate in the crust of the subducted
plate.

Northwest of Mt Ruapehu, the dip of the band of activity at the
top of the Benioff zone steepens to about 70°. There are insufficient
microearthquakes in this section of the band to enable an estimate of
its thickness. Ansell & Smith (1975), who have studied the structure
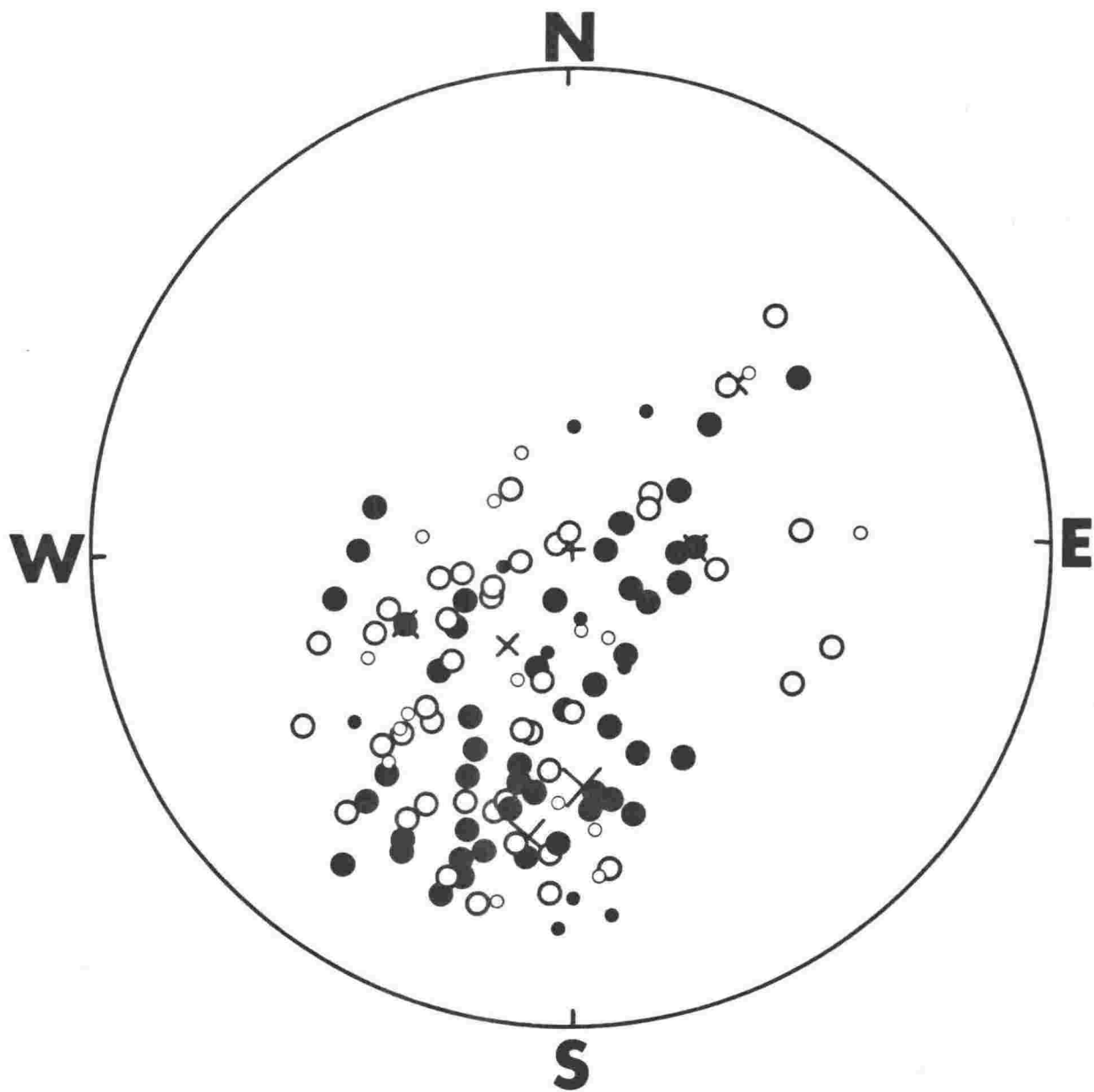
Figure 5.6 A composite focal mechanism diagram for all quality
A and B microearthquakes deeper than 40 km located with the
Dannevirke array. Symbols are as in fig. 5.5.

of the Benioff zone below the North Island using the homogeneous
station method, have suggested that below 100 km the zone is about
9 km thick. This result is in good agreement with the thickness of
the band of microearthquake activity at the top of the Benioff zone
between the Ruahine Range and Mt Ruapehu, and suggests Benioff zone
activity deeper than 100 km is also largely confined to the crust of
the subducted plate.

The prominent bend in the Benioff zone below Mt Ruapehu will
cause problems in the location of microearthquakes in the deeper
part of the zone to the northwest. Ray paths from these events to
southeastern stations of the Ruapehu array will lie partly within
the subducted plate, whereas ray paths to northwestern stations will
lie almost entirely outside it. As a velocity contrast for both P-
and S-waves of 6-10% between paths in and entirely out of the subducted
plate is present below the North Island (Smith, 1977), it is clear that
these events will be located southeast of their true positions. This
mislocation will increase as the depth of an event increases. The
laterally inhomogeneous velocity model of Adams & Ware (1977) compensates
for paths in and outside the subducted plate, and deeper than 100 km
the Benioff zone determined by these authors is to be preferred to
that defined by the microearthquakes of this study.

The four earthquakes underlying the prominent bend in the band
of activity at the top of the Benioff zone all occurred in the same
region, some 60 km southwest of Wanganui. It is unlikely that these
originated in the crust of the subducted plate and have been mislocated,
since nearby earthquakes have been located in the band of activity
identified with this crust. The location of the earthquakes suggests
they represent deformation in the mantle of the subducted plate resulting
from the significant bending of the plate.

A conspicuous feature of the epicentral distribution of micro-
earthquakes deeper than 40 km located with the Ruapehu array is the
southeast-northwest lineation of 10 epicentres passing close to
Mt Ruapehu. When continued into the region of the Dannevirke array,
this lineation coincides with the abrupt change in the depth distribution
of microseismicity along the northeast edge of the array.

The seven microearthquakes grouped beneath the Kaweka Range in fig. 5.2 occurred intermittently during the Ruapehu survey, and cannot be related to a prior large earthquake.

For the construction of a composite focal mechanism diagram, all microearthquakes in the band of activity at the top of the Benioff zone in the 40-100 km depth range were grouped together. This group comprises all microearthquakes interpreted as originating in the crust of the subducted plate except those deeper than 100 km, which are likely to be mislocated as described above. First motion data proved consistent near the centre, but inconsistent near the northeast and southwest edges of the resulting diagram. The inconsistency near the edges of the diagram can be explained when it is realized that as the epicentral distance of one of the above microearthquakes from the Ruapehu array increases, first arrivals are likely to be a mixture of direct phases and phases critically refracted along the subducted plate (cf. sect. 4.2.5), while all first arrivals were interpreted as direct phases in the construction of the diagram.

Because of uncertainties in the position and velocity structure of the top part of the subducted plate, and in the location of a microearthquake, it is difficult to ascertain whether a first arrival from a microearthquake at a large epicentral distance from the Ruapehu array represents a direct or critically refracted phase, and thus plot it accordingly. Consequently, microearthquakes likely to produce critically refracted arrivals were separated from those nearer the array. A measure of the closeness of a microearthquake to the array is provided by DM, the epicentral distance to the nearest station recording the microearthquake. As first motion data becomes inconsistent for microearthquakes with DM >36 km, these were grouped separately, as shown in fig. 5.7.

A well determined composite focal mechanism is defined by the eleven microearthquakes with DM <36 km, as shown in fig. 5.8. In any interpretation of focal mechanisms of Benioff zone earthquakes, allowance must be made for the refraction of P-waves at the upper boundary of the subducted plate (cf. Harris, 1975). The effect of such refraction on the position of the nodal planes of fig. 5.8 should be minimal, since both these planes are nearly perpendicular to the Benioff zone and hence the subducted plate. The alignment of the P and T axes of the
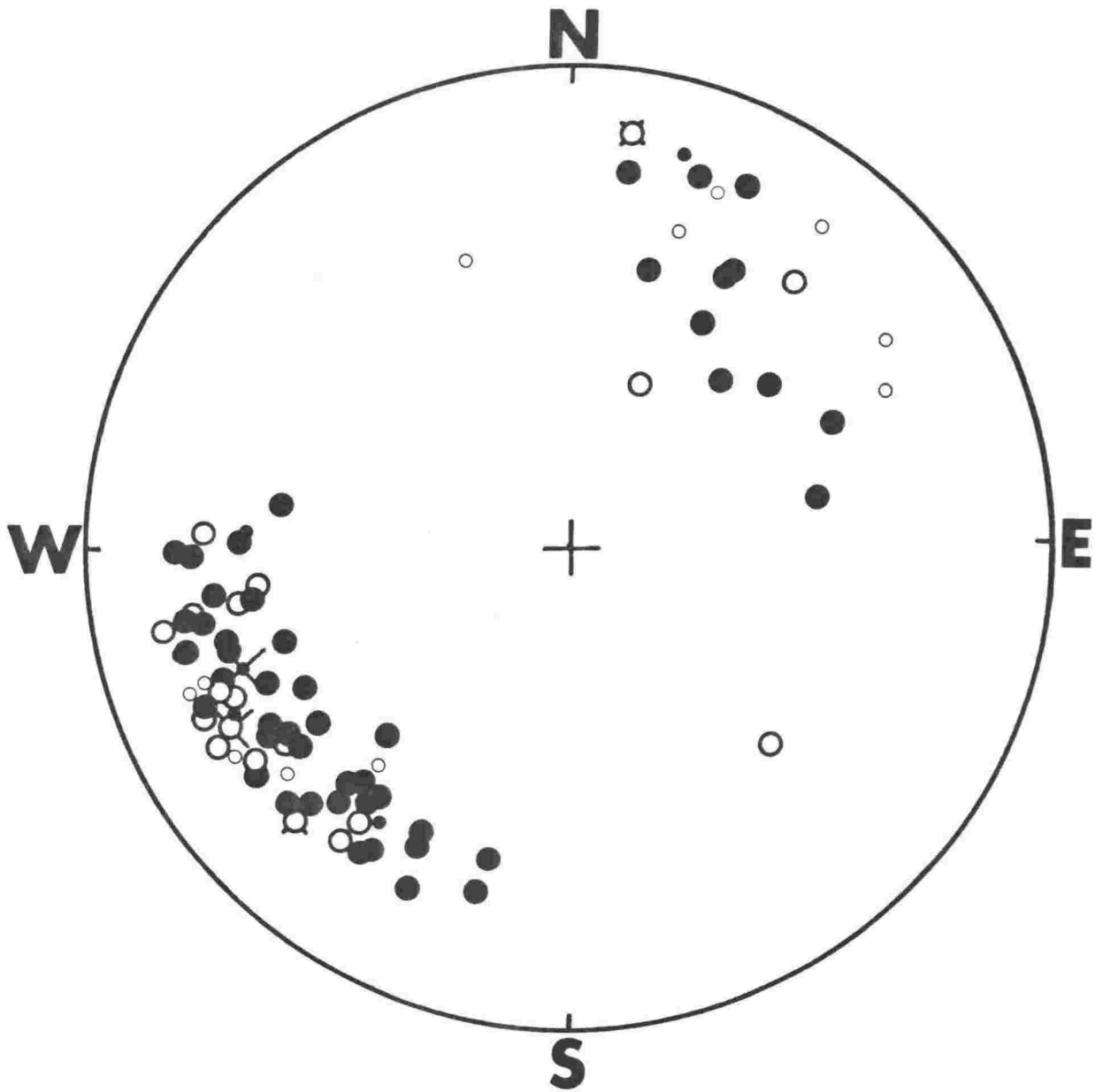
Figure 5.7 A composite focal mechanism diagram for microearthquakes in the band of activity at the top of the Benioff zone, 40 - 100 km deep, and with epicentral distance to the nearest station recording the microearthquake greater than 36 km. Symbols are as in fig. 5.5.

$\phi = 29°$
$\delta = 60°SE$

$\phi = 121°$
$\delta = 85°SW$
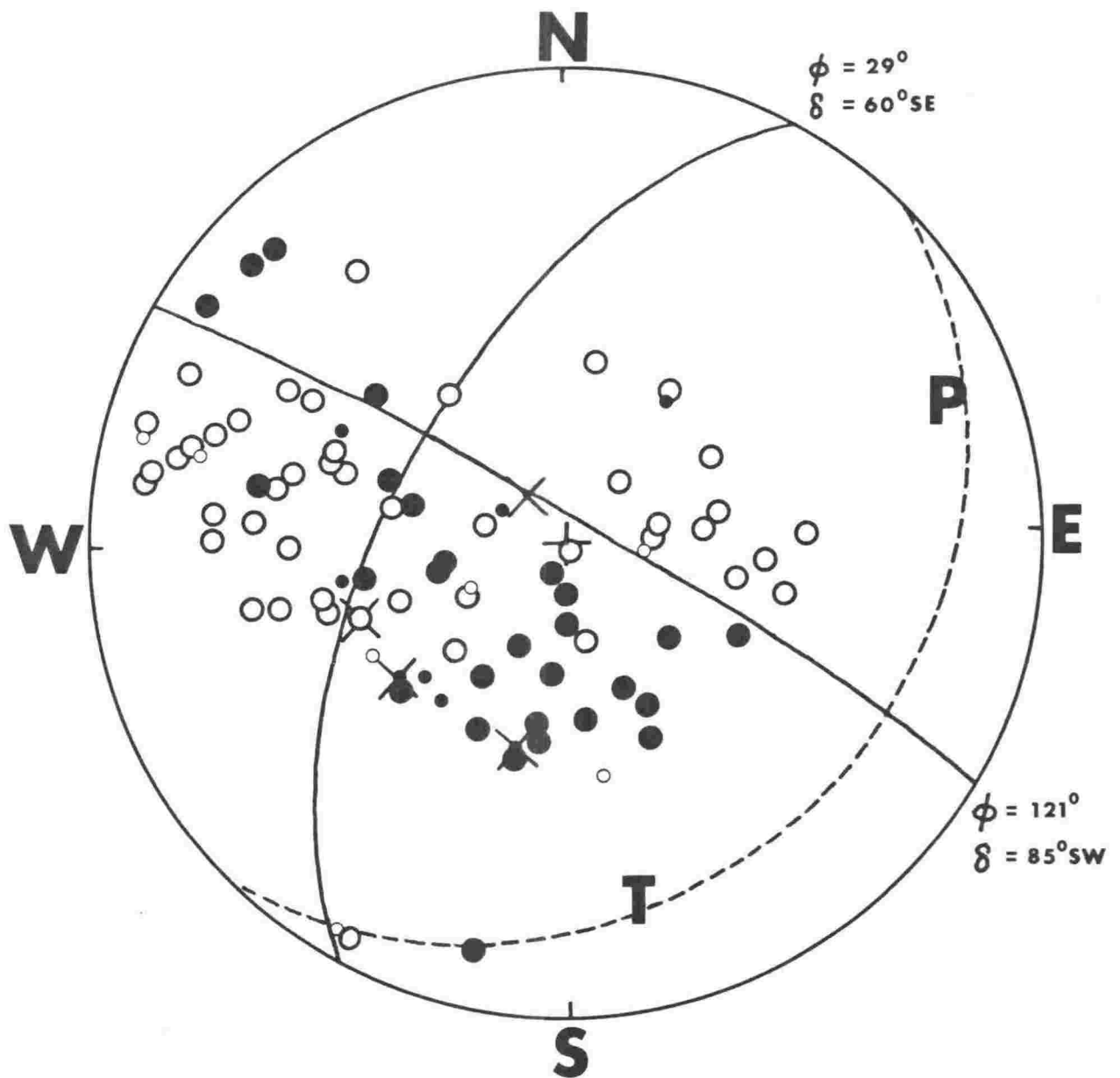
Figure 5.8 A composite focal mechanism for microearthquakes in the band of activity at the top of the Benioff zone, 40 - 100 km deep, and with epicentral distance to the nearest station recording the microearthquake less than 36 km. The dashed curve shows the average orientation of the subducted plate between 40 and 100 km depth. Symbols are as in fig. 5.5.

mechanism parallel to the Benioff zone indicates that the subducted plate acts as a stress guide, as suggested by Isacks & Molnar (1971). The significance of the azimuths of these axes will be discussed in the next chapter in conjunction with focal mechanism results from intermediate depth earthquakes below the North Island. The nodal plane striking at 121° is to be preferred as the fault plane, as eight of the eleven events defining the mechanism form part of the southeast-northwest lineation of microearthquakes discussed previously. Relative to the surface of the subducted plate, sinistral strike-slip motion is indicated on this near-vertical plane.

First motion data for the four Benioff zone microearthquakes deeper than 120 km are plotted in fig. 5.9. Although the data are insufficient to define a composite focal mechanism, they show good agreement with the nodal plane of fig. 5.8 which strikes at 121°. The definition of this plane should not be greatly affected by the previously discussed mislocation of the microearthquakes, as this mis-location is mainly in the direction of dip of the subducted plate. The good fit of a nodal plane of fig. 5.8 to the data of fig. 5.9 suggests that the stress regime in the crust of the subducted plate may be continuous across the prominent bend in the plate below Mt Ruapehu.

Because the four earthquakes underlying the prominent bend in the band of activity at the top of the Benioff zone occurred in a restricted area well outside the Ruapehu array, their first motion data, shown in fig. 5.10, cover a limited area of the focal sphere, and no composite focal mechanism can be defined.

5.2.4 Crustal microearthquakes near Waiouru

During the Ruapehu survey, a high level of crustal microearthquake activity was recorded near Waiouru (fig. 5.1). Persistent earthquake activity near Waiouru is also a feature of the longer term seismicity located by the Seismological Observatory, this activity being characterised by lower magnitude shocks which rarely reach magnitude 5.0. It is likely that a large part of the activity recorded during the Ruapehu survey represents microaftershocks of a magnitude 4.6 earthquake which occurred near Waiouru five weeks prior to the survey, since
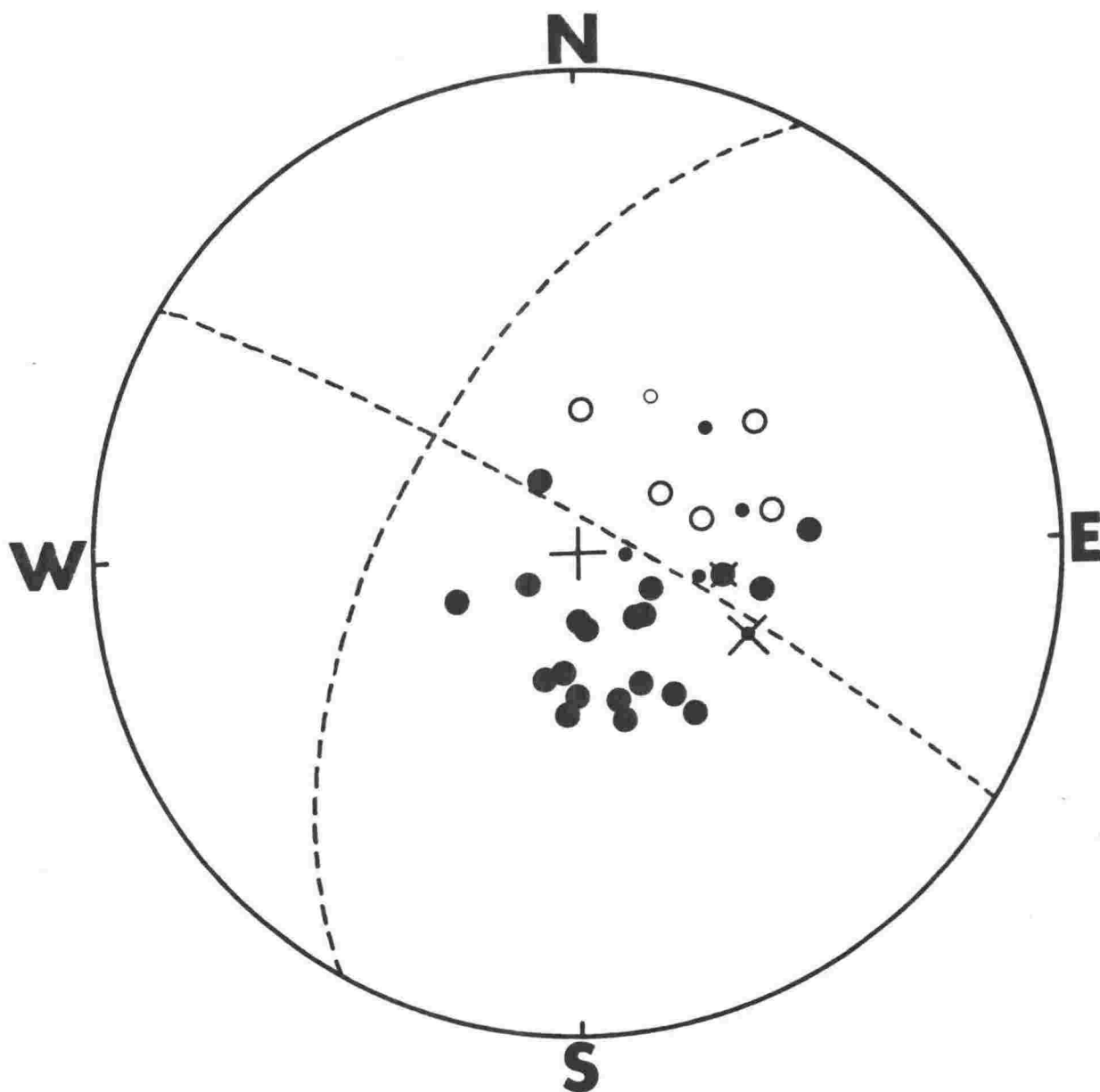
Figure 5.9 A composite focal mechanism diagram for the four
Benioff zone microearthquakes deeper than 120 km. The nodal planes
of the composite focal mechanism of fig. 5.8 (dashed lines) are
included for comparison. Symbols are as in fig. 5.5.
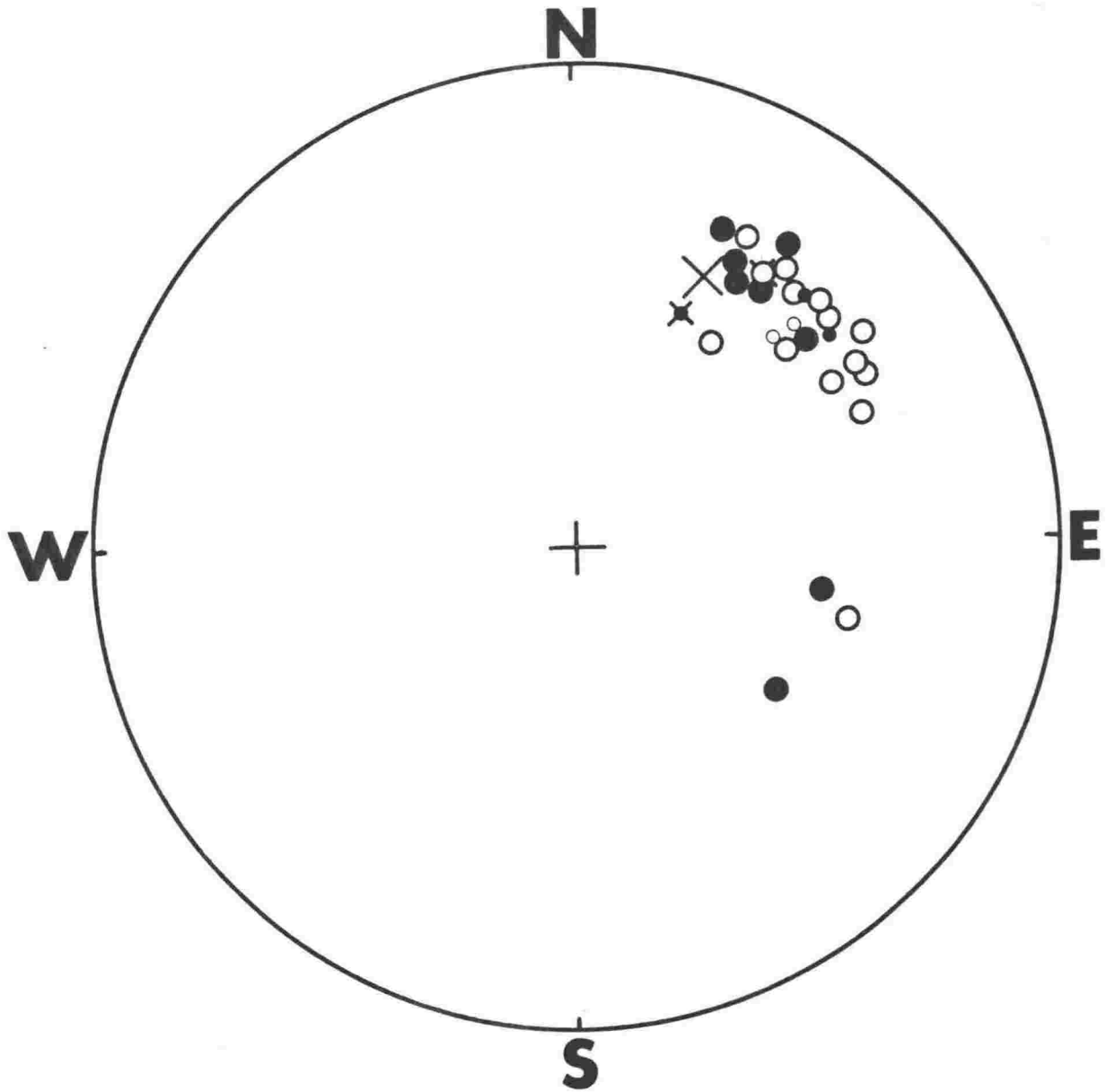
Figure 5.10 A composite focal mechanism diagram for the four
earthquakes underlying the prominent bend in the band of activity
at the top of the Benioff Zone. Symbols are as in fig. 5.5.

a)   the microearthquake hypocentres lie near the hypocentre of this
earthquake as determined by the Seismological Observatory and

b)   the level of microearthquake activity recorded is about that
expected for microaftershocks of the earthquake. The empirical
relation of Arabasz & Robinson (1976) for estimating the duration
of microaftershock sequences suggests microaftershock activity
of about one event per day of magnitude 0.7 or greater during
the Ruapehu survey. In fact 19 microearthquakes of magnitude 0.7
or more occurring during the 30-day Ruapehu survey were located
near Waiouru, indicating a level of activity in good agreement with
the estimated level of microaftershock activity, considering the data
set of located microearthquakes in this region cannot be considered
complete at the 0.7 magnitude level because of the location criteria
adopted.

The scatter of microearthquake hypocentres near Waiouru shown
in figs 5.11 and 5.12 is greater than that normally expected for
microaftershocks of a magnitude 4.6 earthquake. For example, the
empirical formula of Utsu (1961), namely $\log D = 0.5M - 1.8$, estimates
the linear dimension (D) of the aftershock area of an earthquake with
a magnitude (M) of 4.6 as about 3 km. In order to determine if this
scatter is real and not caused by different subsets of stations being
used to locate different microearthquakes, nine microearthquakes were
relocated using the homogeneous station method. This method requires that
the same phases from the same set of stations are used to locate each
microearthquake. The homogeneous data set used included seven phases:
the P recorded at WUB, and both the P and S recorded at TMO, TNG and WHA.
All P readings were equally weighted in the hypocentre calculation, as
were all S readings, and the HYPO71 options of azimuthal weighting and
Jeffreys' weighting of residuals were not used.

The distribution of the relocated hypocentres is similar to that
of the original hypocentres, the difference between the two solutions
being less than the standard errors of location for the majority of the
microearthquakes. The scatter of the hypocentres persists, and there
appears to be no enhancement of the lineations and clustering evident
in the original hypocentres. The congruence of hypocentres determined
by the two methods demonstrates the efficiency of the station corrections
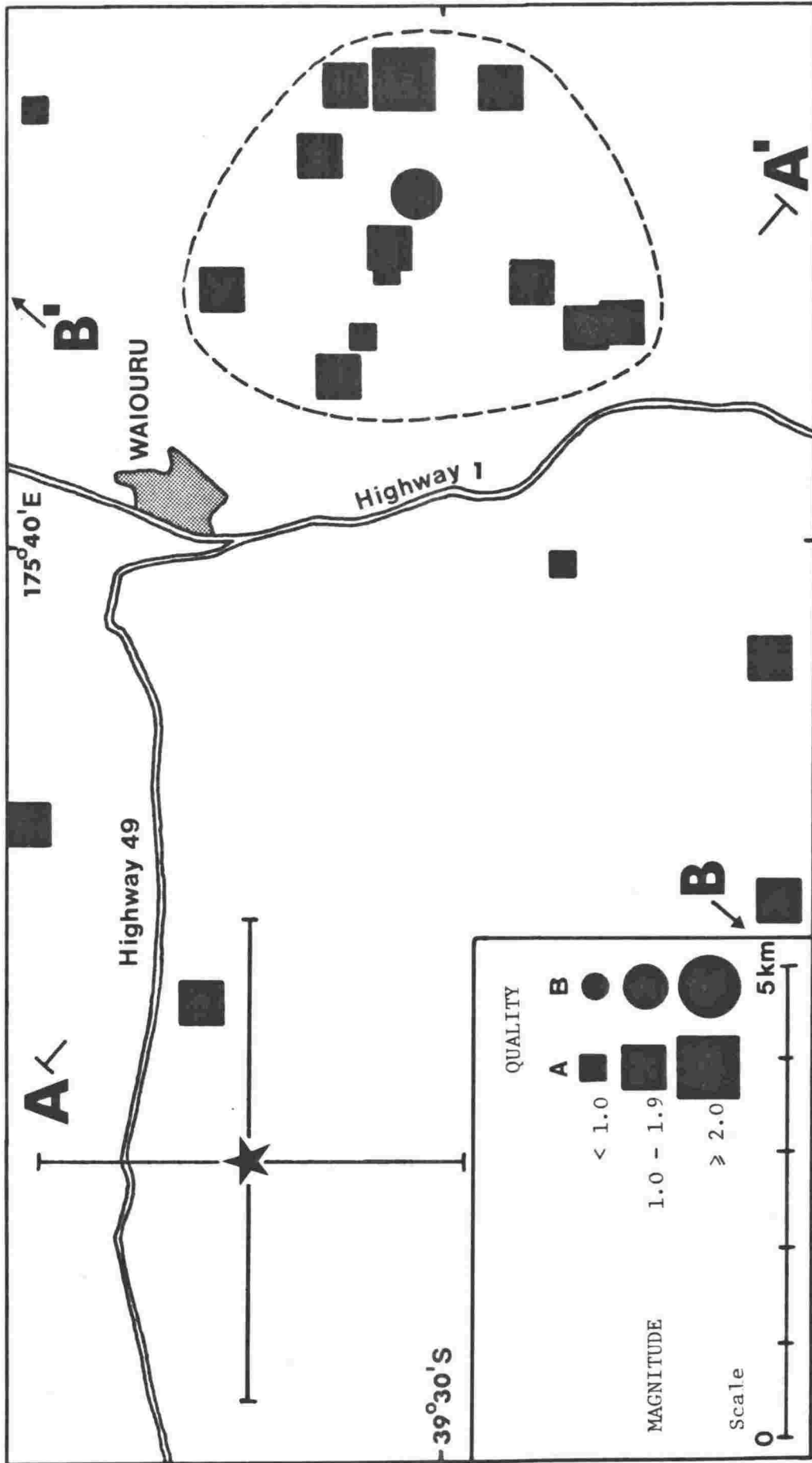
Figure 5.11 Epicentres of microearthquakes near Waiouru located with the Ruapehu array. The star indicates the epicentre (with standard error bars) of the earthquake of 1974 August 25th 19^h 46^m determined by the Seismological Observatory. The dashed line encloses microearthquakes used in the construction of fig. 5.14.
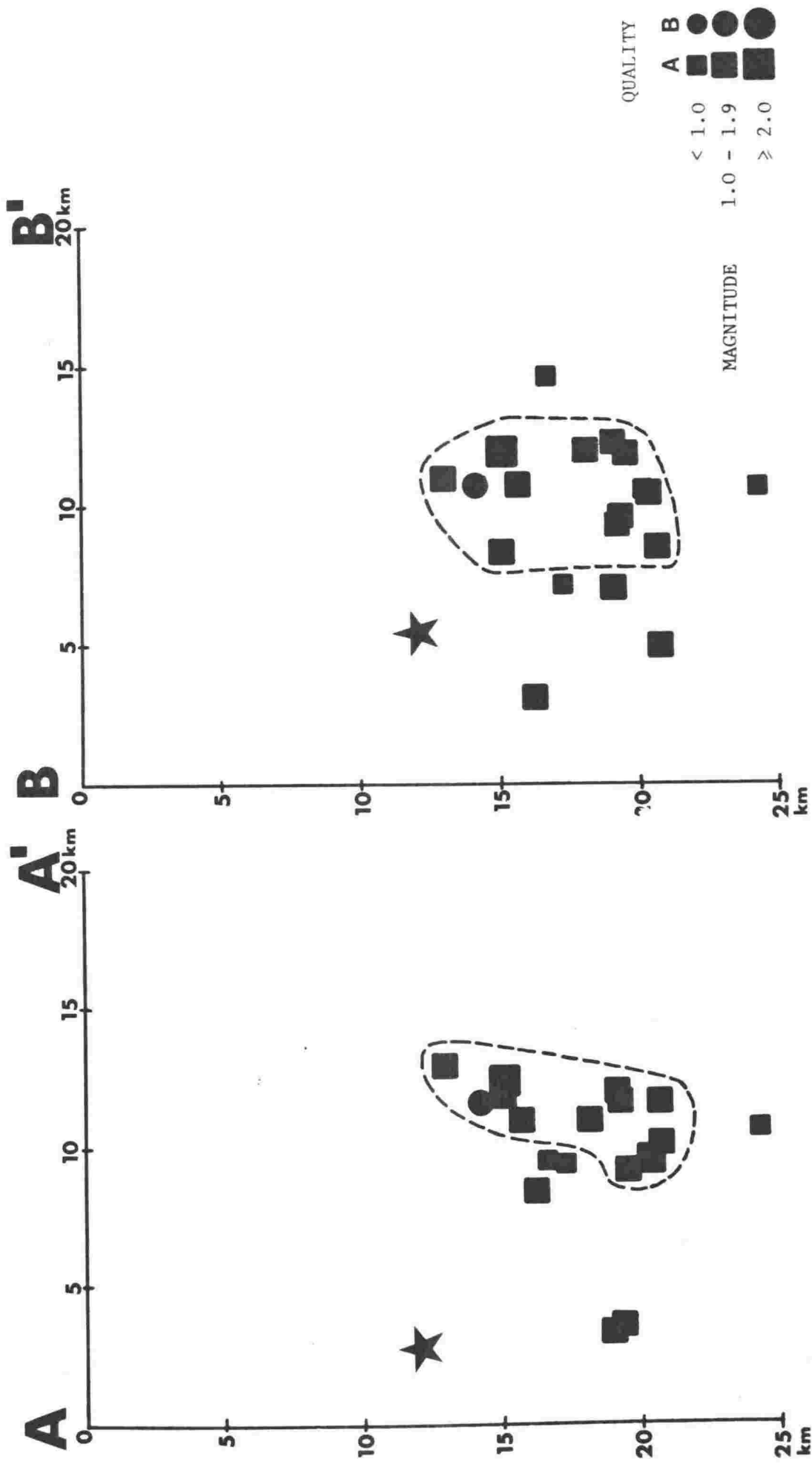
Figure 5.12 Vertical cross sections of microearthquake activity near Waiouru located with the Ruapehu array. The location of the sections is shown in fig. 5.11. The star denotes the earthquake of 1974 August 25th 19^h 46^m, the depth of which was restricted to 12 km by the Seismological Observatory for the purpose of hypocentre calculation. The dashed lines enclose microearthquakes used in the construction of fig. 5.14.

and azimuthal weighting routinely used in the determination of the hypocentres of Ruapehu survey microearthquakes in minimizing the effect of using different subsets of stations to locate different microearthquakes.

A composite focal mechanism diagram for all microearthquakes near Waiouru is shown in fig. 5.13. Interpretation of the diagram is rendered difficult by the great predominance of compressions over dilatations and the lack of data in the northeast quadrant of the focal sphere. The positions of the nodal planes of the double-couple solution shown were dictated by the large areal distribution of compressions. Although both the near-nodal arrivals and the few dilatations indicate a nodal plane dipping towards the northeast at a low angle, its exact position is uncertain owing to the reduced reliability of data near the edge of the focal sphere (see sect. 4.5).

Subsets of the microearthquakes indicate composite focal mechanisms very similar to that of fig. 5.13. For example, fig. 5.14 shows that an adequate solution of the composite focal mechanism diagram of the tight cluster of activity immediately southeast of Waiouru outlined in figs 5.11 and 5.12 is provided by the nodal planes of fig. 5.13.

The composite focal mechanism shown in fig. 5.13 indicates predominantly thrust movement on either a steeply-dipping plane striking at 128° or a gently-dipping plane striking at 120°. Which plane is to be preferred as the fault plane cannot be ascertained from the surface geology. In contrast to the nodal planes of fig. 5.13, Recent faulting near Waiouru strikes N-S and ENE-WSW (N.Z. Geological Survey, 1973). A preferred fault plane is also not suggested by the distribution of the microearthquake hypocentres.

5.2.5 Crustal microearthquakes near Taihape

Although the Ruapehu array provided good coverage of the Taihape region, only five crustal microearthquakes were located there, all these being to the west of Taihape, as shown in fig. 5.1. These all occurred in the lower crust, the depth of the events increasing towards the southwest. The composite focal mechanism diagram for these micro-earthquakes (fig. 5.15) is fairly consistent. However a lack of data in the southern half of the focal sphere leads to poor control of the
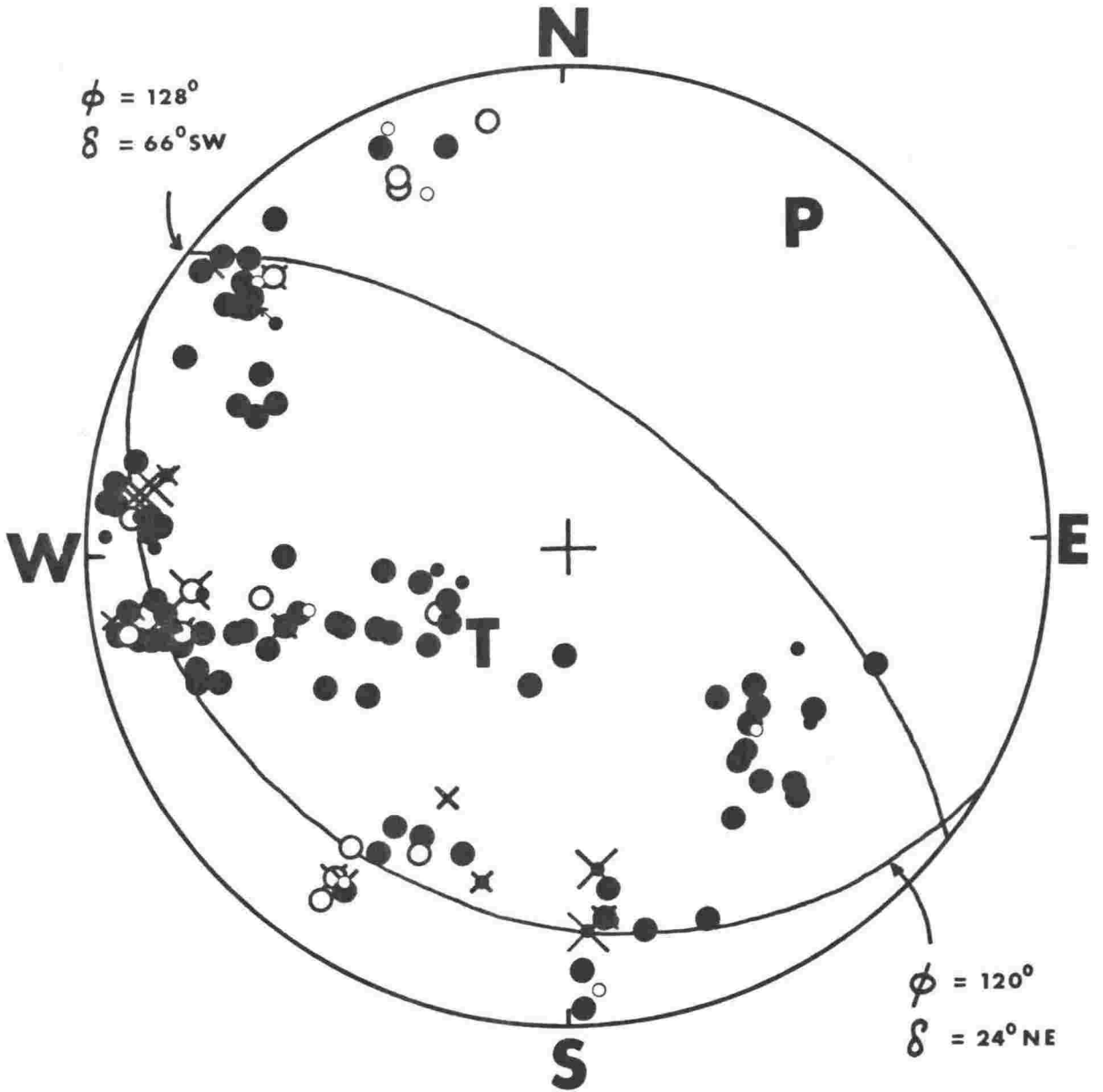
Figure 5.13 A composite focal mechanism for all microearthquakes near Waiouru. Symbols are as in fig. 5.5.

90
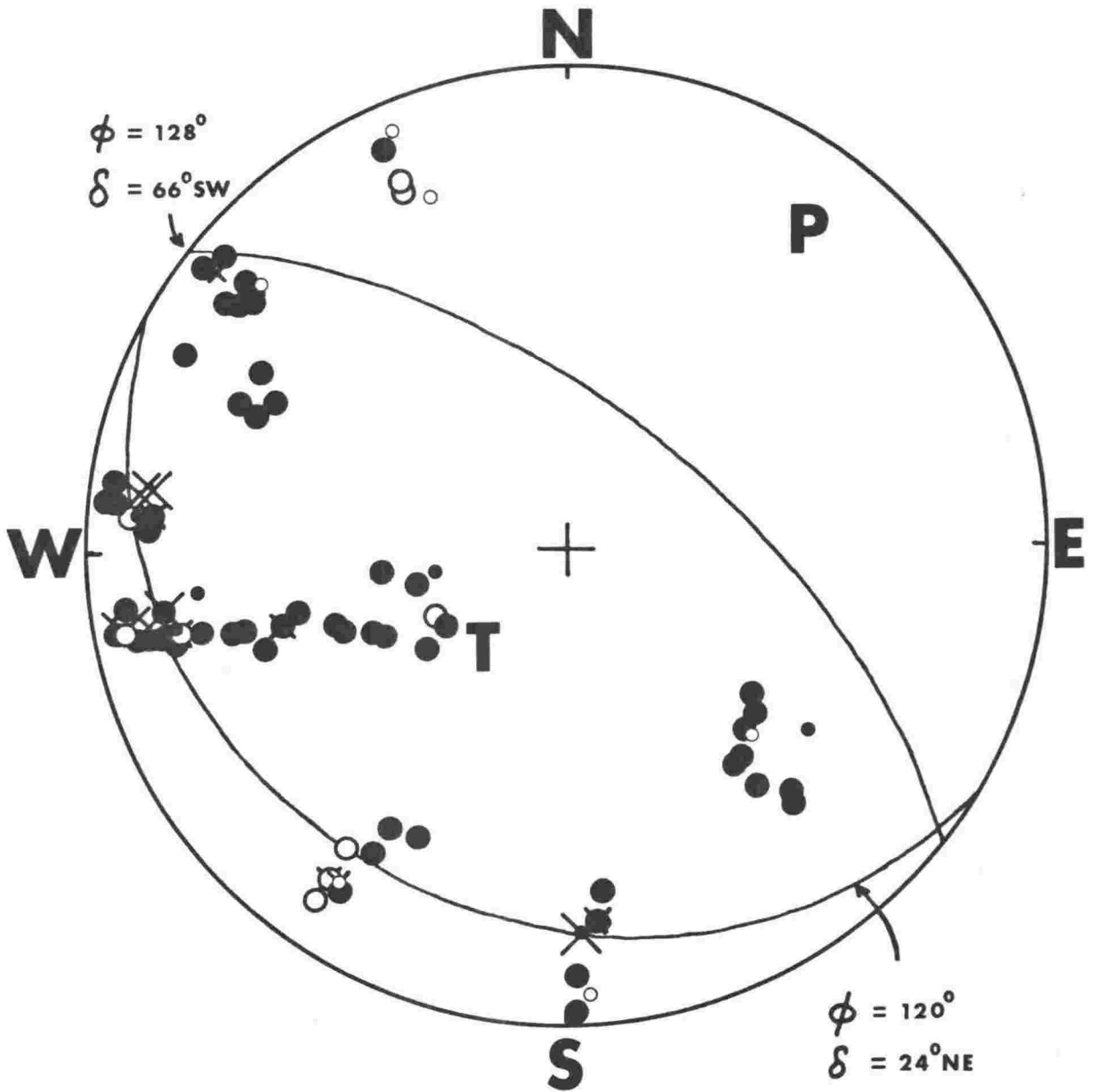
Figure 5.14 A composite focal mechanism for the tight cluster of microearthquakes immediately southeast of Waiouru outlined in figs. 5.11 and 5.12. Symbols are as in fig. 5.5.
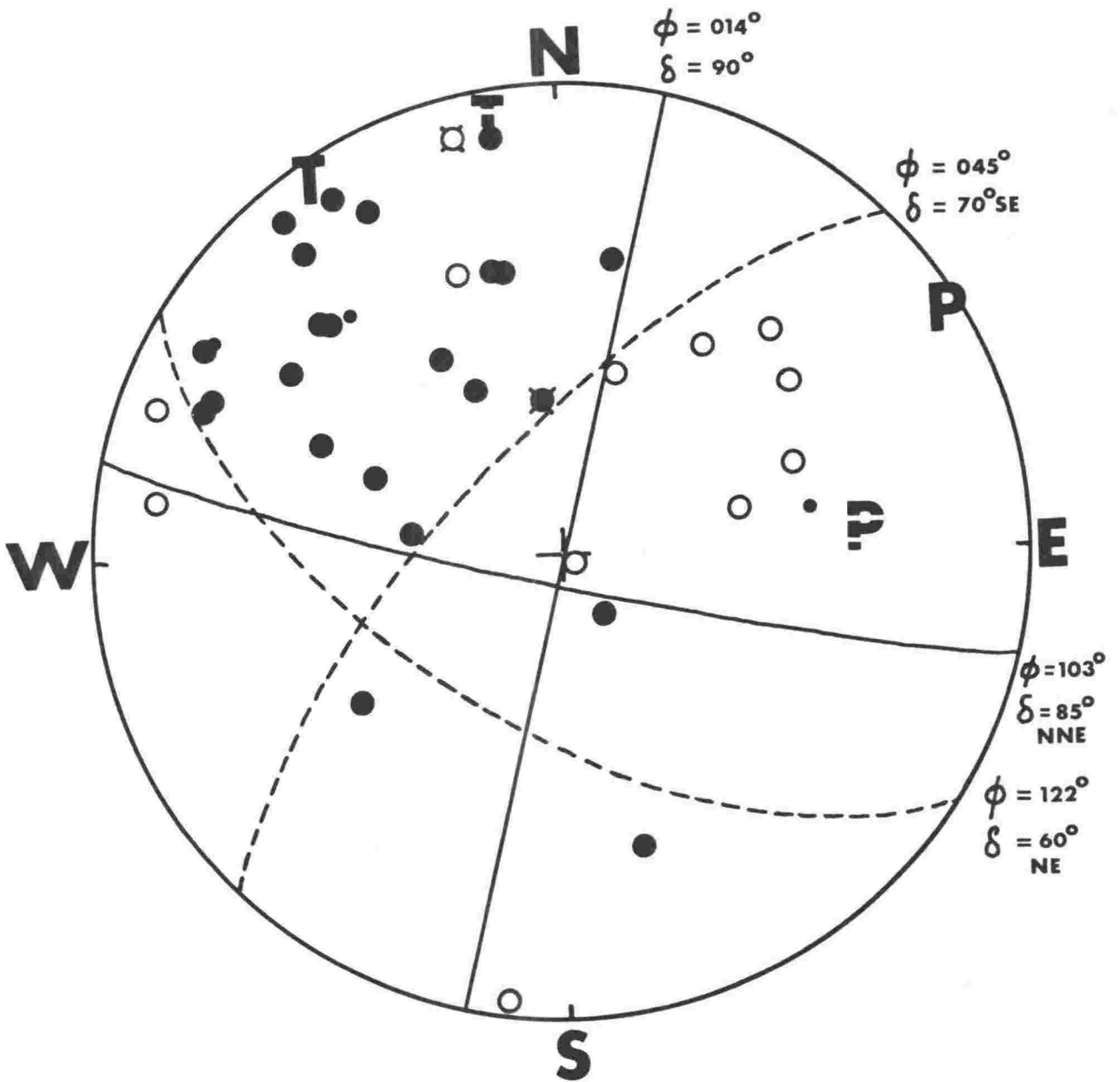
Figure 5.15 A composite focal mechanism diagram for crustal
microearthquakes near Taihape. Two equally valid double-couple
solutions are shown by the solid and dashed nodal planes. Symbols
are as in fig. 5.5.

nodal planes of a double-couple solution, and two equally valid solutions
are shown. Strike-slip faulting is indicated by the solid nodal plane
solution, while the dashed nodal planes indicate a mixture of strike-slip
and normal faulting, the strike-slip component predominating. If
microearthquakes occurring in the lower crust can be related to surface
geology, the NNE and NE nodal planes of fig. 5.15 are to be preferred as
the fault planes, as these planes have a similar strike to the major
faults of the Taihape region (fig. 2.7). Also, dextral strike-slip motion
on these planes is in agreement with Recent movement on the major faults
(Kingma, 1962).

5.2.6 Shallow microearthquakes in the upper basin of the Wanganui River

During the Ruapehu survey, a large number of shallow microearthquakes
occurred in the upper basin of the Wanganui River, west of Mt Ruapehu.
The epicentral distribution of these microearthquakes (fig. 5.1) is very
similar to that of the correspondingly large number of larger earthquakes
that occurred in the same area in the nineteen-year period prior to the
survey (fig. 2.4). In both cases the activity is elongated in an east-
west direction, and stretches from Mt Ruapehu to just west of the township
of Whangamomona. The vertical cross section shown in fig. 5.3 reveals
microearthquakes in the western part of the basin are largely confined to
the 29 to 42 km depth range, while those in the east of the basin extend
from the lower crust almost to the surface.

The first motion data of the microearthquakes suggest a variation
in focal mechanism with depth, and the microearthquakes have been divided
into subsets to monitor this change. Because its first motion pattern
differs markedly from that of all the other microearthquakes, the
shallowest event has been considered separately (fig. 5.16). The first
motion data of the remaining microearthquakes can be satisfactorily
explained by two composite focal mechanisms, one for events between 5 and
25 km deep (fig. 5.17), the other for events between 25 and 42 km deep
(fig. 5.18).

It is possible, assuming a double-couple model, to fit quadrantal
nodal planes to the first motions in fig. 5.16. The simplest interpretation
is one of thrust faulting, although the orientation of the P-axis of
such a mechanism cannot be determined from the scant data. An interesting
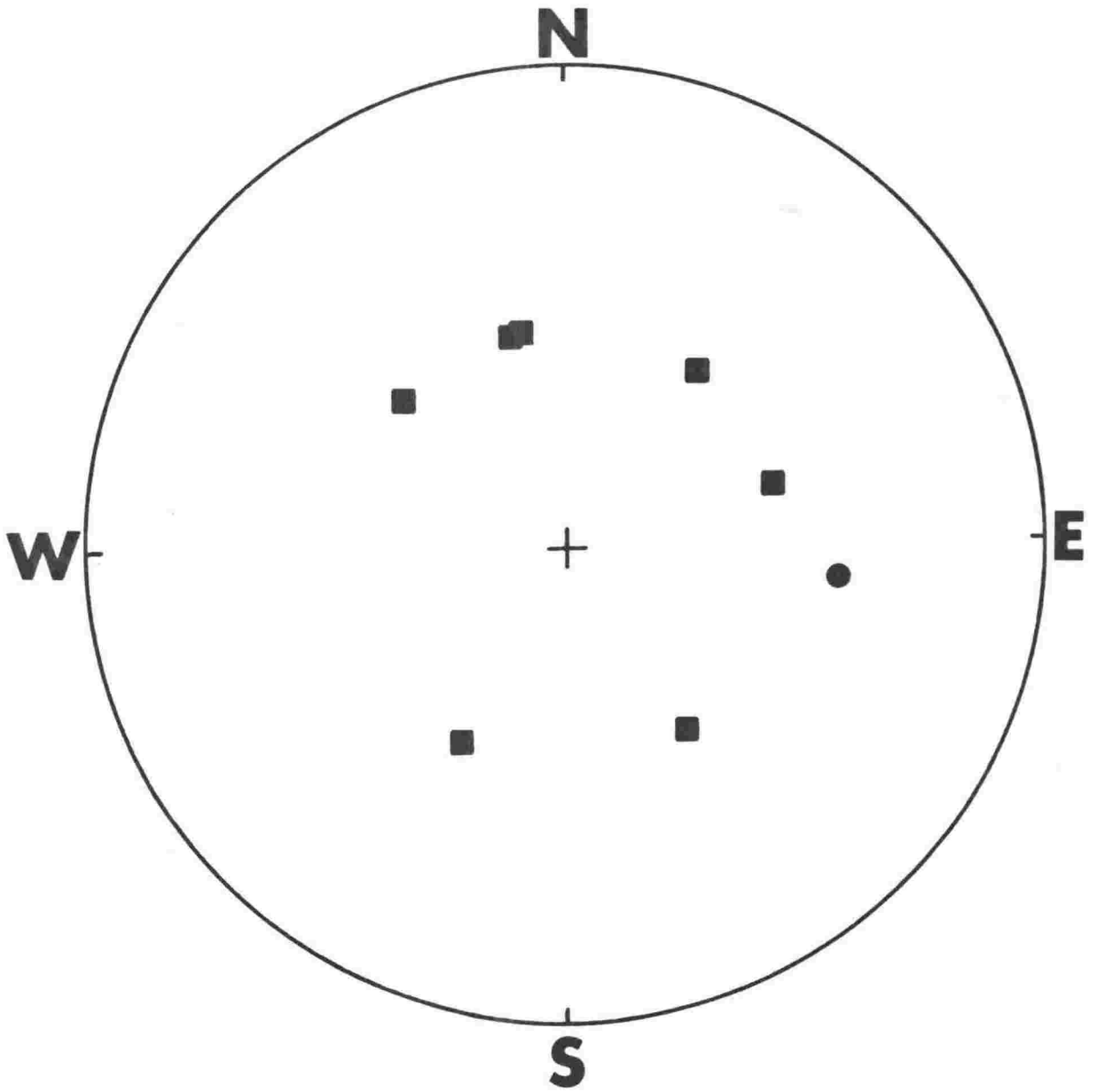
Figure 5.16 First motions of the microearthquake of 1974 October 3rd
05^{h}30^m, which occurred near Ohakune at a depth of 1.4 ± 0.4 km.
Symbols are as in fig. 5.5

Figure 5.17 A composite focal mechanism for microearthquakes between 5 and 25 km deep occurring in the upper basin of the Wanganui River. Symbols are as in fig. 5.5.
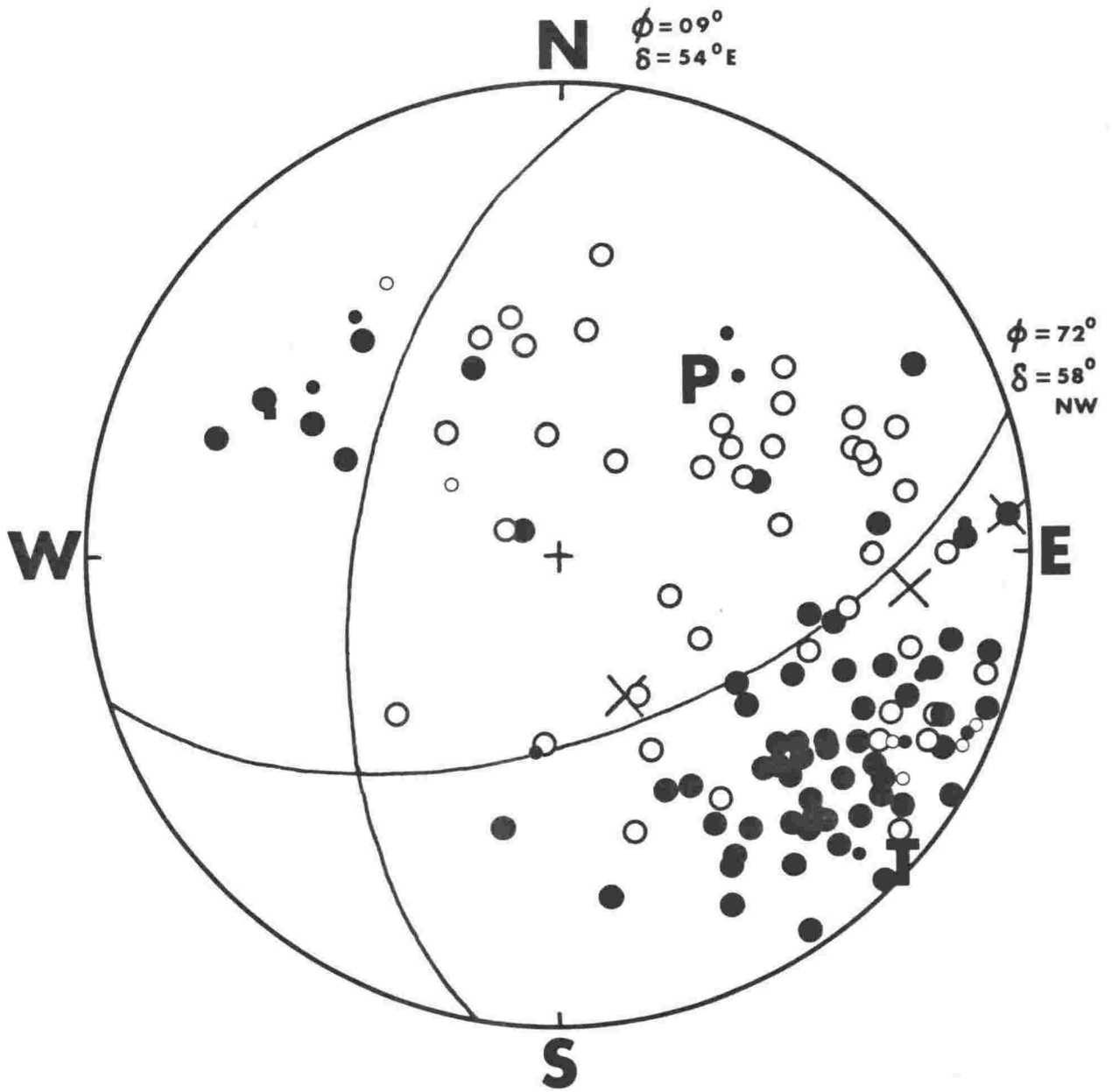
Figure 5.18 A composite focal mechanism for microearthquakes between 25 and 42 km deep occurring in the upper basin of the Wanganui River. Symbols are as in fig. 5.5.

alternative explanation of the first motion pattern is that of an explosive mechanism associated with volcanic activity. Such a mechanism is suggested by the shallow focus of the microearthquake (1.4 ± 0.4 km) and its location less than 2 km north of a group of at least five volcanic vents 1 km NW of Ohakune (Cole, 1978).

The nodal planes of fig. 5.17 are well determined by both first motions and near-nodal arrivals, and indicate pure normal faulting. The east-west strike of both these planes parallels the trend in micro-earthquake epicentres (fig. 5.1), isogals of the Bouguer and isostatic gravity anomalies (Reilly et al., 1977) and the strike of Recent faulting (Hay, 1967) in the upper basin of the Wanganui River. On the basis of surface faulting near Raetihi, which is consistently downthrown to the south (Hay, 1967), the southerly-dipping nodal plane is to be preferred as the fault plane.

The composite focal mechanism for microearthquakes between 25 and 42 km deep (fig. 5.18) is again well determined. Movement has been either dextral with a slightly smaller normal component on a plane striking at 009°, or sinistral with an equal normal component on a plane striking at 072°. Which plane is to be preferred as the fault plane is not suggested by the microearthquake distribution.

The first motion data of microearthquakes occurring in the upper basin of the Wanganui River are insufficient to resolve whether the change in focal mechanism with depth apparent in figs 5.17 and 5.18 represents a gradual change or a discontinuity in the stress field. The 25 km depth used to partition the microearthquakes was chosen merely to give the best separation of the first motion data into two composite focal mechanisms. There is no evidence to suggest a physical discontinuity is present at this depth.

5.2.7 Shallow microearthquakes in the lower basin of the Wanganui River

This group of five microearthquakes is centred some 20 km NNE of Wanganui city (fig. 5.1). Microearthquakes of the group show a similar depth distribution to those occurring in the western part of the upper basin of the Wanganui River, their depths ranging from 25 to 38 km. The first motion data of the microearthquakes are poorly distributed in a composite focal mechanism diagram (fig. 5.19), owing to the occurrence of the events in a restricted area outside the Ruapehu array. Nevertheless,
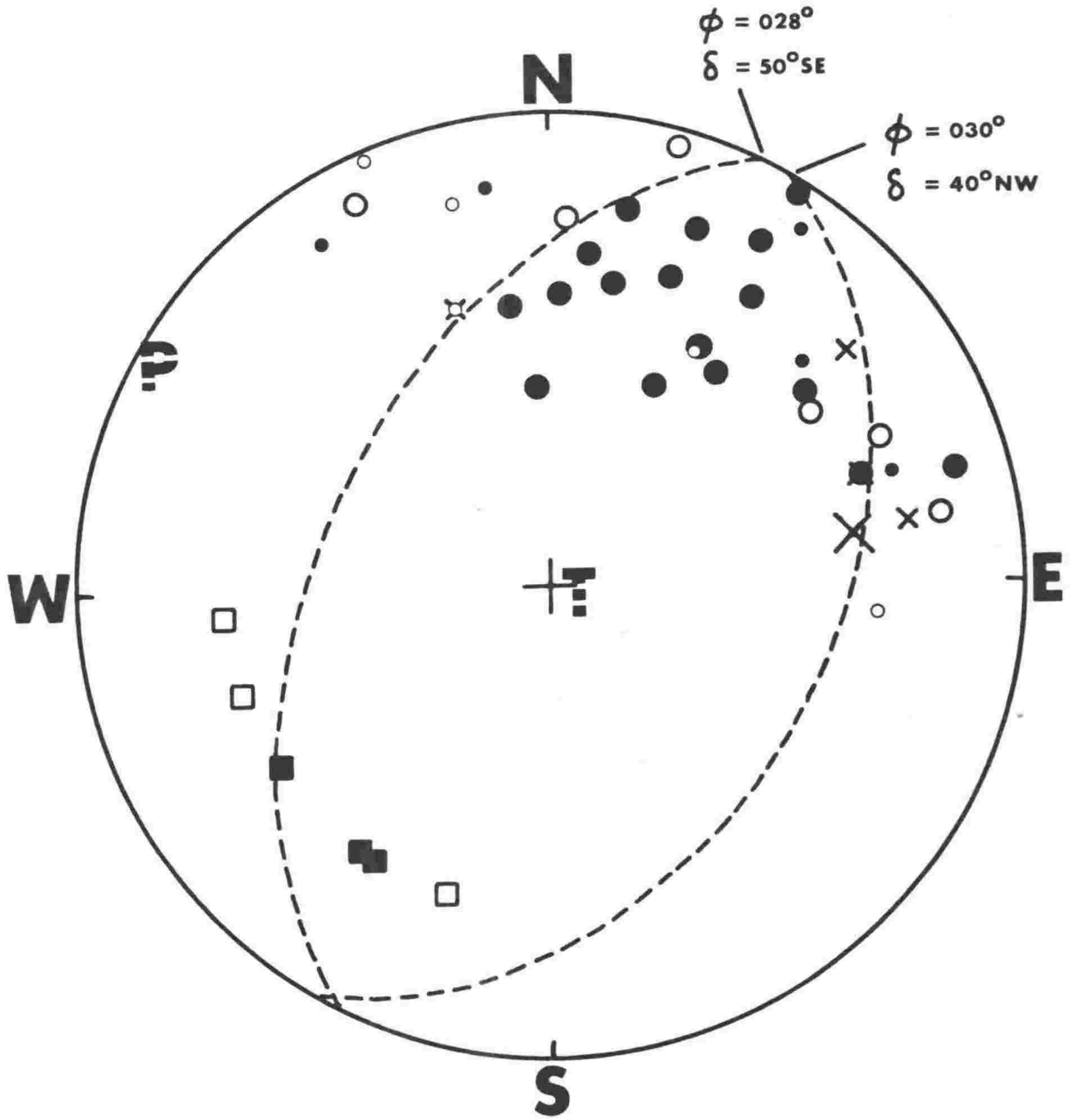
Figure 5.19 A tentative focal mechanism for microearthquakes between
25 and 38 km deep occurring in the lower basin of the Wanganui River.
Symbols are as in fig. 5.5.

some consistency in the data is apparent, and tentative nodal planes, shown dashed in fig. 5.19, can be fitted. The NE-SW elongation of the microearthquake epicentres is in general agreement with the strike of both these nodal planes. Thrust faulting is indicated by the tentative nodal planes, a mechanism markedly different from the mixture of strike-slip and normal faulting determined for microearthquakes in a similar depth range in the upper basin of the Wanganui River. Surface faulting is also at variance with the tentative mechanism, since although it strikes NE, it is predominantly normal (Lensen, 1959).

5.2.8 Microearthquakes immediately south of the city of Wanganui

A conspicuous feature of the shallow seismicity of the North Island is the frequent occurrence of earthquakes within a small area situated 20 km south of the city of Wanganui (fig. 2.4). As shown in fig. 5.1, this feature is reproduced by microearthquakes located with the Ruapehu array. Thirty microearthquakes, ranging in magnitude from 2.3 to 3.4, were located immediately south of Wanganui. The magnitude distribution of these microearthquakes indicates a high value of the coefficient b in the frequency-magnitude relationship of Gutenberg and Richter; this is also suggested by the numerous earthquakes located by the Seismological Observatory in the same region, which rarely exceed magnitude 4.5.

The velocity model used to determine hypocentres of these micro-earthquakes differed from that in sect. 4.2.4 in that it incorporated an upper mantle velocity of 7.80 km/sec, which has been found by Haines (1976) to be appropriate for the Wanganui region. An interesting feature of the hypocentre determinations was that arrivals at the permanent station MNG, some 75 km southeast of the microearthquake activity (fig. 2.7), disagreed with hypocentres determined with the Ruapehu array. These arrivals were consistently early, by up to 1.5 sec for the P-wave, indicating that paths to this station are of higher velocity than paths to the stations of the Ruapehu array. The depth of the microearthquakes suggests the first arrivals seen at MNG are likely to be head waves, refracted either along the Mohorovičić discontinuity of the Indian plate or along the top of the underlying subducted plate. Both these paths can be expected to be of higher velocity than paths to stations of the Ruapehu array (Haines, 1976; Smith, 1977). Because of this difference in path, MNG readings were not used in the determination of the microearthquake hypocentres.

The 30 microearthquakes located cluster more tightly than earthquakes in the same region located by the Seismological Observatory, a circle of radius 12 km serving to delimit their epicentres. As the microearthquakes occurred well outside the Ruapehu array, depth control is generally poor. Nevertheless, the 9 hypocentres of quality A and B, which range from 28 to 33 km in depth, suggest the microearthquake activity is likely to be tightly clustered in depth.

The first motion data of a composite focal mechanism diagram for the quality A and B microearthquakes (fig. 5.20) show little consistency, and no double-couple solution has been attempted. The inconsistency of the data may in part be due to errors in the interpretation of first arrivals as direct waves (P*) or head waves (Pn) arising from errors in the velocity model used to determine the microearthquake hypocentres. The possibility that the earthquake activity immediately south of Wanganui has a consistent mechanism is suggested by the earthquakes located there by the Seismological Observatory, the great majority of which produce compressional first motions at MNG (E.G.C. Smith, pers. comm.,1978). All first motions of the microearthquakes recorded at MNG were also compressions.
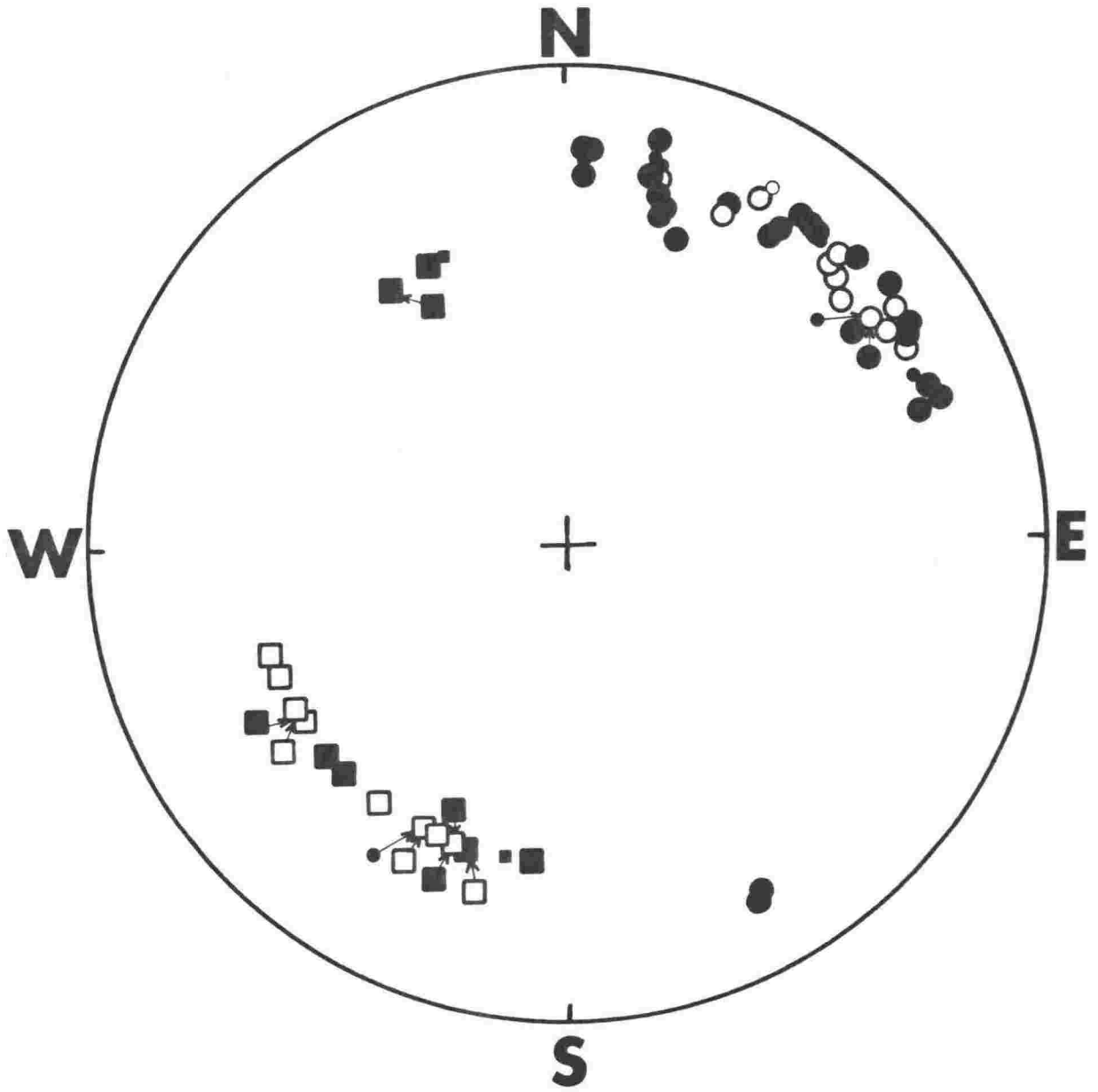
Figure 5.20 A composite focal mechanism diagram for quality A and B microearthquakes of the dense cluster of activity immediately south of the city of Wanganui. Symbols are as in fig. 5.5.

CHAPTER 6

ACTIVE DEFORMATION AT THE NORTH ISLAND PLATE BOUNDARY

6.1 ACTIVE DEFORMATION OF THE PACIFIC PLATE

6.1.1 The geometry of the subducted Pacific plate

When microearthquakes located in this study are combined with well-located earthquakes deeper than 100 km, as shown in fig. 6.1, a fairly complete cross section of the Benioff zone associated with the subducted Pacific plate is obtained. The open triangles in fig. 6.1 denote earthquakes studied by Ansell & Smith (1975) using the homogeneous station method and subsequently relocated with a laterally inhomogeneous velocity model by Adams & Ware (1977). The epicentres of all earthquakes and microearthquakes shown in fig. 6.1 lie within 132 km of the line of section. Microearthquakes thought to be badly mislocated owing to inadequacies in the velocity model, as discussed in the previous chapter, have been omitted from fig. 6.1. Those omitted are the four microearthquakes deeper than 120 km, the three microearthquakes approximately 30 km below the Ruahine Range and the six southeastern-most microearthquakes located with the Dannevirke array (see fig. 5.3).

As discussed in sects. 5.2.3 and 4.2.2, the dipping band of concentrated activity at the top of the Benioff zone, and the continuation of this band below the Dannevirke array, can be identified with the crust capping the subducted Pacific plate. This interpretation enables the delineation of an approximate upper surface of the subducted plate, as shown by the solid line in fig. 6.1. The line represents an attempt to fair a smooth curve to the upper envelope of earthquakes of the band of activity, with some discretion exercised in the exclusion of points judged to represent scatter due to location errors, and bearing in mind that before subduction the crust of the Pacific plate is some 7 km thick (e.g. Worzel, 1974). The dip of this surface below the Dannevirke array indicates that subduction commences in the vicinity of the Hikurangi Trench, and the dashed southeasterly extrapolation of the surface shown in fig. 6.1 assumes a sediment thickness of 3 km (a
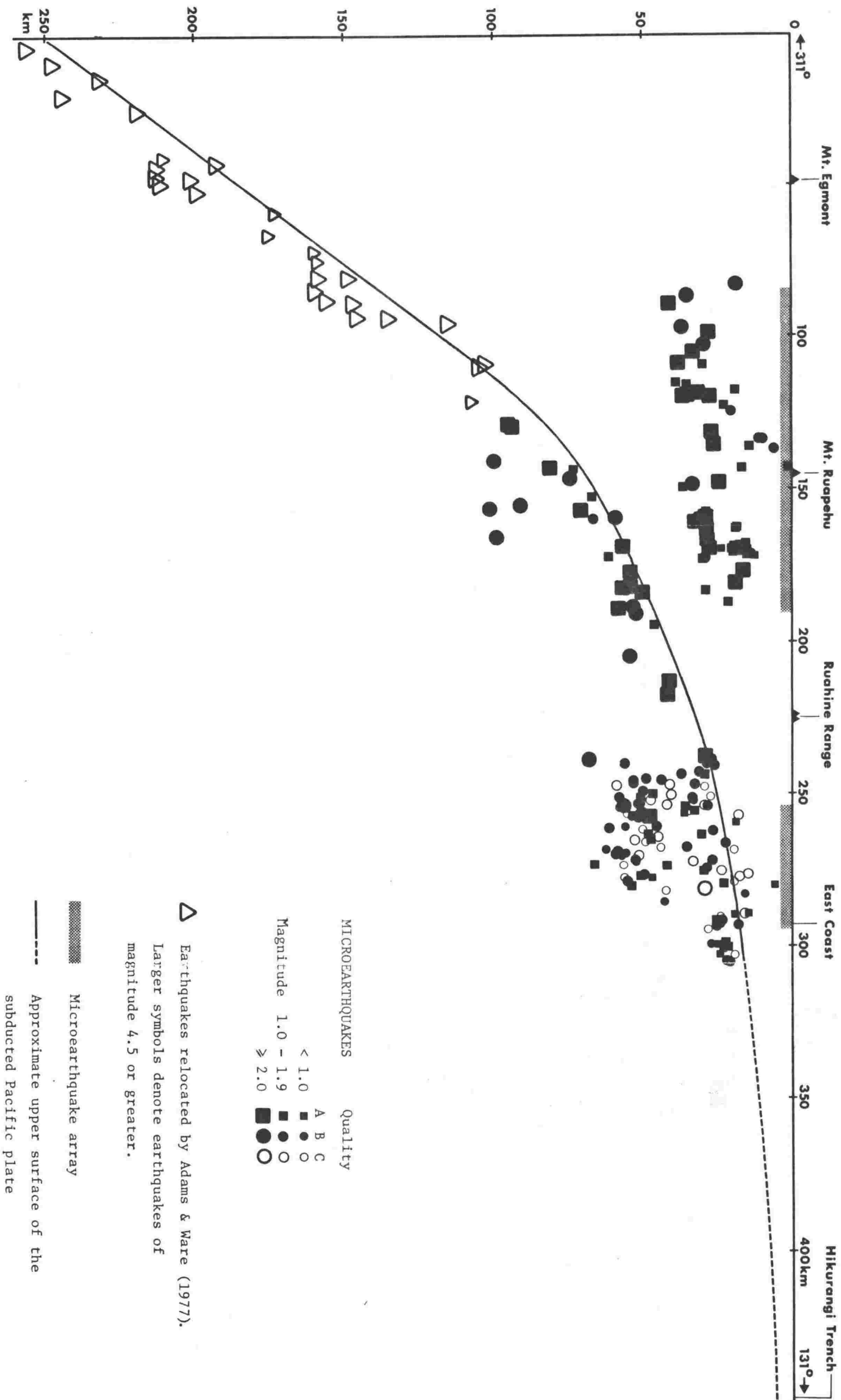
Figure 6.1   A vertical cross section along the microearthquake traverse showing well-determined earthquakes and microearthquakes and the inferred geometry of the upper surface of the subducted Pacific plate.

minimum value - D. Bennett, pers. comm., 1978) and a near-horizontal
plate in the deepest part of the trench.

The geometry of the subducted plate determined from the
distribution of seismicity must be consistent with observed gravity.
The absence of deep seismic sounding in the region of the microearth-
quake traverse precludes any detailed modelling of gravity. Moreover,
modelling of gravity at the subduction zone in the central Aleutians
(Grow, 1973) has revealed that even when control of crustal and upper
mantle structure is good, differing geometries of the subducted plate
suggested by the seismicity cannot be distinguished using gravity.

Hatherton (1970a) has given two interpretations of the negative
gravity anomaly over the North Island; one associates the mass deficiency
with the subcrustal seismicity above 80 km depth, while the other
associates it with a thickening of the continental crust. Interpre-
tation of the same anomaly by Woodward (1976) involves a crustal
thickening closely related to the top of the subducted plate. The
geometry of the subducted plate determined in this study provides a
constraint on future interpretations of the gravity anomaly.

The subducted Pacific plate delineated in fig. 6.1 appears to
contain two knee-like bends, one below the northwest edge of the
Dannevirke array, where the top of the plate is about 25 km deep,
and the other below Mt Ruapehu, where the top of the plate is about
70 km deep. Seaward of the shallower bend, the dip of the plate is
very small, averaging some 5°. Various explanations have been
proposed for an initial small dip of a subducted plate. These include
(a) Loading and depression of the descending plate through sediment
    accretion at the trench (Karig et al., 1976).
(b) Inhibition of subduction through the incorporation of low density
    terrigenous sediments into the descending plate (Jacob et al., 1977).
(c) The sliding of continental margin slivers along an arc as a
    result of oblique subduction (Fitch, 1972; Karig, 1974).
(d) Suction of the descending plate to the overlying continental
    wedge (Jischke, 1975).

The presence of thick sediments in the Hikurangi Trench (e.g. Katz,
1974) suggests both (a) and (b) may contribute to the initial small dip
of the subducted plate at the Hikurangi Margin, but the relative
importance of each process cannot be determined as the proportion of

sediment subducted with the Pacific plate is currently not known. As subduction at the Hikurangi Margin is oblique, (c) can also be expected. The numerous NNE-striking transcurrent faults of the eastern North Island (fig. 2.7) provide evidence of the sliding of continental fragments along the margin. (d) is unlikely to control the initial small dip of the subducted plate. Composite focal mechanisms of microearthquakes in the top of the subducted plate seaward of its shallower bend (mechanisms A-F, fig. 6.2) indicate compression normal to the plate interface, rather than the tension that would be expected if suction was occurring.

Various explanations can also be proposed for the shallower bend in the subducted plate. Jacob et al. (1977) attribute a similar bend in the Alaska-Aleutian Benioff zone at 40 km depth to an increase in the average density of the subducted plate. They suggest this density increase can be produced either by shearing off the terrigenous sedimentary components of the subducted plate, or by initiation of extensive dehydration of the subducted and altered oceanic crust, or by a combination of both. Alternatively, the bend can be explained in terms of contraction of the bottom of the subducted plate owing to the initiation of a phase change there. A likely candidate for such a phase change is that of spinel peridotite to garnet peridotite (e.g. Wyllie, 1971). A visco-elastic finite element analysis of subduction zones (Woodward, 1976) indicates phase changes play an important role in the bending of the subducted plate, as they lower the effective Young's modulus and hence the flexural rigidity of the plate. Woodward calculates that stresses due to phase changes are an order of magnitude larger than those due to the negative buoyancy of the subducted plate in the asthenosphere.

The 40-70 km deep microseismicity in the region of the Dannevirke array appears closely related to the shallower bend in the subducted plate, as it is limited to the vicinity of the bend. If one likens the subducted plate to a bending beam, this activity can be interpreted as due to compression, the apparent gap in microseismicity at about 40 km depth being interpreted as the neutral fibre of the beam and the activity at the top of the plate as due to tension. This interpretation is supported by the significant component of down-dip tension shown by microearthquakes at the top of the subducted plate (fig. 5.5). However,
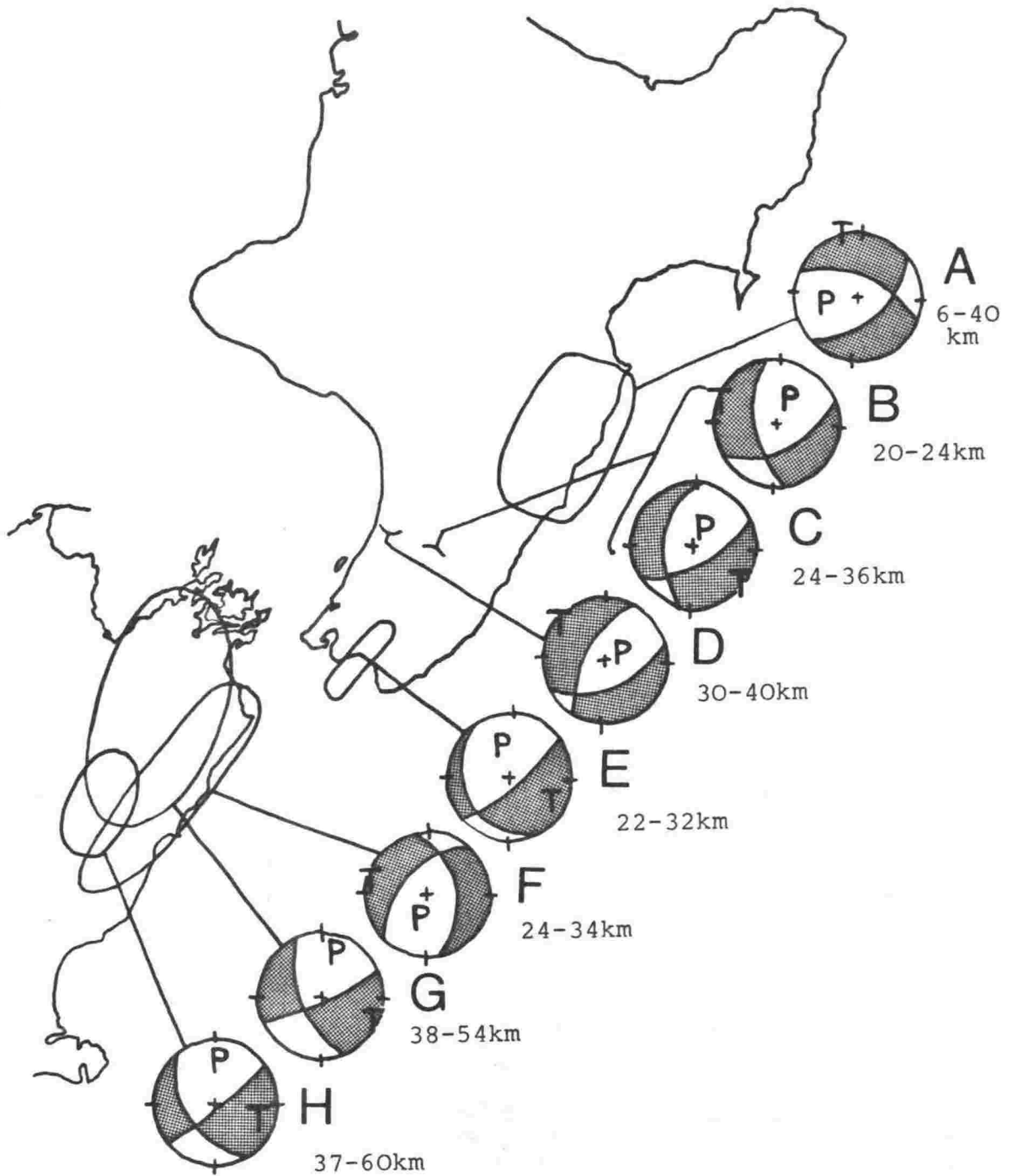
Legend

A: This study

B-D: Arabasz & Lowry (in prep.)

E: Robinson (in press)

F,G: Arabasz & Robinson (1976)

H: Kieckhefer (1977)

Figure 6.2   Composite focal mechanisms for shallow
        microearthquakes in the subducted plate.
        Compressional quadrants are shaded.

the 40-70 km deep microearthquakes do not share a common focal mechanism (fig. 5.6). The elastic thickness of the subducted plate suggested by the microearthquakes, and the depth of the interpreted neutral fibre of bending, are in line with a reduction of the flexural rigidity of the lower part of the plate through phase changes and creep.

Woodward (1976) has shown that bending stresses extend the area of a phase change. Extension of the spinel peridotite to garnet peridotite phase change throughout the mantle of the subducted plate is likely to be accompanied by the gabbro-basalt to eclogite phase change (Green & Ringwood, 1967) in the crust of the subducted plate, as shown schematically in fig. 6.8. Herein lies an explanation of the apparent restraightening of the subducted plate between the Ruahine Range and Mt Ruapehu (fig. 6.1) - the plate has now changed phase throughout its entire thickness, and consequently the bending associated with the unequal running of a phase change at different depths in the plate is no longer present. The restraightened plate does not revert to the dip it had seaward of its shallower bend because bending is continuing seaward of the restraightened section. Whereas the plate is moving, the areas of phase change, being dependent on temperature and pressure, remain comparatively fixed in space.

The occurrence of the deeper bend in the subducted plate directly below Mt Ruapehu suggests it is closely related to volcanism. Similar coincidence of a bend in the Benioff zone with the volcanic front has been found in the Alaska-Aleutian arc (Jacob et al., 1977; Engdahl, 1977). Because of a dramatic change in focal mechanisms and in the character of seismicity at the bend in the Benioff zone underlying the volcanic front in the central Aleutians, Engdahl (1977) postulates the bend represents the onset of segmentation of the subducted plate,owing to either lateral variation in plate properties or tearing. Such an explanation of the bend in the subducted plate below Mt Ruapehu is unlikely, since there appears to be no dramatic change in focal mechanisms (see fig. 6.3) or in the character of seismicity across the bend. As the generation of magma involves the removal of lighter volatile or hydrous components from the subducted plate (e.g. Anderson et al., 1976), the bend in the subducted plate below Mt Ruapehu may simply reflect an increase in the density of the plate.

Microearthquakes of this study

Harris (1975) group A earthquakes
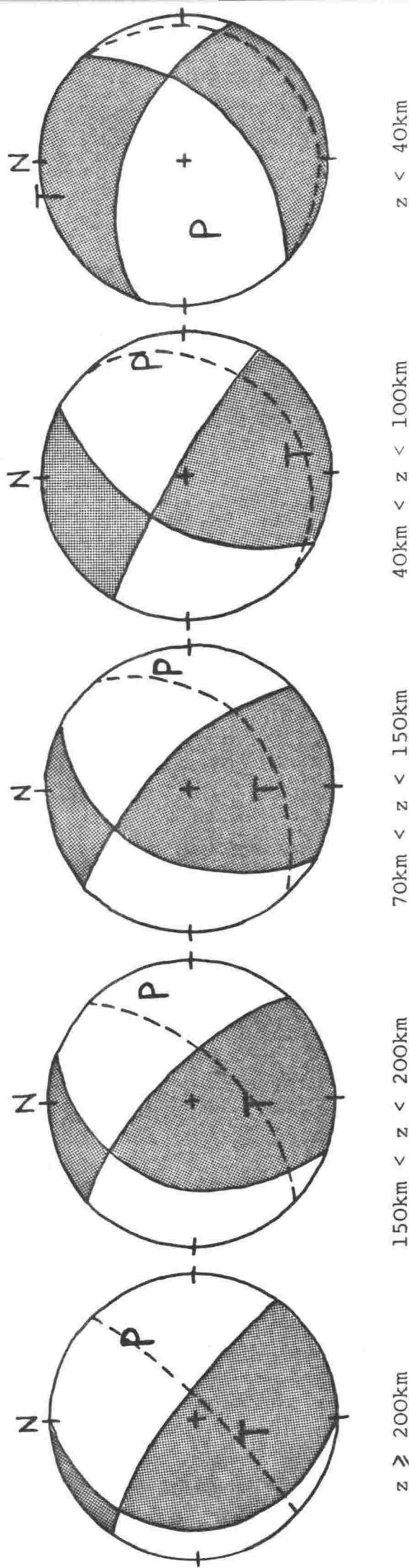
z < 40km

40km < z < 100km

70km < z < 150km

150km < z < 200km

z ⩾ 200km

z = focal depth. The dotted line shows the average orientation of the subducted plate in the appropriate depth range.

Figure 6.3 Composite focal mechanisms for earthquakes in the top of the subducted plate below the central North Island. Compressional quadrants are shaded.

The location of the four earthquakes in the mantle of the subducted plate in the vicinity of the deeper bend (fig. 6.1) suggests they are closely related to the bend. As with activity in the mantle of the subducted plate in the vicinity of its shallower bend, these earthquakes can be considered to be a response to bending stresses.

The depth to the subducted plate below the volcanic front of approximately 70 km determined in this study is shallower than that found in other areas, where it is normally about 100 km (e.g. Isacks & Barazangi, 1977). Clearly, this depth reflects the low upper mantle velocities used to locate the microearthquakes (see sect. 4.2.4). Nevertheless, the shallow depth seems to be a real feature, as a similarly shallow depth of about 80 km is indicated when the standard New Zealand crustal model is used (see fig. 4.1). A depth of approximately 80 km is also suggested by earthquakes studied by Ansell & Smith (1975) using the homogeneous station method and subsequently relocated with a laterally inhomogeneous velocity model (Adams & Ware, 1977; fig. 17). It appears that the depth to the subducted plate below the volcanic front in the North Island is similar to that in the northeastern Japan arc, where microearthquakes have revealed the top of the Benioff zone to lie some 80 km below the volcanic front (Hasegawa et al., 1978).

Beyond its deeper bend the subducted plate is closely planar and dips into the asthenosphere at about 50° (fig. 6.1). This dip may be controlled by deflection of the plate from the vertical by mantle flow entrained by, or associated with, the plate (Davies, 1977). Alternatively, the dip may be a result of the convergence rate and the sinking rate of the subducted plate being nearly equal (cf. Luyendyk, 1970). How the subducted plate restraightens after its deeper bend is open to speculation. It is interesting to note that cross sections of intermediate depth earthquakes below the North Island (e.g. Adams & Ware, 1977; Smith, 1977) show little evidence of a double-planed Benioff zone similar to that found in the Japan arc (e.g. Hasegawa et al., 1978), the Kurile arc (e.g. Veith, 1974) and the central Aleutian arc (Engdahl & Scholz, 1977). If such a double-planed Benioff zone reflects elastic unbending of the subducted plate, as suggested by Engdahl & Scholz (1977), its absence below the North Island may indicate elastic unbending is relatively unimportant there.

6.1.2 The stress regime in the subducted Pacific plate

Pioneering work on the stresses set up in the Pacific plate as
it subducts below the North Island has been carried out by Harris (1975),
who has studied the focal mechanisms of 215 intermediate depth
earthquakes between latitudes 38°S and 40°S. Harris has found

1) For 155 of the intermediate depth shocks (group A - see fig. 6.3)
    composite focal mechanisms indicate that both the P and T axes
    are parallel to the Benioff zone. The T axis is inclined some 30°
    to the dip of the Benioff zone, and Harris has related this
    orientation to the sloping bottom edge of the subducted Pacific
    plate, the plate being interpreted as sinking through the astheno-
    sphere under its own weight.

2) For a further 41 intermediate depth earthquakes (group B - see
    fig. 6.4) a composite focal mechanism gives the T axis in the
    direction of dip of the Benioff zone and the P axis normal to the
    zone. Most of these earthquakes were 150 km to 200 km deep, and
    Harris proposes that at such depths the occurrence of a group A
    earthquake temporarily removes the effect of the sloping bottom
    edge of the subducted Pacific plate on the local stress field.

3) The focal mechanism of the deepest well-observed earthquake between
    latitudes 38°S and 40°S,which was at 274 km (see fig. 6.4), gives
    a down-dip P axis, suggesting that at this depth the subducted plate
    has encountered resistance to its downward motion.

It is apparent from fig. 6.3 that the T axes of the composite
focal mechanisms for microearthquakes in the top of the subducted
plate located in this study, being nearly parallel to the subducted
plate and inclined some 30° to its dip, agree closely with the T axes
of the group A earthquakes of Harris. Clearly the subducted plate is
acting as a stress guide, the effect attributed to the sloping bottom
edge of the plate being transmitted to the section of the plate seaward
of its shallower bend. The composite focal mechanism for microearthquakes
between 40 and 100 km deep is very similar to those of the group A
earthquakes of Harris, having both the P and T axes parallel to the
subducted plate and thus indicating strike-slip motion relative to
the surface of the plate. The P axis of the composite focal mechanism
for microearthquakes shallower than 40 km is more nearly normal to the

The earthquake of October 12, 1972

z = 274km

Group B earthquakes

150km ≤ z < 200km

z = focal depth. The dotted line shows the average orientation of the subducted plate in the appropriate depth range.

Figure 6.4 Composite focal mechanisms for earthquakes in the subducted plate below the central North Island (after Harris, 1975). Compressional quadrants are shaded.

subducted plate. This suggests that seaward of its shallower bend, the subducted plate is being loaded by the overlying plate.

All currently available composite focal mechanisms for shallow microearthquakes with hypocentres believed to be in the subducted plate at the Hikurangi Margin are shown in fig. 6.2. The mechanisms of microearthquakes shallower than 40 km (A-F) all indicate predominantly normal faulting relative to the surface of the subducted plate, while the mechanisms of microearthquakes 37 to 60 km below Marlborough (G,H) indicate a mixture of strike-slip and normal faulting relative to the surface of the subducted plate, intermediate to the normal faulting at the top of the subducted plate when the plate is shallower, and the strike-slip faulting when the plate is deeper (fig. 6.3). The tendency toward the vertical of the P-axes of mechanisms A-F is consistent with the suggestion that seaward of its shallower bend, the subducted plate is being loaded by the overlying plate. Although the T axes of all the mechanisms of fig. 6.2 are nearly parallel to the subducted plate, the strike of the T axis of mechanism A differs significantly from the consistent SE-NW to ESE-WNW strike of the T axes of mechanisms B-H. This suggests that the stress regime in the shallow part of the subducted plate in the region of this study differs from that in the southern part of the Hikurangi Margin. This may be a consequence of locking of the plates, as discussed later.

6.1.3 Lateral segmentation of the subducted Pacific plate

Lateral segmentation of the descending plate at subduction zones has often been proposed (e.g. Kanamori, 1971; Abe, 1972; Carr et al., 1973; Van Wormer et al., 1974), and there is evidence to suggest that this is occurring in the subducted Pacific plate at the Hikurangi Margin. For example, Arabasz & Robinson (1976) have found the Benioff zone beneath the Marlborough region (northern South Island) to be segmented, the zone in south Marlborough being much shorter than that further to the north-east. Eiby (1977) has suggested that the northern part of the Main Seismic Region is separated from the southern end of the Kermadec Seismic Region by a transverse fracture. In addition, a lineation defined by relocated earthquakes in the Gisborne region has been tentatively interpreted by Smith (1977) as a fault striking roughly down the dip of the subducted Pacific plate.

There is also evidence for a major discontinuity striking down
the dip of the subducted plate and passing beneath the Tongariro volcanic
centre. This evidence, summarized in fig. 6.5, includes:

1) The distribution of subcrustal earthquakes. The occurrence of very
    deep shocks beneath an area in which there is a discontinuity in the
    depth of maximum activity in the Benioff zone (see fig. 2.3) has
    led Adams & Ware (1977) to suggest that both these features may be
    related to some past disturbance or dislocation in the lithospheric
    material forming the zone.

2) The intermediate depth earthquake of January 5, 1973 and its after-
    shocks, which define a lineation which strikes down the dip of the
    subducted plate (Harris, 1975).

3) The distribution of microearthquakes of this study, including the
    prominent lineation of ten Benioff zone microearthquakes striking
    down the dip of the subducted plate and passing beneath the Tongariro
    volcanic centre (fig. 5.2), and the abrupt change in the depth
    distribution of microseismicity along the northeast edge of the
    Dannevirke array (fig. 5.4).

4) Bathymetric features. The southeasterly extrapolation of the
    discontinuity defined by (1)-(3) meets the Hikurangi Trench in an
    area where the trench undergoes a significant change in strike
    (fig. 2.1) and a prominent piercement structure, probably of igneous-
    volcanic origin (Katz, 1974; D. J. Bennett, pers. comm., 1978)
    occurs in the trench. Also, such an extrapolation passes through
    Madden Canyon, a major bathymetric feature transverse to the trench
    which is difficult to explain in terms of erosion. The change in strike
    of the trench, the piercement structure and Madden Canyon can all be
    related to a discontinuity striking down the dip of the subducted
    plate (cf. Carr et al., 1973).

    Focal mechanisms of earthquakes and microearthquakes on this
discontinuity (fig. 6.5) indicate it represents a near vertical, sinistral,
strike-slip fault. Why should such a fault occur in the subducted plate?
It may be a product of the contortion of the subducted plate needed to
accommodate the change in strike of the Hikurangi Trench. Then again,
it may have developed in response to the stresses produced by the sloping
bottom edge of the subducted plate (cf. Harris, 1975).
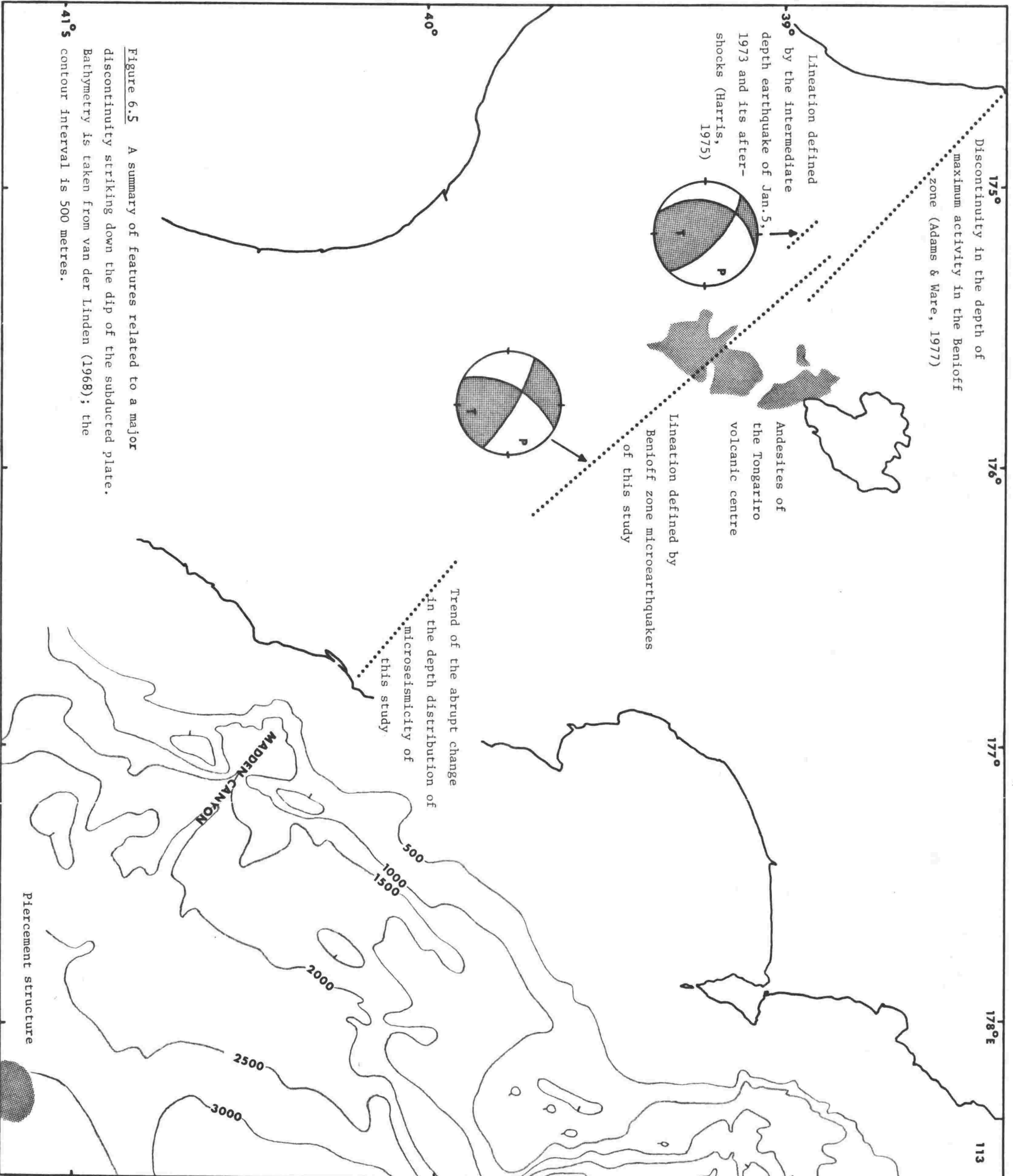
Figure 6.5   A summary of features related to a major discontinuity striking down the dip of the subducted plate. Bathymetry is taken from van der Linden (1968); the contour interval is 500 metres.

6.2 ACTIVE DEFORMATION OF THE INDIAN PLATE

6.2.1 The east coast of the North Island

On the evidence of retriangulation results, Walcott (1978b) has proposed that deformation in the Indian plate along the east coast of the North Island involves episodic compressional and extensional strain normal to the plate boundary, together with a continuing regional dextral shear parallel to the boundary. The episodes of compression and extension are suggested to be the result of locking and unlocking of the subducted and overlying plates, and Walcott has interpreted retriangulation data for the period after 1931 (fig. 6.6) as indicating that the plates are currently decoupled along the east coast of the North Island, except in the southern North Island where they are locked together, resulting in the accumulation of elastic strain.

Focal mechanisms of earthquakes in both the subducted and overlying plates appear to support this interpretation. Mechanisms A and B of fig. 6.7 indicate compression in the Indian plate normal to the Hikurangi Trench in the southern North Island, whereas mechanism S indicates extension in the Indian plate normal to the Hikurangi Trench in the Hastings area. The almost exact coincidence of the T axes of mechanisms B-E of fig. 6.2 with the P axes of mechanisms A and B of fig. 6.7 further suggests locking of the plates in the southern North Island, while the significantly different orientation of the T axis of mechanism A of fig. 6.2, compared with mechanisms B-E of the same figure, suggests this locking does not extend as far north as the Dannevirke region.

In the Wellington region, where the plates are interpreted as being locked, significant microearthquake activity occurs in the overlying plate (Robinson, in press). By analogy, the occurrence of microearthquakes in the overlying plate beneath and southwest of the Dannevirke array (fig. 5.4) may indicate a locking of the plates, while the complete absence of microearthquakes in the overlying plate northeast of the array may indicate a decoupling of the plates. Thus the northeastern boundary of the postulated locked zone may coincide with the fault striking down the dip of the subducted plate discussed in the previous section. The inferred sinistral, strike-slip movement on this fault is that expected from differential subduction caused by a locking of the

Figure 6.6   Shear strain components from retriangulation data for
the period after 1931, after Walcott (1978b). The numbers are
rates of shear strain in units of 10^{-7}/yr, and the bars mark the
direction of the principal axis of horizontal compression.

Figure 6.7 Focal mechanisms for shallow earthquakes in
the Indian plate.
Compressional quadrants are shaded.
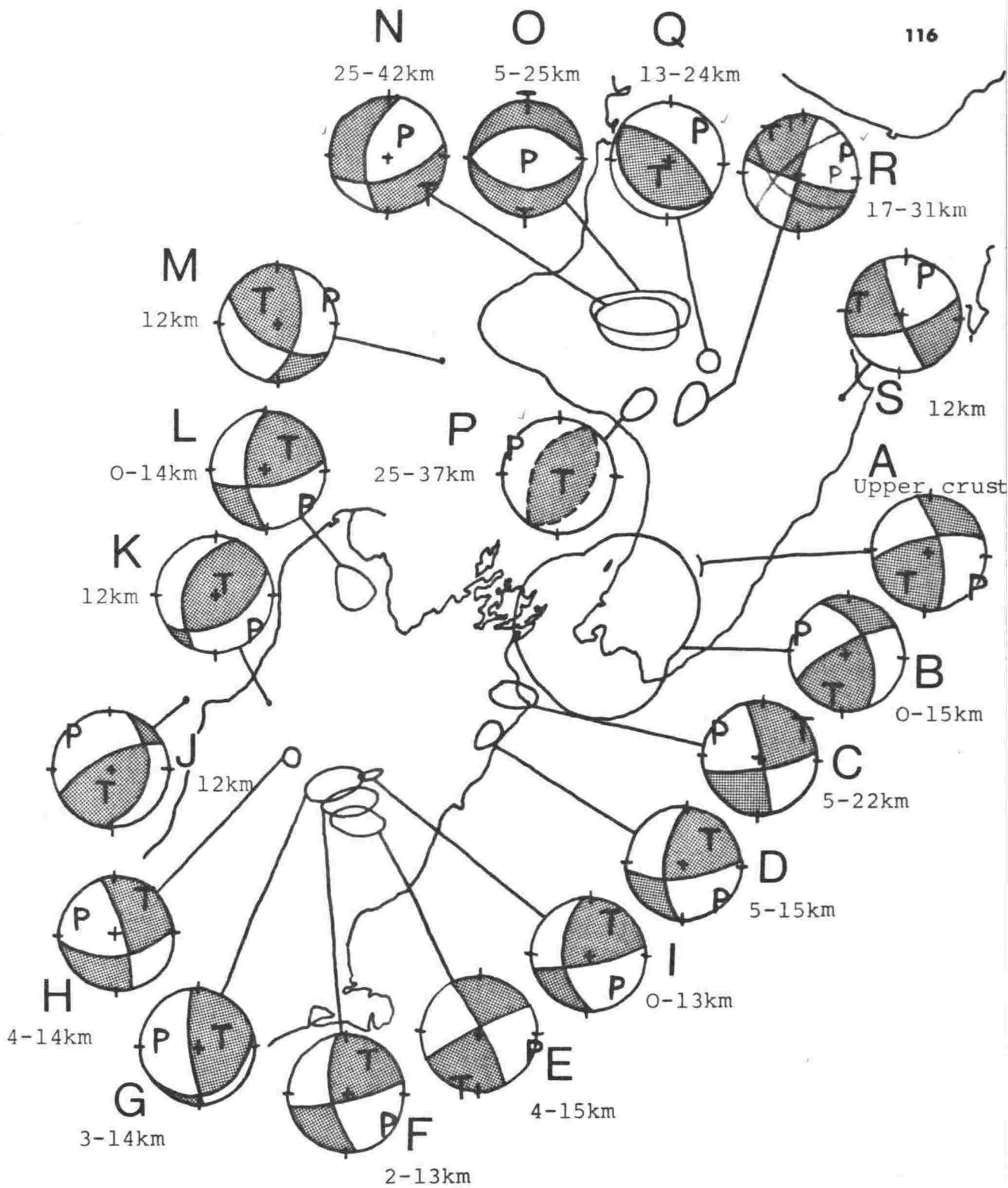
Legend

A:	Arabasz & Lowry (in prep.)	L:	Robinson & Arabasz (1975)
B:	Robinson (in press)	M:	Robinson et al. (1976)
C-H:	Arabasz & Robinson (1976)	N-R	This study. Two alternative mechanisms are shown for R.
I:	Kieckhefer (1977)		
J:	Adams & LeFort (1963)	S:	Robinson (pers.com. 1976)
K:	Evison et al. (1973)		

plates to the southwest. The fault may in fact control the extent of the postulated locked zone, in line with the observation of Carr et al. (1973) that transverse faults form the lateral margins of the focal regions of great earthquakes in the Japanese arcs.

Seaward of the shallower bend in the subducted plate, locking of the plates will be facilitated by the loading of the subducted plate by the overlying plate evident from focal mechanisms of microearthquakes in the subducted plate (see sect. 6.1.2), and by the shallow dip of the plate interface (cf. Kelleher et al., 1974). At the shallower bend in the subducted plate, however, unlocking of the plates is to be expected as here

1) the bending of the subducted plate leads to a decrease in the normal stress across the plate interface (since this stress is of gravitational origin, being produced by the loading effect of the overlying plate), and hence leads to a decrease of friction at the plate interface; and

2) bending stresses, as well as stresses driving the relative plate motion, are available to rupture a locked portion of the plate interface.

Indeed, there may be a sympathetic relationship between the unlocking of the plates and the shallower bend in the subducted plate. An unlocking of the plate interface will produce a decrease in tensional stress in the top of the subducted plate, as tensional stress produced by the deeper, sinking part of the plate will be relieved. This will promote bending, and thus lead to an increase in compressional stress in the interior of the plate. Vice versa, the relief of compressional stress in the interior of the subducted plate through fracture and/or phase changes will also promote bending, leading to an increase in tensional stress at the top of the plate which may in turn unlock the plate interface.

The great Hawke's Bay earthquake of 1931 (see sect. 2.2) illustrates the above ideas. Hypocentres determined by both Adams et al. (1933) and Bullen (1938a) place this earthquake in a position that can now be recognized as situated in the overlying plate close to the shallower bend in the subducted plate. Deformation of the overlying plate associated with the earthquake (Henderson, 1933) has been interpreted by Walcott (1978b)

as indicating movement on a thrust fault through most of the thickness
of the overlying plate, with attendant unlocking of the plate interface.
An interesting feature of aftershocks of the earthquake is that some
felt intensely in New Zealand were not recorded overseas, while others
not felt as intensely in New Zealand were well recorded overseas
(Bullen, 1938a). This suggests that some aftershocks may have occurred
in the interior of the subducted plate. As explained above, deformation
there would be an expected result of the unlocking of the plate interface.
The relationship of the 80 km deep earthquake of June 28th, 1921 (see
sect. 2.2) to the 1931 Hawke's Bay earthquake is also interesting.
Bullen (1937) has conjectured that "it is possible this earthquake
contributed substantially towards an instability nearer the surface
which resulted in the disastrous earthquake of 1931". His location for
this earthquake places it in the interior of the subducted plate. Thus
if the earthquake reduced the compressive stress there, it will have
promoted bending of the subducted plate and thus will have contributed
to the tensional stress in the top of the plate which was eventually
relieved in the Hawke's Bay earthquake.

The Wairarapa earthquakes of June 24th and August 1st 1942 (see
sect. 2.2) can also be interpreted in terms of the plate bending ↔
unlocking mechanism. On this interpretation, the earthquake of June 24th,
which was about 20 km deep, would have unlocked the plates, thus producing
an increase in compressive stress in the interior of the subducted plate
which resulted in the 55 km-deep earthquake of August 1st.

6.2.2 The Ruahine Range

A conspicuous lack of microseismicity in the Indian plate in the
region of the Ruahine Range has been revealed in this study. This is
a real feature, since although there were no microearthquake recorders
in the Ruahine Range, both the Dannevirke and Ruapehu arrays were capable
of recording microearthquakes, and roughly locating them, had they
occurred there. Also, this lack of microseismicity is in agreement with
the low level of shallow macroseismicity in the same area, as shown by
fig. 2.4.

Jacob et al. (1977) have found a similar aseismic region to be
present in the overlying plate landward of the shallower bend in the
subducted plate at the Alaska-Aleutian arc. They have suggested that

aseismic creep promoted by the upward migration of water produced by
dehydration of the subducted oceanic crust is occurring in this region.
Although similar aseismic creep in the Indian plate below the Ruahine
Range cannot be discounted, the aseismicity there can be simply attributed
to a low level of stress resulting from the plate interface being currently
unlocked in the Dannevirke region. In the Wellington region, where the
plates are interpreted as being currently locked, the southwesterly
extension of the Ruahine Range (i.e. the Tararua-Rimutaka Range) is
underlain by significant activity in the Indian plate, both on the
macroseismic and microseismic level (fig. 2.4 and Robinson, in press).

The structure of the Ruahine Range has been described as that
of a horst (Kingma, 1957). A lack of any gravitational anomaly directly
associated with the range has led Robertson & Reilly (1958) to suggest
that it is not underlain by a crustal root. Clearly, the shallow depth
of the subducted plate below the range, which is inferred to be about
32 km (fig. 6.1), precludes the development of such a root in the Indian
plate. Nevertheless, the crust of the subducted plate, if it has not
yet transformed to eclogite, will constitute a de facto root to the range.

Uplift of the Ruahine range can be interpreted as a response to
compression resulting from episodic locking of the plates at the
Hikurangi Margin. The major active faults intersecting and bordering
the range, which show both dextral transcurrent and vertical movement
(fig. 2.7; Kingma, 1962), are suitably positioned to take up deformation
resulting from such episodic locking of the plates, as they lie landward
of the shallower bend in the subducted plate and hence beyond the inferred
region of locking.

6.2.3 The Wanganui Basin

A distinctive feature of the microseismicity of the Wanganui Basin
is the concentration of activity in the 25-42 km depth range, shallower
activity being largely confined to the northeast edge of the basin,
near Mt Ruapehu and Waiouru. Composite focal mechanisms for the
25-42 km deep activity, summarized in fig. 6.7, suggest it is a response
to stresses set up by the locking and unlocking of the plates at the
Hikurangi Margin. The orientation of the P axis of the tentative mechanism

P of fig. 6.7 is very similar to that of mechanisms A-L, and can be related to a locking of the plates in the southern North Island and northern South Island. Similarly, the T axes of mechanisms N and R are in general agreement with that of mechanism S, and can be related to the plates being unlocked in and northeast of the Dannevirke region.

In contrast, microearthquakes shallower than 25 km at the northeast edge of the basin appear to be a response to local stresses. The normal faulting shown by microearthquakes shallower than 25 km near Mt Ruapehu (mechanism O, fig. 6.7) can be related to local volcanic phenomena, such as an upward migration of magma, or subsidence caused by the depletion of a magma reservoir. The tight clustering of both macro-seismic and microseismic activity near Waiouru, and the dissimilarity of the focal mechanism of this activity (mechanism Q, fig. 6.7) with the mechanisms of nearby activity, suggest that it is likewise a response to local stresses. Such stresses could be produced by volcanic activity in the nearby Tongariro volcanic centre or, on a larger scale, active spreading of the Taupo Volcanic Zone, as proposed by Calhaem (1973) (see sect. 2.3).

The tectonic significance of the continuing activity immediately south of the city of Wanganui, evident at both the macroseismic and microseismic level, is open to speculation. The activity may simply represent aftershocks of the large earthquakes that have previously occurred in the same region (see sect. 2.2). An unusual feature of the magnitude 6.1 Opunake earthquake of November 5, 1974, which occurred some 140 km WNW of the Wanganui activity, was the long duration and high b-value of its aftershock sequence (Robinson et al., 1976). If it is assumed that the parameters of the aftershock sequence of the Opunake earthquake are appropriate for earthquakes near Wanganui, and that they do not change with time, one would expect the present rate of occurrence of aftershocks of magnitude 4.0 or greater to be about 7 per year for the magnitude 7 earthquake of 1897 and about 21 per year for the magnitude 7.5 earthquake of 1843. The rate of occurrence of Wanganui activity of magnitude 4.0 or greater is currently observed to be 3.3 per year. Thus, taking into account the large uncertainties involved in the calculation of the aftershock rates, interpretation of the activity as aftershocks appears plausible.

Such an interpretation of the Wanganui activity begs the question of why the large earthquakes occurred in the first place. The proximity of the Wanganui activity to the largest negative gravity anomaly in New Zealand, the Rangitikei anomaly (fig. 2.5), is highly suggestive of some basic connection between the two phenomena. As pointed out by Robertson & Reilly (1958), the gravitational effect of thick Pliocene sediments near the centre of the Rangitikei anomaly is some 400 μN/kg, leaving a Bouguer anomaly of about 1200 μN/kg to be ascribed to deep-seated causes. They prefer to explain the anomaly in terms of a crustal downwarp. There is, however, no independent evidence that this exists.

In order to account for the shortening determined from plate tectonic considerations to have occurred in the South Island in the last 10 Myr, Walcott (1978a) has speculated that continental crust caught between the converging Indian and Pacific plates in the vicinity of the South Island may have been squeezed northeastwards and thrust back over the Pacific plate at the Hikurangi Margin. If similar rafting of continental crust is currently occurring in the Wanganui region, the Wanganui earthquake activity could be interpreted as deformation resulting from a resistance to such rafting of a local downwarp of the crust.

Alternatively, the Wanganui earthquake activity can be explained in terms of incipient volcanism. A well-developed Benioff zone underlies the activity at a depth at which magma genesis is likely to occur (e.g. Adams & Ware, 1977; fig. 13). Volcanism near Wanganui would continue the southward migration of the North Island magmatic arc that has occurred during the Upper Cenozoic (e.g. Ballance, 1976); this migration may be related to a southward migration of subduction (Scholz et al., 1973a; Arabasz & Robinson, 1976). Also, volcanism would provide an explanation of the Rangitikei gravity anomaly - that of an upwelling of low density volcanics in the lower crust and upper mantle.

The qualitative interpretation of active deformation at the North Island plate boundary presented in this chapter is summarized in fig. 6.8. This interpretation in terms of stress-strain fields is put forward as a basis for further work. A large amount of research will be needed before the interpretation can be represented rigorously by means of a quantitative model.
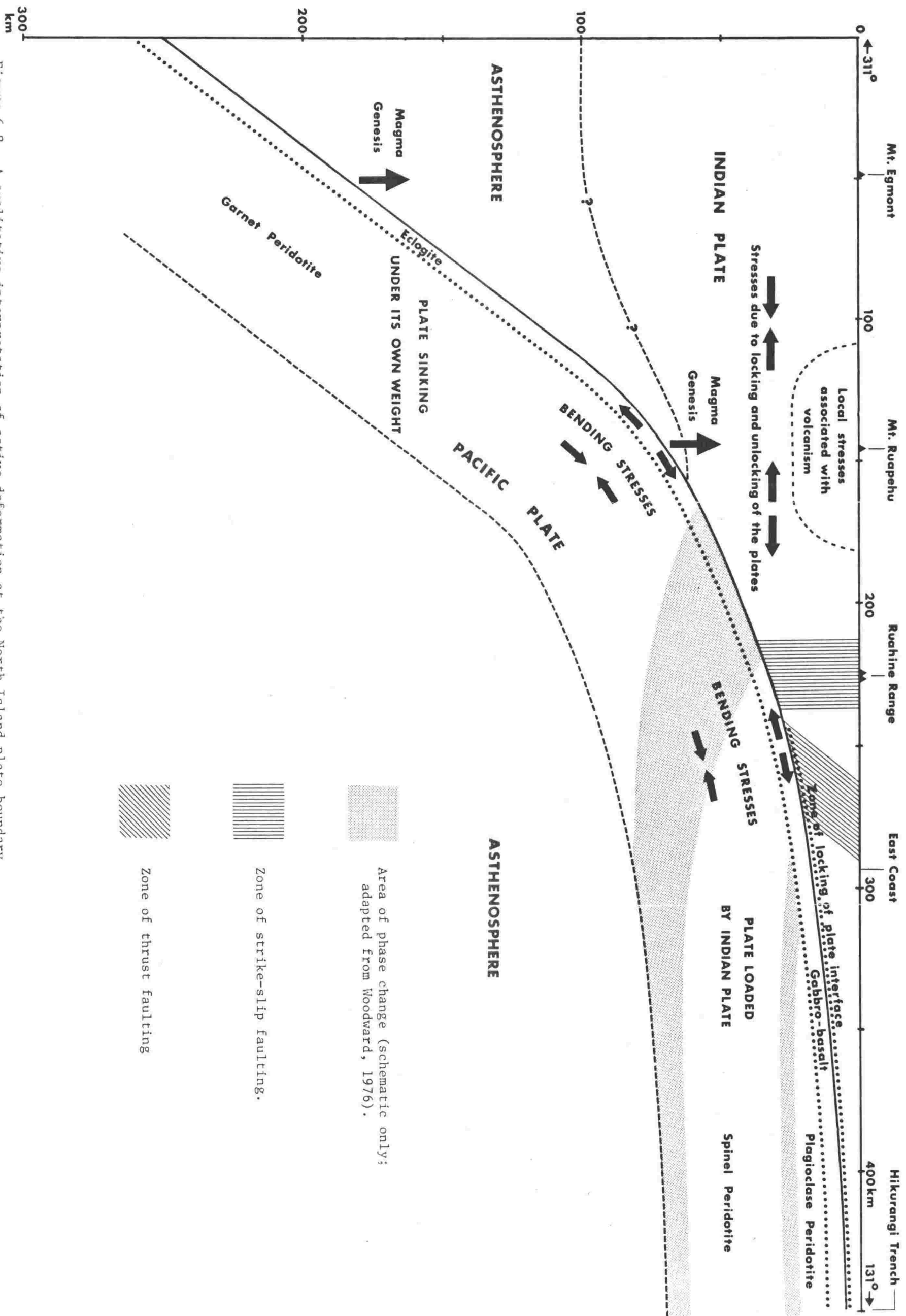
Figure 6.8   A qualitative interpretation of active deformation at the North Island plate boundary.

CHAPTER 7

CONCLUSION

A major achievement of this study has been the accurate determination of the depth distribution of microseismicity at the North Island plate boundary. From this the geometry of the subducted Pacific plate at shallow depths has been inferred, and the relationship of the Hikurangi Trench to the intermediate depth seismicity below the North Island resolved. Microearthquake activity below the North Island appears to be exclusively intraplate; there is no evidence of thrusting focal mechanisms which might be related to interplate activity.

The microearthquake traverse lies in a region where a marked change in the stress regime at the plate boundary occurs. Interpretation of this change has been hampered by the paucity of microearthquake studies to the north of the traverse. A recent microearthquake study in the East Cape - Bay of Plenty area (R. Frith, pers. comm., 1978) will remedy this to some extent. Further studies to the north of the traverse are both desirable and logistically feasible. For example, a microearthquake traverse could be carried out from Napier to Taupo.

Further study of the 40-70 km deep microseismicity between the east coast of the North Island and the Ruahine Range is needed in order to test the interpretation that this activity represents compression in the interior of the subducted plate due to bending of the plate. More work is also needed on the enigmatic earthquake activity immediately south of the city of Wanganui. A recent microearthquake study in the Wanganui region (E.G.C. Smith, pers. comm., 1978) has confirmed the lower crustal depth of this activity determined in the present study.

If the level of microseismicity in the Indian plate in the eastern North Island is related to the degree of coupling of the plates, as suggested in this study, periodic monitoring of this activity may prove valuable in identifying areas where the plates have locked, resulting in the accumulation of elastic strain which may be released in a large earthquake.

Finally, it must be remembered that earthquake studies cannot provide information on anelastic, aseismic strain. Thus future work must include geodetic and geologic earth deformation studies before a quantitative model of active deformation at the North Island plate boundary can be constructed.

APPENDIX

DANNEVIRKE SURVEY AND RUAPEHU SURVEY LOCATED MICROEARTHQUAKES

LEGEND

MAG   Microearthquake duration magnitude.

NO   Number of phases (both P and S) used in locating a microearthquake.

DM   Epicentral distance in km to the nearest station.

RMS   Root mean square error of the time residuals in seconds.

ERH   Standard error of the epicentre in km.

ERZ   Standard error of the focal depth in km.

ND   Standard error not determined.

Q   Hypocentre quality. See sect.4.3 for explanation.

C   Classification of microearthquakes of the Ruapehu Survey.

   A: Aftershock of the earthquake of 1974 August 25th 19^h46^m.

   B: Microearthquake occurring in the Benioff Zone.

   U: Microearthquake occurring in the upper basin of the Wanganui River.

   W: Microearthquake in the dense cluster of activity immediately south of the city of Wanganui.

DANNEVIRKE SURVEY LOCATED MICROEARTHQUAKES

Origin Time			Epicentre		Depth	MAG	NO	DM	RMS	ERH	ERZ	Q
h m	sec		Lat. S	Long. E	km			km	sec	km	km	

February 8th 1974

Origin Time		Epicentre		Depth	MAG	NO	DM	RMS	ERH	ERZ	Q
0709	16.8	39°59.2'	176°43.4'	33.6	1.8	5	20	0.01	0.4	0.2	C
1827	19.2	40 19.9	176 29.4	42.8	0.7	6	14	0.03	1.3	0.7	C

February 9th

0605	05.5	40 12.0	176 53.2	4.6	0.5	5	16	0.01	0.3	23	D

February 10th

0713	56.1	40 15.5	176 31.2	23.2	0.4	5	7	0.21	6.6	8.5	D
1056	53.2	40 22.9	176 23.7	19.8	0.4	5	11	0.04	1.1	1.2	C
1121	51.9	40 36.7	176 09.5	11.5	1.2	5	43	0.04	3.0	9.5	D
1317	04.2	40 04.7	176 24.0	18.3	1.2	6	16	0.14	3.0	3.5	C
1332	15.9	40 02.3	176 20.8	27.8	0.7	6	22	0.02	0.6	0.5	C

February 11th

0227	00.9	39 58.9	176 15.2	26.5	1.4	7	32	0.09	2.4	2.3	B
0451	39.4	40 21.0	176 31.3	43.4	0.8	7	9	0.13	3.2	2.5	B
0502	01.6	40 12.2	176 28.8	30.2	1.5	6	10	0.19	4.1	6.6	D
0746	52.5	40 12.1	176 28.9	26.9	1.1	7	11	0.03	0.5	0.4	B
0929	33.8	40 21.4	176 29.0	16.2	0.8	8	8	0.26	2.5	2.7	B
1124	58.6	40 28.4	176 19.4	29.5	2.0	6	23	0.10	3.7	2.3	C
1222	48.8	39 53.6	176 29.5	40.9	1.2	5	27	0.03	2.4	1.1	C
2145	19.1	39 56.5	176 23.7	41.6	1.4	6	26	0.08	3.5	2.1	C
2242	38.5	40 37.8	176 11.1	3.9	2.0	5	44	0.05	28.7	51.6	D

February 12th

0239	46.5	40 00.3	176 15.7	31.8	1.2	7	30	0.13	4.5	3.7	B
0257	09.5	39 42.8	177 00.2	30.2	2.1	7	59	0.11	4.4	171	D
1302	27.3	40 22.0	176 35.8	24.4	0.1	5	4	0.04	1.3	1.1	C
1311	50.4	40 17.9	176 41.3	29.5	0.5	10	11	0.33	4.0	3.1	D
1312	53.2	40 25.3	176 11.1	19.9	0.8	6	26	0.08	2.7	2.6	C
1728	44.4	40 20.8	176 48.1	19.6	0.4	5	18	0.01	0.7	0.7	C
1755	37.6	39 56.8	176 24.0	29.8	0.9	5	25	0.02	1.0	1.2	C
1817	01.3	39 43.4	176 36.1	49.7	1.6	8	45	0.12	5.0	4.1	B
1834	22.2	40 00.0	176 19.4	33.1	1.6	7	26	0.10	2.7	3.0	B

DANNEVIRKE SURVEY LOCATED MICROEARTHQUAKES – continued

Origin Time		Epicentre		Depth	MAG	NO	DM	RMS	ERH	ERZ	Q
h m	sec	Lat. S	Long. E	km			km	sec	km	km	
February 13th											
0110	36.8	40°00.0'	176°13.8'	41.3	1.0	6	33	0.08	5.2	4.3	D
0213	51.9	39 57.6	176 07.3	19.0	1.8	7	43	0.19	8.0	16.5	D
0510	46.3	40 01.1	176 39.1	51.9	1.3	6	14	0.07	3.9	2.9	C
0704	04.7	40 15.3	176 41.9	15.2	0.5	8	30	0.14	1.6	1.5	A
1056	32.8	40 22.2	176 17.2	53.6	1.0	6	29	0.10	10.4	6.4	D
1316	33.7	40 29.9	176 49.0	18.4	1.9	7	20	0.18	4.1	5.6	D
1858	30.2	39 35.7	176 32.2	43.8	2.3	10	59	0.12	4.7	6.9	D
2009	18.5	40 09.2	176 33.3	57.1	0.5	5	3	0.02	1.6	0.5	C
2107	47.8	40 37.4	176 02.3	52.4	1.6	5	50	0.06	6.8	8.7	D
February 14th											
0050	55.9	39 43.7	176 39.4	50.5	1.9	9	45	0.13	4.9	3.7	B
0312	00.8	39 58.8	176 13.6	28.7	1.6	9	34	0.11	2.4	2.8	B
0448	45.7	39 50.5	176 32.4	47.3	1.7	9	32	0.05	1.8	1.4	A
0825	38.2	39 47.5	176 30.3	29.5	1.7	8	38	0.09	2.1	0.6	A
0835	37.1	39 45.8	176 29.0	29.2	1.8	8	41	0.15	4.0	1.0	B
1109	33.4	39 44.5	175 59.5	30.6	2.5	7	66	0.07	3.3	44.3	D
1243	55.2	40 27.7	176 05.8	3.5	1.9	7	35	0.08	70.6	126	D
1500	35.2	40 22.9	176 10.6	53.3	1.4	6	25	0.05	3.7	1.7	C
1510	41.6	40 15.9	176 15.6	60.5	1.1	7	16	0.11	5.9	2.8	D
1527	04.2	40 31.1	175 58.8	26.9	1.9	7	47	0.05	2.2	2.8	B
1527	59.0	40 33.3	176 59.3	5.1	1.8	7	44	0.32	7.8	487	D
1553	52.6	39 50.0	176 47.8	22.9	1.4	7	38	0.08	2.4	3.2	B
2026	43.1	39 42.4	176 45.2	28.8	1.8	7	49	0.11	4.9	0.7	B
February 15th											
0002	59.3	39 59.9	176 16.6	37.7	1.3	8	29	0.12	3.4	3.3	B
0225	28.4	39 47.3	176 40.3	51.7	1.7	6	38	0.09	6.3	3.8	D
0942	20.7	40 26.9	175 54.3	47.9	1.7	5	49	0.02	1.2	2.2	C
1119	56.1	40 37.6	176 36.5	10.7	2.0	10	39	0.23	3.9	13.6	D
1140	27.5	39 53.8	176 44.7	35.7	1.6	8	29	0.14	3.2	3.6	B
1349	12.2	40 44.7	176 50.9	28.1	1.9	6	56	0.08	4.2	0.9	D
1353	58.2	40 47.8	176 55.5	25.3	2.8	9	64	0.14	4.2	0.8	D
1537	25.2	40 33.7	176 47.3	4.8	1.3	7	35	0.21	4.1	312	D
1829	15.1	40 24.2	176 34.9	24.7	1.4	8	14	0.22	3.8	3.1	B
February 16th											
0013	55.0	40 28.4	176 15.2	20.3	1.3	8	26	0.19	3.5	6.4	D
0045	48.6	40 37.1	176 36.5	9.6	1.8	8	38	0.21	5.1	19.6	D

DANNEVIRKE SURVEY LOCATED MICROEARTHQUAKES – continued

Origin Time		Epicentre		Depth	MAG	NO	DM	RMS	ERH	ERZ	Q
h m	sec	Lat. S	Long. E	km			km	sec	km	km	
0057	04.4	40°01.0'	176°31.6'	50.8	0.6	5	13	0.04	2.6	1.6	C
0652	05.1	39 55.4	176 34.4	52.0	1.4	7	23	0.02	1.0	0.6	B
0839	32.9	39 45.2	176 39.4	58.6	1.5	10	42	0.15	4.6	3.2	B
0911	27.1	40 16.6	176 31.6	6.2	0.6	8	7	0.09	0.9	1.5	A
1629	06.2	40 07.7	176 30.8	59.4	1.0	9	5	0.16	4.4	2.4	B
1922	59.5	40 00.3	176 31.8	62.0	1.0	7	15	0.05	2.2	1.6	B
1951	06.4	40 12.7	176 28.9	66.8	1.3	8	9	0.07	2.1	1.0	A
2100	58.4	40 03.7	176 09.5	56.9	1.1	10	19	0.18	4.5	2.5	B
2242	30.3	40 14.3	176 10.8	58.6	0.7	6	23	0.05	2.5	1.4	C

February 17th

0035	30.6	40 08.5	176 18.0	33.1	1.9	10	11	0.10	1.5	1.2	A
0039	20.6	40 06.1	176 19.2	36.1	1.2	8	7	0.08	2.0	1.4	A
0118	57.9	40 06.2	176 17.7	33.3	1.0	8	8	0.17	2.8	2.0	B
0119	16.9	40 07.4	176 15.6	33.5	1.0	8	12	0.24	4.0	3.0	B
0135	04.7	39 53.8	176 34.3	35.4	1.0	6	25	0.09	2.7	2.0	C
0451	36.5	40 21.8	176 25.3	23.4	1.2	10	8	0.16	1.8	1.5	A
0809	14.6	39 47.0	176 56.6	52.9	1.9	7	53	0.03	1.2	1.8	B
1107	17.4	40 07.0	176 23.1	19.3	0.5	9	6	0.11	1.1	1.0	A
1247	16.9	40 21.6	176 44.1	25.1	1.6	10	14	0.08	1.2	0.9	A
1312	37.5	40 23.5	176 47.1	21.5	1.3	7	20	0.03	0.6	0.6	B
1354	48.1	40 21.9	176 43.6	27.5	0.8	7	14	0.24	5.0	4.8	B
1608	07.4	39 20.5	176 55.3	68.8	2.8	8	92	0.04	3.0	3.9	B
1930	44.2	39 59.0	176 47.3	50.4	1.2	7	24	0.05	1.9	1.5	B
2012	37.4	39 59.7	176 29.1	54.2	0.9	7	12	0.05	1.9	0.9	B
2044	06.2	40 17.3	176 03.7	51.2	1.4	8	33	0.07	2.2	1.6	A
2152	13.3	40 32.3	176 10.1	4.6	2.1	8	36	0.43	18.1	957	D

February 18th

0150	10.3	40 24.7	176 31.8	19.7	1.2	9	15	0.12	1.5	1.2	A
0557	13.8	39 59.8	176 46.8	51.1	1.5	8	23	0.05	1.4	1.2	A
1005	46.7	39 48.9	176 36.2	27.9	1.1	8	33	0.19	5.4	5.6	D
1138	12.3	40 50.5	176 09.0	15.5	1.8	5	66	0.02	1.6	11.5	D
1242	08.1	39 59.3	176 32.7	46.0	1.6	10	16	0.13	3.0	1.8	B
1324	40.6	40 18.9	176 48.2	23.6	0.8	10	13	0.16	2.2	1.6	A
1538	26.8	40 36.4	176 21.3	19.9	1.4	7	36	0.20	6.4	8.2	D
1841	52.8	40 04.7	176 37.3	53.0	0.9	9	7	0.12	2.9	1.8	B

DANNEVIRKE SURVEY LOCATED MICROEARTHQUAKES - continued

Origin Time		Epicentre		Depth	MAG	NO	DM	RMS	ERH	ERZ	Q
h m	sec	Lat. S	Long. E	km			km	sec	km	km	
February 19th											
0246	54.0	40°22.6'	176°42.8'	26.2	1.1	6	14	0.17	5.3	4.8	D
0848	31.1	40 51.2	176 07.5	17.3	2.0	8	68	0.17	5.6	31.9	D
1154	39.4	39 28.8	176 24.3	26.3	3.2	8	64	0.09	2.6	0.5	D
1218	16.0	40 23.3	176 45.6	24.5	0.5	8	18	0.09	1.7	1.7	A
1236	30.0	40 21.0	176 40.2	28.6	0.3	6	10	0.17	5.0	3.0	C
1251	30.1	39 58.9	176 29.3	55.9	0.9	6	18	0.08	4.6	2.5	C
1826	31.1	40 29.0	176 38.7	11.2	1.1	5	23	0.10	3.7	10.1	D
February 20th											
0247	08.5	40 37.3	176 49.0	27.7	2.2	6	48	0.08	2.3	0.7	C
0249	16.7	40 36.2	176 50.7	24.8	1.9	5	48	0.03	2.2	3.9	C
0323	50.3	40 38.1	176 52.6	16.2	2.0	6	53	0.03	1.1	4.2	D
0328	19.6	40 36.5	176 51.6	27.4	2.6	5	50	0.07	3.1	1.4	C
0343	24.9	40 38.5	176 48.7	26.9	1.9	5	50	0.03	1.4	0.6	C
0424	07.1	40 37.9	176 47.0	33.6	2.0	6	47	0.04	1.3	0.8	C
0514	09.8	40 30.1	176 13.4	15.2	1.5	5	30	0.08	3.2	4.9	C
0804	11.4	40 01.8	176 32.9	45.3	1.1	5	11	0.05	3.2	2.1	C
0902	18.5	40 36.9	176 52.2	22.9	2.0	6	51	0.03	1.5	3.1	D
0911	39.4	40 35.3	176 51.1	27.6	2.9	4	48	0.00	ND	ND	D
0912	09.4	40 34.6	176 50.5	28.8	2.7	6	46	0.22	7.1	2.6	D
1346	06.1	40 02.4	176 35.8	44.7	0.5	6	10	0.08	2.9	1.6	C
1419	31.3	40 14.3	176 31.6	56.7	0.6	6	9	0.09	4.0	1.5	C
1533	39.1	40 03.1	176 33.0	49.7	0.8	6	9	0.12	4.2	2.1	C
1859	07.7	39 57.3	176 58.2	25.2	1.4	6	39	0.10	3.9	5.4	D
1939	37.2	39 53.1	176 27.2	59.4	1.4	6	20	0.08	3.5	1.6	C
2110	54.3	39 54.5	176 59.0	12.1	2.0	5	42	0.08	4.6	3.8	D
February 21st											
0803	39.3	40 09.2	176 24.0	60.0	0.3	5	2	0.03	25.7	1.4	D
1338	51.7	40 33.7	176 21.8	16.4	1.3	6	31	0.04	1.6	2.0	C
1509	07.5	39 52.1	176 52.0	42.6	1.8	8	38	0.06	1.7	2.0	A
1737	54.3	39 36.8	176 39.4	26.0	2.0	6	55	0.11	5.1	1.5	D
1927	50.5	40 25.7	176 19.0	18.0	1.2	6	19	0.05	1.6	1.5	C
1931	14.7	39 53.9	176 48.2	12.7	1.3	7	32	0.11	2.6	2.2	D

DANNEVIRKE SURVEY LOCATED MICROEARTHQUAKES - continued

Origin Time		Epicentre		Depth	MAG	NO	DM	RMS	ERH	ERZ	Q
h m	sec	Lat. S	Long. E	km			km	sec	km	km	
1931	37.8	39° 54.4'	176° 51.4'	24.0	1.2	5	34	0.03	1.8	2.4	C
2033	34.8	40 37.0	176 57.9	13.1	1.9	6	57	0.08	2.7	142	D
2322	35.4	40 32.6	176 22.4	23.9	1.7	6	28	0.14	5.2	4.7	D
February 22nd											
0659	40.6	39 48.6	176 38.3	42.4	1.4	6	36	0.08	4.5	4.5	C
0707	16.7	39 31.3	176 43.0	39.0	2.3	6	66	0.06	4.0	15.9	D
0927	50.5	39 49.4	176 40.1	50.9	2.1	10	35	0.12	3.3	2.8	B
1411	35.1	39 47.6	177 09.6	34.8	2.3	7	62	0.32	531	ND	D
1756	17.8	40 11.3	176 25.9	62.9	0.8	8	3	0.08	2.7	1.0	B
February 23rd											
0001	17.9	39 38.7	176 51.0	38.3	2.6	9	58	0.10	3.0	6.1	D
0009	03.3	40 32.5	177 03.6	13.2	2.3	6	59	0.20	11.7	338	D
0221	24.3	39 59.5	176 29.7	48.8	1.1	6	13	0.06	2.8	1.3	C
0350	05.4	40 02.1	176 31.7	48.4	1.1	9	11	0.09	2.1	1.5	A
0743	24.8	39 25.2	176 21.2	28.1	2.5	6	71	0.05	8.0	10.1	D
0820	34.0	40 22.5	176 14.9	59.9	1.2	8	19	0.11	3.7	1.7	B
1105	41.9	39 48.3	176 24.1	29.5	2.4	9	28	0.08	1.4	0.4	A
1447	25.2	40 14.7	176 15.7	56.7	0.6	7	5	0.09	4.1	1.3	B
1524	44.1	39 43.9	176 45.9	27.0	1.9	5	47	0.09	11.9	15.4	D
2054	58.9	39 51.5	176 35.3	29.6	1.4	6	30	0.05	1.6	0.3	C
February 24th											
0211	37.2	40 32.4	176 08.2	29.0	1.5	7	38	0.13	3.1	1.6	B
0615	56.5	40 45.3	176 30.2	21.6	1.8	5	52	0.04	3.2	9.1	D
1224	19.9	40 25.0	176 39.6	22.5	1.8	10	23	0.12	1.6	1.9	A
1253	43.3	39 50.0	176 29.3	44.1	1.3	7	27	0.10	3.3	2.9	B
1400	08.7	39 47.1	176 18.8	22.1	1.4	7	31	0.19	5.5	7.8	D
1418	01.9	39 28.9	176 08.8	27.0	2.2	6	67	0.09	3.6	1.6	D
2324	39.1	39 46.5	176 54.6	27.5	2.1	6	55	0.03	1.6	0.5	D
February 25th											
0058	09.5	39 40.0	175 55.4	25.0	2.4	8	58	0.12	2.5	1.0	D
0619	21.5	40 42.1	176 46.1	29.1	2.0	5	53	0.04	4.4	0.8	C
0652	01.3	40 48.4	176 18.0	25.2	2.5	10	58	0.10	2.0	0.8	D
0700	32.8	40 02.1	176 25.9	36.6	0.6	10	6	0.16	2.4	2.2	A

DANNEVIRKE SURVEY LOCATED MICROEARTHQUAKES - continued

Origin Time		Epicentre		Depth	MAG	NO	DM	RMS	ERH	ERZ	Q
h m	sec	Lat. S	Long. E	km			km	sec	km	km	
0736	26.4	40° 24.9'	175° 57.8'	52.1	1.5	8	35	0.09	3.9	3.3	B
0746	26.7	40 04.9	176 23.2	54.2	0.6	10	3	0.08	1.7	0.8	A
0840	46.4	40 01.6	176 46.8	55.4	1.1	7	21	0.06	3.1	1.8	B
0841	39.8	40 45.2	176 21.8	5.0	2.3	8	52	0.17	4.0	236	D
1007	37.9	40 41.7	176 18.6	5.1	2.0	8	46	0.40	11.3	561	D
1120	19.0	40 31.8	176 33.5	22.0	1.9	10	28	0.09	1.6	2.4	A
1239	31.0	39 57.2	176 28.3	51.7	1.2	8	14	0.11	3.6	1.7	B
1321	21.0	40 22.1	176 48.5	22.0	1.2	8	32	0.12	3.0	3.2	B
1336	31.5	40 24.2	176 51.4	11.9	1.7	9	37	0.14	2.6	8.1	D
1507	17.0	40 09.7	175 42.6	14.7	2.1	10	47	0.11	2.1	10.8	D
1849	48.1	40 41.0	175 42.7	9.7	3.0	8	71	0.06	1.6	0.9	D
2017	05.1	39 39.8	176 48.1	56.8	2.2	7	55	0.07	4.3	3.3	B
2026	44.6	40 03.9	176 45.5	54.4	1.3	10	17	0.10	2.5	1.6	A

February 26th

0957	42.5	40 09.7	176 29.2	56.0	0.6	9	8	0.11	2.9	1.9	B
1416	21.5	40 07.6	175 43.0	7.3	1.9	8	57	0.16	3.2	47.8	D
1425	28.1	40 06.6	175 33.3	27.0	2.0	8	61	0.07	3.6	0.6	D
1738	33.1	39 36.3	176 20.3	25.7	2.2	9	51	0.07	1.5	0.5	A
1948	38.1	40 06.6	176 40.3	47.6	0.8	8	8	0.03	0.9	0.8	A
2225	22.6	39 42.2	176 48.5	42.4	1.9	8	51	0.08	3.9	5.7	D

February 27th

0430	52.4	39 58.1	177 04.4	25.6	2.9	9	46	0.11	2.6	4.0	B
0839	27.7	40 06.9	176 32.7	57.8	0.9	7	14	0.05	2.7	0.9	B
0926	41.9	39 58.8	176 36.9	47.8	1.3	10	17	0.09	2.0	1.3	A
1218	05.8	40 18.7	176 23.2	29.0	0.7	9	5	0.20	3.1	2.2	B
1218	27.2	40 18.4	176 24.5	30.2	1.1	10	4	0.18	2.3	2.0	A
1224	25.9	39 52.3	176 53.4	32.9	1.7	7	39	0.10	3.8	5.7	D
1259	53.4	40 19.7	176 38.2	23.7	1.4	10	17	0.25	3.3	3.0	B
1635	37.1	40 18.7	176 41.7	18.5	1.6	9	21	0.15	2.2	2.8	B
2122	38.3	40 08.9	176 09.2	53.8	1.6	10	11	0.15	3.6	1.8	B

March 1st

0758	14.3	40 29.6	175 57.9	31.1	1.6	6	41	0.13	5.8	19.2	D

DANNEVIRKE SURVEY LOCATED MICROEARTHQUAKES - continued

Origin Time			Epicentre		Depth	MAG	NO	DM	RMS	ERH	ERZ	Q
h m	sec		Lat. S	Long. E	km			km	sec	km	km	
1357	27.7		39° 48.9'	176° 41.3'	47.9	2.4	9	36	0.05	1.6	1.4	A
1623	36.0		40 09.3	176 24.2	31.0	1.1	10	2	0.12	1.4	1.5	A
1732	52.3		39 34.6	175 54.7	36.7	2.4	8	75	0.19	12.2	171	D
1758	34.1		39 47.6	176 33.1	53.9	1.7	7	33	0.07	3.4	1.9	B
1816	07.5		39 28.6	176 13.1	23.8	2.4	8	66	0.08	2.8	1.5	D
1838	04.4		39 39.9	176 35.0	28.2	2.4	8	47	0.16	4.9	0.8	B

RUAPEHU SURVEY LOCATED MICROEARTHQUAKES

Origin Time			Epicentre		Depth	MAG	NO	DM	RMS	ERH	ERZ	Q C
h m	sec	Lat. S	Long. E		km			km	sec	km	km	

October 2nd 1974

0719	13.1	39°30.1'	175°16.3'		74.4	1.3	15	7	0.07	1.0	0.6	A B
0841	32.1	39 14.5	175 25.9		11.7	1.6	18	11	0.22	0.9	0.6	B

October 3rd

0018	57.1	39 29.3	175 43.4		19.1	1.6	13	24	0.09	0.8	1.2	A A
0530	54.4	39 23.2	175 24.9		1.4	1.7	12	2	0.15	0.7	0.4	A
0551	42.2	39 40.3	175 10.1		24.9	2.4	15	14	0.16	1.3	1.6	A
0834	34.2	39 06.3	175 20.3		19.7	1.6	12	16	0.19	1.7	1.7	A U
1134	22.8	39 21.1	175 42.0		67.5	1.1	13	21	0.15	3.1	1.8	B B
1517	33.3	39 41.7	177 02.9		32.6	4.6	10.	105	0.20	152	204	D
1651	07.3	40 19.6	175 05.6		52.7	2.9	14	46	0.13	2.9	2.6	B B
1849	24.4	39 19.0	175 03.4		39.8	1.7	11	16	0.08	1.1	0.9	A U
1849	40.2	40 07.8	175 01.3		12.1	2.7	10	66	0.34	4.6	433	D W
1915	12.2	39 08.4	175 06.8		33.6	2.4	19	5	0.13	1.0	0.8	A U

October 4th

0108	11.3	39 25.0	175 00.9		36.3	2.8	13	11	0.16	1.5	2.3	A U
0157	34.1	39 14.4	174 52.3		37.5	2.5	16	13	0.23	2.2	2.0	B U
0321	19.0	39 19.8	175 06.9		34.9	2.3	15	14	0.14	1.0	1.4	A U
0542	20.0	40 00.4	175 02.8		25.2	2.7	15	52	0.23	2.8	6.9	D W
0710	03.1	39 45.3	175 05.1		33.9	2.1	17	25	0.26	2.1	2.0	B
1035	59.1	40 02.8	175 01.7		27.5	3.1	17	57	0.19	1.7	1.4	D W
1200	16.4	40 04.6	174 59.8		28.0	3.2	17	61	0.21	2.2	1.1	D W
1206	11.6	40 03.2	175 01.1		12.7	2.5	10	58	0.24	3.2	307	D W
1452	44.5	39 38.4	176 20.0		31.1	1.9	16	44	0.11	1.5	0.6	A
1559	59.3	39 37.2	176 37.3		21.2	2.2	14	68	0.19	2.6	2.7	D
1716	29.2	39 20.3	174 51.0		30.1	2.6	19	20	0.23	1.4	1.2	B U
1835	46.9	39 14.2	176 31.0		55.2	2.8	16	72	0.12	2.1	3.2	B B
2120	53.5	39 17.1	175 14.1		21.0	1.4	11	7	0.23	2.0	2.2	B U
2121	38.8	39 27.6	175 43.2		16.6	0.8	10	12	0.10	1.3	1.3	A A
2144	41.7	39 44.7	175 06.9		37.5	1.7	13	23	0.19	2.0	1.7	A
2158	14.4	40 04.5	175 00.7		24.4	2.6	16	60	0.30	2.7	2.2	D W

October 5th

0011	23.1	39 19.6	175 06.3		32.4	2.3	12	14	0.08	0.6	0.6	A U
0616	41.4	38 48.7	176 05.9		75.1	3.0	11	85	0.09	3.6	5.0	B B

RUAPEHU SURVEY LOCATED MICROEARTHQUAKES — continued

Origin Time		Epicentre		Depth	MAG	NO	DM	RMS	ERH	ERZ	Q	C
h m	sec	Lat. S	Long. E	km			km	sec	km	km		
0751	28.8	39° 29.1'	175° 49.5'	54.9	2.8	10	12	0.10	1.7	2.0	A	B
0834	02.3	40 18.2	174 24.5	36.0	3.5	13	109	0.31	7.9	129	D	
1044	08.9	40 01.5	174 56.3	29.3	2.7	17	58	0.15	1.2	0.6	A	W
1058	33.1	39 29.8	175 42.6	14.1	1.3	19	9	0.22	0.9	2.1	B	A
1124	15.0	39 17.7	175 22.5	10.2	1.2	13	10	0.21	0.9	1.8	B	
1336	51.1	39 29.5	175 41.6	20.2	0.8	11	8	0.11	1.2	1.2	A	A
1358	41.6	40 15.2	174 22.2	100.9	3.9	16	103	0.11	2.6	2.8	B	B
1801	13.8	39 08.7	175 10.0	30.6	1.7	15	10	0.11	0.9	0.9	A	U
2009	31.9	40 01.7	174 59.0	12.2	2.6	11	59	0.13	1.7	160	D	W
2358	50.8	39 12.1	174 47.6	41.7	3.2	18	5	0.17	1.7	1.0	A	U

October 6th

| 0623 | 38.9 | 39 49.6 | 175 32.5 | 29.6 | 1.8 | 15 | 14 | 0.10 | 0.9 | 0.6 | A | |

October 7th

0749	06.8	39 58.2	176 51.1	30.6	3.7	18	97	0.39	78.1	127	D	
0851	31.9	39 35.8	174 56.9	94.9	2.8	22	23	0.14	1.4	1.2	A	B
1133	59.6	39 18.4	175 38.2	67.9	1.7	17	20	0.15	1.9	1.6	A	B
1402	34.1	39 18.3	175 09.0	28.4	2.1	20	14	0.13	0.6	0.8	A	U

October 8th

| 0623 | 22.4 | 40 05.6 | 175 06.6 | 29.2 | 3.0 | 12 | 60 | 0.21 | 2.8 | 1.0 | D | W |

October 9th

| 0905 | 40.8 | 40 28.2 | 174 30.2 | 99.7 | 4.6 | 15 | 85 | 0.12 | 3.4 | 3.2 | B | B |
| 1159 | 15.0 | 39 25.0 | 175 15.9 | 26.9 | 2.0 | 12 | 12 | 0.06 | 0.5 | 1.0 | A | U |

October 10th

| 1304 | 41.5 | 39 31.0 | 175 41.7 | 15.0 | 1.2 | 11 | 7 | 0.09 | 0.6 | 0.9 | A | A |

October 11th

1250	17.8	39 20.3	175 02.9	35.6	1.9	14	14	0.11	1.2	1.0	A	U
1931	17.8	39 29.6	175 42.2	15.6	1.0	12	9	0.09	0.9	0.8	A	A
2353	47.2	38 54.2	174 27.0	27.0	3.5	16	40	0.39	4.7	1.5	D	

October 12th

0550	07.0	39 13.5	176 12.7	50.8	2.4	17	53	0.10	1.0	1.6	A	B
0646	03.5	39 26.5	175 47.4	62.4	1.8	20	17	0.12	1.1	0.9	A	B
1204	07.7	38 53.8	175 14.9	176.2	2.9	14	38	0.10	3.6	1.7	B	B
1522	40.4	40 03.3	175 02.2	26.0	2.9	20	57	0.24	1.7	1.9	D	W

RUAPEHU SURVEY LOCATED MICROEARTHQUAKES – continued

Origin Time		Epicentre		Depth	MAG	NO	DM	RMS	ERH	ERZ	Q C
h m	sec	Lat. S	Long. E	km			km	sec	km	km	
1729	05.5	39° 15.7'	175° 14.7'	23.2	1.6	12	5	0.15	1.1	1.1	A U
2021	44.6	40 06.6	174 56.6	25.7	2.8	15	66	0.31	4.0	14.2	D W
2025	57.0	40 05.6	175 00.2	29.0	2.9	17	62	0.27	2.4	1.1	D W
2036	07.1	40 01.5	175 05.2	24.2	2.6	15	52	0.13	1.5	4.0	D W
2117	16.2	39 40.7	176 13.7	42.2	2.5	17	36	0.10	1.2	1.2	A B
October 13th											
1849	51.3	39 50.0	176 47.3	30.0	3.5	15	91	0.44	60.8	98.0	D
October 15th											
0654	19.1	39 41.1	176 09.2	41.9	3.5	11	30	0.09	2.0	1.3	A B
1012	59.1	40 00.9	175 00.2	26.5	2.8	13	54	0.18	3.3	8.5	D W
1128	44.1	38 49.8	174 32.9	18.5	3.5	16	42	0.15	2.0	4.3	D
1314	33.8	39 16.2	175 26.5	6.5	1.9	22	12	0.26	0.6	1.3	B
1536	34.1	39 40.6	175 32.8	30.5	1.1	13	1	0.08	0.8	0.7	A
1758	40.0	39 30.8	175 41.6	20.6	1.4	13	7	0.11	0.7	0.9	A A
2006	26.4	40 05.9	174 50.3	59.9	3.1	15	69	0.15	2.5	3.6	B B
October 16th											
0207	50.8	39 15.7	175 26.9	15.0	1.4	18	11	0.15	0.7	1.2	A
0331	28.3	39 41.7	175 39.1	19.4	2.0	13	8	0.14	1.3	1.3	A
0851	55.3	39 30.5	175 42.0	19.2	1.2	15	8	0.10	0.6	0.8	A A
0920	51.2	39 16.4	174 51.8	28.8	2.7	19	15	0.13	0.8	1.1	A U
1651	07.6	39 39.2	176 48.9	45.3	3.2	7	85	0.09	6.3	8.5	D
1827	10.3	39 38.3	176 19.0	29.6	3.6	14	42	0.16	2.0	0.7	A
2156	21.3	39 29.3	175 41.3	20.3	1.4	16	8	0.13	0.6	1.2	A A
2253	23.1	38 50.6	175 40.4	106.2	3.0	11	55	0.25	7.7	8.6	D B
2356	56.2	39 06.0	176 19.1	54.6	3.0	16	67	0.10	1.4	2.3	A B
October 17th											
0621	58.3	39 29.7	175 42.0	24.2	0.7	9	9	0.16	1.9	1.8	A A
1405	17.9	40 28.5	176 07.1	60.0	3.4	11	86	0.17	5.2	5.4	D
1524	34.1	40 04.7	175 05.2	30.0	3.1	17	59	0.24	2.0	1.0	B W
2332	56.5	40 03.2	175 04.3	21.5	2.5	11	57	0.19	2.9	11.4	D W
October 18th											
0118	14.4	39 28.6	175 41.9	19.5	1.6	17	9	0.09	0.5	0.6	A A
1139	48.8	39 17.0	176 13.5	59.0	3.5	14	49	0.07	1.1	1.2	A B
1207	36.5	39 12.5	176 18.4	53.8	2.2	14	60	0.13	2.0	2.8	B B

RUAPEHU SURVEY LOCATED MICROEARTHQUAKES - continued

Origin Time			Epicentre		Depth	MAG	NO	DM	RMS	ERH	ERZ	Q C
h m	sec		Lat. S	Long. E	km			km	sec	km	km	
1525	32.5		40°10.1'	176°44.5'	23.0	3.7	11	98	0.27	6.9	2.0	D
October 19th												
2054	34.7		39 02.4	176 11.3	57.3	2.7	14	58	0.09	1.4	1.8	A B
October 20th												
1330	33.4		40 01.2	174 56.9	30.7	2.9	14	57	0.15	1.5	0.7	A W
1335	09.1		40 01.3	174 57.0	31.4	3.0	17	57	0.14	1.3	0.5	A W
1714	15.3		40 11.1	174 41.4	102.0	3.3	14	83	0.15	3.0	2.3	B B
1835	51.2		40 03.9	174 59.7	29.2	3.0	20	60	0.19	1.4	0.6	D W
2217	35.5		39 09.8	173 46.0	23.8	3.8	20	53	0.26	4.9	1.2	D
October 21st												
0151	21.5		40 00.4	175 05.1	29.9	2.5	13	51	0.15	2.3	5.5	D W
0231	09.7		40 02.2	175 05.0	28.5	2.7	11	55	0.08	1.3	1.5	A W
1056	13.4		39 32.2	175 13.6	82.1	2.0	13	3	0.06	0.9	0.6	A B
1216	51.0		39 29.8	175 43.5	15.0	2.1	11	10	0.06	0.4	0.9	A A
1545	01.9		39 30.3	175 43.4	12.9	1.0	8	10	0.08	0.9	0.9	A A
1614	58.5		39 29.2	175 42.9	18.1	1.2	14	10	0.08	0.4	0.9	A A
1716	10.5		39 56.3	175 05.8	29.4	2.7	16	44	0.09	0.7	0.5	A W
October 22nd												
0112	44.4		40 28.7	174 52.1	31.4	3.4	10	54	0.21	10.5	10.7	D
0356	26.2		39 16.2	175 01.2	38.8	2.4	19	17	0.09	0.6	0.7	A U
0617	57.6		40 06.4	174 57.9	25.0	2.8	16	65	0.37	5.0	17.4	D W
0856	14.9		39 31.9	175 37.4	16.2	1.6	16	2	0.07	0.3	0.8	A A
0905	20.8		39 08.6	176 16.7	57.8	2.8	19	63	0.15	1.9	2.5	A B
1727	30.6		40 07.6	174 58.1	23.5	3.0	18	67	0.36	2.9	3.3	D W
2216	14.8		40 08.8	174 59.7	12.2	2.6	13	68	0.20	2.1	244	D W
2334	12.9		39 28.6	175 36.6	19.0	1.1	14	5	0.15	0.9	1.1	A A
October 23rd												
0914	04.7		39 19.5	175 18.3	27.5	2.2	18	9	0.11	0.5	0.8	A U
1004	41.8		39 17.2	173 40.4	8.9	5.0	21	93	0.27	4.8	5.8	D
1322	07.2		39 48.7	175 01.9	32.9	2.8	20	33	0.15	1.3	0.4	A
1914	40.3		39 30.7	175 39.9	17.2	0.9	18	5	0.18	0.7	1.1	A A
2001	01.2		38 54.9	175 15.8	11.1	2.6	20	29	0.28	2.0	0.9	D U
October 24th												
0132	30.6		39 36.9	175 40.6	16.9	2.0	12	12	0.09	0.6	1.4	A

RUAPEHU SURVEY LOCATED MICROEARTHQUAKES - continued

Origin Time		Epicentre		Depth	MAG	NO	DM	RMS	ERH	ERZ	Q	C
h m	sec	Lat. S	Long. E	km			km	sec	km	km		
0216	43.2	39° 36.6'	175° 56.6'	46.8	1.4	15	10	0.07	1.0	0.8	A	B
0806	09.9	39 51.7	175 04.4	71.6	2.8	22	36	0.15	1.8	1.3	A	B
1049	31.0	39 43.8	175 42.1	22.1	1.0	12	4	0.13	1.2	1.1	A	
1055	29.7	39 59.4	175 05.5	29.0	2.3	11	49	0.06	1.1	2.3	A	W
1632	46.4	40 23.0	174 26.3	91.6	5.6	14	92	0.07	2.0	2.7	B	B
1643	22.5	39 00.1	175 16.3	132.4	3.1	9	23	0.08	3.3	1.7	B	B
1924	22.9	39 43.5	175 15.3	29.5	1.5	20	18	0.18	1.3	1.2	A	
2129	55.5	39 12.2	174 41.4	19.1	3.6	22	6	0.25	1.4	1.1	B	U
2206	10.7	39 39.1	174 42.7	125.4	3.1	18	42	0.08	1.6	1.0	A	B

October 25th

0726	49.5	39 15.4	174 41.5	35.8	3.3	21	10	0.27	2.3	2.4	B	U
1232	42.4	39 25.2	174 54.5	136.2	2.8	15	19	0.11	3.3	1.5	B	B
1532	00.4	40 01.7	176 21.2	22.5	3.0	15	61	0.11	1.8	0.9	D	
1720	22.4	40 02.4	175 03.9	24.8	2.8	17	55	0.14	1.6	4.6	D	W
1811	52.7	39 56.9	175 05.1	28.3	2.6	17	45	0.11	0.9	0.7	A	W
1915	11.9	39 04.2	175 32.8	96.2	2.4	13	14	0.09	1.8	1.2	A	B
2040	05.9	40 05.1	175 02.1	25.0	3.1	16	61	0.27	2.3	2.0	D	W
2043	07.9	39 56.5	175 03.6	32.9	3.4	14	45	0.12	1.8	1.1	A	W

October 27th

1200	30.0	39 22.2	175 26.1	17.3	1.5	16	2	0.16	0.8	1.0	A	
2029	32.9	39 27.5	175 38.0	19.3	1.4	14	7	0.19	1.3	1.5	A	A

October 28th

0051	39.5	39 31.9	175 39.2	20.7	1.2	11	4	0.04	0.3	0.5	A	A

REFERENCES

Abe, K., 1972. Seismological evidence for a lithospheric tearing beneath the Aleutian arc. Earth Planet. Sci. Lett., 14: 428-432.

Adams, C. E., Barnett, M.A.F. & Hayes, R. C., 1933. Seismological report of the Hawke's Bay earthquake of 3rd February, 1931. N.Z. J. Sci. Technol., 15: 93-107.

Adams, R. D. & Hatherton, T., 1973. Seismological and geothermal research in New Zealand. Nature, 246: 262-264.

Adams, R. D. & Le Fort, J. H., 1963. The Westport earthquakes, May 1962. N.Z. J. Geol. Geophys. 6: 487-509.

Adams, R. D. & Ware, D. E., 1977. Subcrustal earthquakes beneath New Zealand; locations determined with a laterally inhomogeneous velocity model. N.Z. J. Geol. Geophys. 20: 59-83.

Adams, R. D., Robinson, R. & Lowry, M. A., 1974. A micro-earthquake survey of the Benmore-Pukaki region; February-March 1973. Report No. 86, Geophysics Division, Dept. Sci. Indust. Res., Wellington, N.Z.

Aggarwal, Y. P., Sykes, L. R., Armbruster, J. & Sbar, M. L., 1973. Premonitory changes in seismic velocities and prediction of earthquakes. Nature, 241: 101-104.

Aggarwal, Y. P., Sykes, L. R., Simpson, D. W. & Richards, P. G., 1975. Spatial and temporal variations in t_s/t_p and in P wave residuals at Blue Mountain Lake, New York: application to earthquake prediction. J. Geophys. Res., 80: 718-732.

Anderson, O. L. & Liebermann, R. C., 1966. Sound velocities in rocks and minerals. VESIAC State-of-the-art Report, 7885-4-X, Institute of Science and Technology, University of Michigan.

Anderson, R. N., Uyeda, S. & Miyashiro, A., 1976. Geophysical and geochemical constraints at converging plate boundaries - Part I: Dehydration in the downgoing slab. Geophys. J. R. astr. Soc., 44: 333-357.

Ansell, J. H. & Smith, E.G.C., 1975. Detailed structure of a mantle seismic zone using the homogeneous station method. Nature, 253: 518-520.

Arabasz, W. J. & Robinson, R., 1976. Microseismicity and geologic structure of the northern South Island, New Zealand. N.Z. J. Geol. Geophys., 19: 569-601.

Ballance, P. F., 1976. Evolution of the Upper Cenozoic magmatic arc and plate boundary in northern New Zealand. Earth Planet. Sci. Lett., 28: 356-370.

Berryman, K. R., 1977. Dating recent tectonic events in parts of New Zealand with dendrochronology. B.Sc.(Hons.) project, Geology library, Victoria University of Wellington, N.Z.

Brown, R., 1973. Precursory changes in V_p/V_s before strike-slip events. Proceedings of the conference on tectonic problems of the San Andreas fault system, Stanford University, pp.463-472.

Brune, J. N. & Allen, C., 1967. A microearthquake survey of the San Andreas fault system in southern California. Bull. Seismol. Soc. Am., 57: 277-296.

Bullen, K. E., 1936. On near earthquakes in the vicinity of New Zealand. N.Z. J. Sci. Technol., 18: 493-507.

Bullen, K. E., 1937. The Hawke's Bay earthquake of 1921, June 29. N.Z. J. Sci. Technol., 19: 199-205.

Bullen, K. E., 1938a. An analysis of the Hawke's Bay earthquakes during February 1931. N.Z. J. Sci. Technol., 19: 497-519.

Bullen, K. E., 1938b. On the epicentre of the 1934 Pahiatua earthquake. N.Z. J. Sci. Technol., 20B: 61-66.

Burdick, L. J. & Langston, C. A., 1977. Modelling crustal structure through the use of converted phases in teleseismic body-wave forms. Bull. Seismol. Soc. Am., 67: 677-691.

Caldwell, J. G. & Frohlich, C., 1975. Microearthquake study of the Alpine fault zone near Haast, South Island, New Zealand. Bull. Seismol. Soc. Am., 65: 1097-1104.

Calhaem, I. M., 1973. Heat flow measurements under some lakes in North
    Island, New Zealand. Ph.D. thesis, Victoria University of Wellington,
    New Zealand.

Carr, M. J., Stoiber, R. E. & Drake, C. L., 1973. Discontinuities in
    the deep seismic zones under the Japanese arcs. Geol. Soc. Am.
    Bull., 84: 2917-2930.

Chase, C. G., 1978. Plate kinematics: the Americas, East Africa, and
    the rest of the world. Earth Planet. Sci. Lett., 37: 355-368.

Cole, J. W., 1978. Andesites of the Tongariro volcanic centre, North
    Island, New Zealand. J. Volcanol. Geotherm. Res., 3: 121-153.

Cope, R. N., 1965. The Taranaki Basin: a subsurface review.
    Shell, B.P. and Todd Oil Services Ltd. Open file Petroleum Report
    No. 456, N.Z. Geol. Surv. Library, Lower Hutt, N.Z.

Cope, R. N., 1966. The hydrocarbon prospects of the Wanganui Basin.
    Shell, B.P. and Todd Oil Services Ltd. Open file Petroleum
    Report No. 459, N.Z. Geol. Surv. Library, Lower Hutt, N.Z.

Crompton, J. S. & Butler, D., 1976. Comments on "Statistical analysis
    of microearthquake activity near San Andreas Geophysical Observatory,
    Hollister, California" by Udias and Rice, 1975 (Letter). Bull.
    Seismol. Soc. Am., 66: 997-998.

Crosson, R. S., 1976. Crustal structure modelling of earthquake data.
    1. Simultaneous least squares estimation of hypocenter and
    velocity parameters. J. Geophys. Res., 81: 3036-3046.

Davies, G. F. 1977. Viscous mantle flow under moving lithospheric
    plates and under subduction zones. Geophys. J. R. astr. Soc., 49:
    557-563.

Dibble, R. R., 1964. A portable slow motion magnetic tape recorder for
    geophysical purposes. N.Z. J. Geol. Geophys., 7: 445-465.

Druce, A. P., 1966. Tree-ring dating of recent volcanic ash and lapilli,
    Mt Egmont. N.Z. J. Botany, 4: 3-41.

Eaton, J. P., O'Neill, M.E. & Murdock,J.N., 1970. Aftershocks of the
    1966 Parkfield-Cholame, California, earthquake: a detailed study.
    Bull. Seismol. Soc. Am., 60: 1151-1197.

Eiby, G. A., 1957. Crustal structure project. Geophys. Mem. N.Z. 5. 40 pp.

Eiby, G. A., 1958. The structure of New Zealand from seismic evidence. Geol. Rundsch., 47: 647-662.

Eiby, G. A., 1964. The New Zealand sub-crustal rift. N.Z. J. Geol. Geophys., 7: 109-133.

Eiby, G. A., 1968a. A descriptive catalogue of New Zealand earthquakes. Part I - shocks felt before the end of 1845. N.Z. J. Geol. Geophys., 11: 16-40.

Eiby, G. A., 1968b. An annotated list of New Zealand earthquakes, 1460-1965. N.Z. J. Geol. Geophys., 11: 630-647.

Eiby, G. A., 1971. Seismic regions of New Zealand. In: B. W. Collins and R. Fraser (Editors), Recent Crustal Movements, N.Z. R. Soc. Bull., 9: 153-160.

Eiby, G. A., 1977. The junction of the main New Zealand and Kermadec seismic regions. International symposium on geodynamics in south-west Pacific, Noumea (New Caledonia), 27 August-2 September 1976. Editions Technip, Paris, pp. 167-178.

Engdahl, E. R., 1973. Relocation of intermediate depth earthquakes in the central Aleutians by seismic ray tracing. Nature Phys. Sci., 245: 23-25.

Engdahl, E. R., 1977. Seismicity and plate subduction in the central Aleutians. In: Island arcs, deep sea trenches and back-arc basins. Editors M. Talwani and W. C. Pitman III, Am. Geophys. Union, Maurice Ewing Series 1, pp. 259-271.

Engdahl, E. R. & Scholz, C. H., 1977. A double Benioff zone beneath the central Aleutians: an unbending of the lithosphere. Geophys. Res. Lett., 4: 473-476.

Evison, F. F., Robinson, R. & Arabasz, W. J., 1973. Late aftershocks, tectonic stress and dilatancy. Nature 246: 471-473.

Evison, F. F., Robinson, R. & Arabasz, W. J. 1976. Microearthquakes, geothermal activity, and structure, central North Island, New Zealand. N.Z. J. Geol. Geophys., 19: 625-637.

Ewing, W. M., Jardetzky, W. S. & Press, F., 1957. Elastic waves
    in layered media. McGraw-Hill, New York, 380 pp.

Fedotov, S. A., 1968. On deep structure, properties of the upper
    mantle, and volcanism of the Kuril-Kamchatka island arc according
    to seismic data. In: The crust and upper mantle of the Pacific
    area. Geophysical Monograph 12, Am. Geophys. Union, pp. 131-139.

Feng, Te-Yi; Tan, Ai-Na & Wang, Ke-Fen, 1974. Velocity anomalies
    of seismic waves from near earthquakes and earthquake prediction.
    Acta Geophys. Sinica, 17: 84-98.

Field, H. C., 1897. Notes on the recent earthquake. Trans. N.Z.
    Inst., 30: 447-457.

Fitch, T. J., 1972. Plate convergence, transcurrent faults, and
    internal deformation adjacent to southeast Asia and the western
    Pacific. J. Geophys. Res., 77: 4432-4460.

Fleming, C. A. & Steiner, A., 1951. Sediments beneath Ruapehu
    volcano. N.Z. J. Sci. Technol., 32B(6): 31-32.

Garrick, R. A., 1968. A reinterpretation of the Wellington crustal
    refraction profile (Letter). N.Z. J. Geol. Geophys., 11: 1280-1294.

Garrick, R. A., 1969. Some physical properties of rocks in the East
    Cape - Mahia Peninsula region, North Island, New Zealand.
    N.Z. J. Geol. Geophys., 12: 738-760.

Gibowicz, S. J. & Hatherton, T., 1975. Source properties of shallow
    earthquakes in New Zealand and their tectonic associations.
    Geophys. J. R. astr. Soc., 43: 589-605.

Green, D. H. & Ringwood, A. E., 1967. An experimental investigation of
    the gabbro to eclogite transformation and its petrological
    applications. Geochim. Cosmochim. Acta, 31: 767-833.

Grindley, G. W., 1960. Sheet 8 Taupo (1st Ed.), Geological Map of
    New Zealand 1:250,000. Dept. Sci. Indust. Res., Wellington, N.Z.

Grow, J. A., 1973. Crustal and upper mantle structure of the central
    Aleutian arc. Geol. Soc. Am. Bull., 84: 2169-2192.

Haines, A. J., 1976. Compressional and shear velocities in the upper mantle beneath New Zealand determined using local crustal earthquakes. M.Sc. thesis, Victoria University of Wellington, N.Z.

Haines, A. J., 1978. Local magnitudes for New Zealand earthquakes. Report No. 132, Geophysics Division, Dept. Sci. Indust. Res., Wellington, N.Z.

Hamilton, R. M., 1966. The Fiordland earthquake sequence of 1960 and seismic velocities beneath New Zealand. N.Z. J. Geol. Geophys., 9: 224-238.

Hamilton, R. M. & Gale, A. W., 1968. Seismicity and structure of North Island, New Zealand. J. Geophys. Res., 73: 3859-3876.

Hamilton, R. M. & Gale, A. W., 1969. Thickness of the mantle seismic zone beneath the North Island of New Zealand. J. Geophys. Res., 74: 1608-1613.

Harris, F., 1975. Focal mechanisms of intermediate depth and deep earthquakes in the North Island, New Zealand. M.Sc. thesis, Victoria University of Wellington, N.Z.

Hasegawa, A., Umino, N. & Takagi, A., 1978. Double-planed structure of the deep seismic zone in the northeastern Japan arc. Tectonophysics, 47: 43-58.

Hashizume, M., 1970. Investigation of microearthquakes - on the accuracy of hypocenter determination. Bull. Disaster Prevention Res. Inst., Kyoto University, 19(3): 1-17.

Hatherton, T., 1969. The geophysical significance of calc-alkaline andesites in New Zealand. N.Z. J. Geol. Geophys., 12: 436-459.

Hatherton, T., 1970a. Upper mantle inhomogeneity beneath New Zealand: surface manifestations. J. Geophys. Res., 75: 269-284.

Hatherton, T., 1970b. Gravity, seismicity, and tectonics of the North Island, New Zealand. N.Z. J. Geol. Geophys., 13: 126-144.

Hatherton, T., 1971. The association of gravity with seismicity and tectonism in New Zealand. In: B. W. Collins and R. Fraser (Editors), Recent Crustal Movements, N.Z. R. Soc. Bull., 9: 167-170.

Hay, R. F. 1967. Sheet 7 Taranaki (1st Ed.), Geological Map of New
    Zealand 1:250,000. Dept. Sci. Indust. Res., Wellington, N.Z.

Hayes, D. E., Talwani, M. & Christoffel, D. A., 1972. The Macquarie
    Ridge complex. In: Antarctic Geology and Geophysics, ed. Adie,
    R. J., Int. Un. Geol. Sci., Series B, No.1, pp.767-772,
    Universitetsforlaget, Oslo.

Hayes, R. C., 1937. The Pahiatua earthquake of 1934 March 5: a report
    on the seismological aspects. N.Z. J. Sci. Technol., 19: 382-388.

Hayes, R. C., 1942. The Wairarapa earthquake of 24th June 1942. Dominion
    Observatory Bulletin S-66, Dept. Sci. Indust. Res., Wellington, N.Z.

Hayes, R. C., 1943. Earthquakes in New Zealand during the year 1942.
    N.Z. J. Sci. Technol., 24B: 191-194.

Hayes, R. C., 1953. Some aspects of earthquake activity in the New
    Zealand region. Proc. 7th Pacif. Sci. Congr., 2: 629-636.

Helmberger, D. V., 1977. Fine structure of an Aleutian crustal section.
    Geophys. J. R. astr. Soc., 48: 81-90.

Henderson, J., 1933. The geological aspects of the Hawke's Bay earthquakes.
    N.Z. J. Sci. Technol., 15: 38-75.

Hogben, G., 1898. The Wanganui earthquake of the 8th December, 1897.
    Trans. N.Z. Inst., 31: 583-590.

Hogben, G., 1904. Notes on the East Coast earthquake of 9th August, 1904.
    Trans. N.Z. Inst., 37: 421-424.

Honda, H., 1957. The mechanism of the earthquakes. Science Reports of
    the Tohoku University, Series 5, Geophysical Supplement 9: 1-46.

Ingham, C. E., 1971. Tongariro power development geophysical survey:
    (5) Seismic survey - Mangaio tunnel line area. Report No.66,
    Geophysics Division, Dept. Sci. Indust. Res., Wellington, N.Z.

Isacks, B. L. & Barazangi, M., 1977. Geometry of Benioff zones: lateral
    segmentation and downwards bending of the subducted lithosphere.
    In: Island arcs, deep sea trenches and back-arc basins. Editors
    M. Talwani and W. C. Pitman III, Am. Geophys. Union, Maurice Ewing
    Series 1, pp. 99-114.

Isacks, B. & Molnar, P., 1971. Distribution of stresses in the descending lithosphere from a global survey of focal-mechanism solutions of mantle earthquakes. Rev. Geophys. Space Phys., 9: 103-174.

Jacob, K. H., Nakamura, K. & Davies, J. N., 1977. Trench-volcano gap along the Alaska-Aleutian arc: facts, and speculations on the role of terrigenous sediments for subduction. In: Island arcs, deep sea trenches and back-arc basins. Editors M. Talwani and W. C. Pitman III, Am. Geophys. Union, Maurice Ewing Series 1, pp. 243-258.

James, D. E., Sacks, I. S., Lazo, E. & Aparicio, P., 1969. On locating local earthquakes using small networks. Bull. Seismol. Soc. Am., 59: 1201-1212.

Jischke, M. C., 1975. On the dynamics of descending lithospheric plates and slip zones. J. Geophys. Res., 80: 4809-4813.

Kaan, J. F., 1960. Interim report on the seismic survey of the Tarata area. Shell, B. P. and Todd Oil Services Ltd. Open file Petroleum Report No. 429, N.Z. Geol. Surv. Library, Lower Hutt, N.Z.

Kanamori, H., 1971. Focal mechanism of the Tokachi-Oki earthquake of May 16, 1968: contortion of the lithosphere at a junction of two trenches. Tectonophysics, 12: 1-13.

Karig, D. E., 1970. Kermadec arc - New Zealand tectonic confluence. N.Z. J. Geol. Geophys., 13: 21-29.

Karig, D. E., 1974. Tectonic erosion at trenches? Earth Planet. Sci. Lett., 21: 209-212.

Karig, D. E., Caldwell, J. G. & Parmentier, E. M., 1976. Effects of accretion on the geometry of the descending lithosphere. J. Geophys. Res., 81: 6281-6291.

Katz, H. R., 1974. Margins of the southwest Pacific. In: The geology of continental margins. Editors C. A. Burk and C. L. Drake, Springer-Verlag, N.Y., pp. 549-565.

Kelleher, J., Savino, J., Rowlett, H. & McCann, W., 1974. Why and where great thrust earthquakes occur along island arcs. J. Geophys. Res., 79: 4889-4899.

Kieckhefer, R. M., 1977. Microseismicity in the vicinity of the Clarence Fault, New Zealand. N.Z. J. Geol. Geophys., 20: 165-177.

Kingma, J. T., 1957. The tectonic setting of the Ruahine-Rimutaka Range. N.Z. J. Sci. Technol., 38B: 858-861.

Kingma, J. T., 1962. Sheet 11 Dannevirke (1st Ed.), Geological Map of New Zealand 1:250,000. Dept. Sci. Indust. Res., Wellington, N.Z.

Kosminskaya, I. P. & Kapustian, N. K., 1976. Generalized seismic model of the typical oceanic crust. In: Volcanoes and tectonosphere. Editors H. Aoki and S. Iizuka, Tokai University Press, pp. 143-156.

Langenkamp, D. & Combs, J., 1974. Microearthquake study of the Elsinore fault zone, southern California. Bull. Seismol. Soc. Am., 64: 187-203.

Lawrence, P., 1967. New Zealand region; bathymetry, 1:6,000,000. N.Z. Oceanogr. Inst. Chart, Miscellaneous Series, 15.

Lee, W.H.K., Bennett, R. E. & Meagher, K. L., 1972. A method of estimating magnitude of local earthquakes from signal duration. Open File Report, U.S. Geol. Surv., 28 pp.

Lee, W.H.K. & Lahr, J. C., 1975. HYPO71: a computer program for determining hypocenter, magnitude, and first motion pattern of local earthquakes. Open File Report, U.S. Geol. Surv., 50 pp., Third Printing.

Lensen, G. J., 1959. Sheet 10 Wanganui (1st Ed.), Geological Map of New Zealand 1:250,000. Dept. Sci. Indust. Res., Wellington, N.Z.

Le Pichon, X., 1968. Seafloor spreading and continental drift. J. Geophys. Res., 73: 3661-3697.

Leslie, W. C. & Hollingsworth, R.J.S., 1972. Exploration in the East Coast Basin, New Zealand. Austral. Petrol. Explor. Assoc. J., 12: 39-44.

Lewis, K. B., 1971. Growth rate of folds using tilted wave-planed surfaces: coast and continental shelf, Hawke's Bay, New Zealand. In: Recent Crustal Movements, B. W. Collins and R. Fraser (Editors), N.Z. R. Soc. Bull., 9: 225-231.

Luyendyk, B. P., 1970. Dips of downgoing lithospheric plates beneath island arcs. Geol. Soc. Am. Bull., 81: 3411-3416.

Neef, G., 1976. Probable faulting on a minor, reverse, bedding fault adjacent to the Alfredton Fault, north Wairarapa, during the 1 August 1942 earthquake (Note). N.Z. J. Geol. Geophys., 19: 737-742.

Nersesov, I. L., Semenov, A. N. & Simberiva, I. G., 1971. Space time distribution of ratios of travel times of P and S waves in the Garm region. In: Experimental Seismology, Science Publishers, Moscow, pp. 334-345.

New Zealand Geological Survey, 1972. North Island (1st Ed.), Geological Map of New Zealand 1:1,000,000. Dept. Sci. Indust. Res., Wellington, N.Z.

New Zealand Geological Survey, 1973. Quaternary Geology - North Island 1:1,000,000 (1st Ed.), N.Z. Geol. Surv. Miscell. Ser. Map 5, Dept. Sci. Indust. Res., Wellington, N.Z.

New Zealand Seismological Observatory, 1978a. New Zealand seismological report for 1974. N.Z. Seismol. Obs. Bull. E-155.

New Zealand Seismological Observatory, 1978b. New Zealand seismological report for 1976. N.Z. Seismol. Obs. Bull. E-158.

Nur, A., 1972. Dilatancy, pore fluids, and premonitory variations of t_s/t_p travel times. Bull. Seismol. Soc. Am., 62: 1217-1222.

Oliver, J. & Isacks, B., 1967. Deep earthquake zones, anomalous structures in the upper mantle, and the lithosphere. J. Geophys. Res., 72: 4259-4275.

Oliver, J., Ryall, A., Brune, J. N. & Slemmons, D. B., 1966. Micro-earthquake activity recorded by portable seismographs of high sensitivity. Bull. Seismol. Soc. Am., 56: 899-924.

Ongley, M., 1943. Wairarapa earthquake of 24th June, 1942, together with map showing surface traces of faults recently active. N.Z. J. Sci. Technol., 25B: 67-78.

Reilly, W. I., 1962. Gravity and crustal thickness in New Zealand. N.Z. J. Geol. Geophys., 5: 228-233.

Reilly, W. I., 1965. Gravity Map of New Zealand 1:4,000,000, isostatic
     anomalies (1st Ed.). Dept. Sci. Indust. Res., Wellington, N.Z.

Reilly, W. I., Whiteford, C. M. & Doone, A., 1977. North Island
     (1st Ed.), Gravity Map of New Zealand 1:1,000,000, Bouguer and
     isostatic anomalies. Dept. Sci. Indust. Res., Wellington, N.Z.

Research Group for Explosion Seismology, 1977. Regionality of the
     upper mantle around northeastern Japan as derived from explosion
     seismic observations and its seismological implications.
     Tectonophysics, 37: 117-130.

Richter, C. F., 1971. Sporadic and continuous seismicity of faults
     and regions. In: Recent Crustal Movements, B. W. Collins and
     R. Fraser (Editors), N.Z. R. Soc. Bull., 9: 171-173.

Robertson, E. I. & Reilly, W. I., 1958. Bouguer anomaly map of New
     Zealand. N.Z. J. Geol. Geophys., 1: 560-564.

Robinson, R., in press. Seismicity within a zone of plate convergence -
     the Wellington region, New Zealand. Geophys. J. R. astr. Soc.

Robinson, R. & Arabasz, W. J., 1975. Microearthquakes in the north-
     west Nelson region, New Zealand. N.Z. J. Geol. Geophys., 18:
     83-91.

Robinson, R., Arabasz, W. J. & Evison, F. F., 1975. Long-term behaviour
     of an aftershock sequence: the Inangahua, New Zealand, earthquake
     of 1968. Geophys. J. R. astr. Soc., 41: 37-49.

Robinson, R., Calhaem, I. M. & Thomson, A. A., 1976. The Opunake,
     New Zealand, earthquake of 5 November 1974. N.Z. J. Geol. Geophys.,
     19: 335-345.   \

Rynn, J.M.W. & Scholz, C. H., 1978. Study of the seismic velocity
     ratio for several regions of the South Island, New Zealand:
     evaluation of regional t_s/t_p and near source V_p/V_s values.
     Geophys. J. R. astr. Soc., 53: 87-112.

Scholz, C. H., Wyss, M. & Smith, S. W., 1969. Seismic and aseismic
     slip on the San Andreas Fault. J. Geophys. Res., 74: 2049-2069.

Scholz, C. H., Rynn, J.M.W., Weed, R. W. & Frohlich, C., 1973a.
     Detailed seismicity of the Alpine fault zone and Fiordland
     region, New Zealand. Geol. Soc. Am. Bull., 84: 3297-3316.

Scholz, C. H., Sykes, L. R. & Aggarwal, Y. P., 1973b. Earthquake
    prediction: a physical basis. Science, 181: 803-810.

Smith, E.G.C., 1977. The theory of multi-earthquake location by least
    squares and applications to groups of North Island, New Zealand
    mantle earthquakes. Ph.D. thesis, Victoria University of Wellington,
    N.Z.

Smith, W. D., 1970. S to P conversion as an aid to crustal studies.
    Geophys. J. R. astr. Soc., 19: 513-519.

Topping, W. W., 1974. Some aspects of Quaternary history of Tongariro
    volcanic centre. Ph.D. thesis, Victoria University of Wellington, N.Z.

Udias, A. & Rice, J., 1975. Statistical analysis of microearthquake
    activity near San Andreas Geophysical Observatory, Hollister,
    California. Bull. Seismol. Soc. Am., 65: 809-827.

Utsu, T., 1961. A statistical study on the occurrence of aftershocks.
    Geophys. Mag., 30: 521-605.

van der Linden, W.J.M., 1968. Cook bathymetry. N.Z. Oceanogr. Inst.
    Chart, Oceanic Series, 1:1,000,000.

Van Wormer, J. D., Davies, J. & Gedney, L., 1974. Seismicity and plate
    tectonics in south central Alaska. Bull. Seismol. Soc. Am., 64:
    1467-1475.

Veith, K. F., 1974. The relationship of island arc seismicity to
    plate tectonics (abstract). Trans. Am. Geophys. Union, 55: 349.

Wadati, K., 1933. On the travel time of earthquake waves. Part II,
    Geophys. Mag., 7: 101-111.

Walcott, R. I., 1978a. Present tectonics and Late Cenozoic evolution
    of New Zealand. Geophys. J. R. astr. Soc., 52: 137-164.

Walcott, R. I., 1978b. Geodetic strains and large earthquakes in
    the axial tectonic belt of North Island, New Zealand. J. Geophys.
    Res., 83: 4419-4429.

Ward, P. L., Gibbs, J., Harlow, D. & Arturo Aburto Q, 1974. Aftershocks
    of the Managua, Nicaragua, earthquake and the tectonic significance
    of the Tiscapa Fault. Bull. Seismol. Soc. Am., 64: 1017-1029.

Watson, J. S. & Allen, D.C.K., 1964. Compilation of seismic results in
     the Wanganui Basin. Shell, B. P. and Todd Oil Services Ltd. Open
     file Petroleum Report No. 448. N.Z. Geol. Surv. Library, Lower
     Hutt, N.Z.

Weissel, J. K., Hayes, D. E. & Herron, E. M., 1977. Plate tectonics
     synthesis: the displacements between Australia, New Zealand,
     and Antarctica since the Late Cretaceous. Mar. Geol., 25: 231-277.

Whiteford, C. M. & Woodward, D. J., 1975. Sheet 11 Dannevirke (1st Ed.),
     Gravity Map of New Zealand 1:250,000, Bouguer anomalies.
     Dept. Sci. Indust. Res., Wellington, N.Z.

Woodward, D. J., 1976. Visco-elastic finite element analysis of
     subduction zones. Ph.D. thesis, University of Durham.

Worzel, J. L., 1974. Standard oceanic and continental structure.
     In: The geology of continental margins. Editors C. A. Burk and
     C. L. Drake, Springer-Verlag, N.Y., pp. 59-66..

Wyllie, P. J., 1971. The dynamic earth: textbook in geosciences.
     John Wiley & Sons, N.Y., 416 pp.

Wyss, M., 1973. The thickness of deep seismic zones. Nature, 242:
     255-256.